HHS Public Access

Author manuscript

Compr Physiol. Author manuscript; available in PMC 2015 April 15.

Published in final edited form as:

Compr Physiol. 2013 October ; 3(4): 1437–1471. doi:10.1002/cphy.c100085.

Particle transport and deposition: basic physics of particle kinetics

Akira Tsuda[1], **Frank S. Henry**[1], and **James P. Butler**[1,2]

[1]Harvard School of Public Health, Boston, MA, 02115

[2]Dept. Medicine, Harvard Medical School, Boston, MA 02115

Abstract

The human body interacts with the environment in many different ways. The lungs interact with the external environment through breathing. The enormously large surface area of the lung with its extremely thin air-blood barrier is exposed to particles suspended in the inhaled air. Whereas the particle-lung interaction may cause deleterious effects on health if the inhaled pollutant aerosols are toxic, this interaction can be beneficial for disease treatment if the inhaled particles are therapeutic aerosolized drug. In either case, an accurate estimation of dose and sites of deposition in the respiratory tract is fundamental to understanding subsequent biological response, and the basic physics of particle motion and engineering knowledge needed to understand these subjects is the topic of this chapter.

A large portion of this chapter deals with three fundamental areas necessary to the understanding of particle transport and deposition in the respiratory tract. These are: 1) the physical characteristics of particles, 2) particle behavior in gas flow, and 3) gas flow patterns in the respiratory tract. Other areas, such as particle transport in the developing lung and in the diseased lung are also considered. The chapter concludes with a summary and a brief discussion of areas of future research.

Keywords

pulmonary acinus; PM; Inhalation therapy; chaotic mixing; nanoparticles

Introduction

Adult humans inhale over 10,000 liters of air per day. Contained within this air are somewhere between 100 billion and 10 trillion particles. A fraction of this astronomically large number of particles deposits on the lung surface. Pathogenic effects may occur if the deposited particles are not properly dealt with by the lung's defense mechanisms. In inhalation drug therapy, one puff of a metered-dose inhaler (MDI), for instance, contains several million particles, but only a fraction of those drug particles reach the target site in the respiratory tract. What fraction of the particles we inhale reaches the lung's respiratory surface is a function of the particles' physical characteristics and the dynamics of the gas flow. This in turn leads to a clear distinction between “exposure-response”, the subject of epidemiology, and the causal relationship between “exposure-dose” and “dose-response”.

The focus of this chapter is to review the basic engineering knowledge needed to understand the exposure-dose relationship.

This chapter aims to provide the basic information necessary to understand current research on the relationship between particle exposure and the number of particles depositing on a unit area of the lung's surface (dose). The chapter starts with describing the physical and chemical characteristics of a particle, which are important factors in determining its behavior in the gas flow (Particle Characteristics). This is followed by a discussion of transport and deposition mechanics in a conduit (Particle Transport and Particle Deposition, respectively). Particle Transport and Deposition in the Respiratory Tract, the main part of this chapter, describes the transport and deposition phenomena along the respiratory tract in the anatomical order an inhaled particle experiences. The Special Issues section describes some specific topics that are important in lung physiology but are not covered in the previous section. The chapter ends with a summary and suggestions of future research directions.

Particle Characteristics

Particle size

The size of an aerosol particle is the fundamental characteristic that determines its transport properties. For spherical particles, the size is given by particle diameter (d_p). In the case of irregularly-shaped particles (see below), an equivalent diameter is used, defined by the diameter of a sphere of equal volume. Respirable particles range from a few nanometers to, typically, a few microns.

The transport behavior of an aerosol particle depends on its interaction with the surrounding gas molecules. This interaction can be characterized by considering the particle size (d_p) relative to the mean free path of the gas molecules (ℓ); the ratio between d_p and ℓ is the Knudsen number ($Kn = \ell/d_p$). When $Kn \gg 1$ (i.e., $\ell \gg d_p$) the behavior of the particle and surrounding gas requires the kinetic theory of gases. On the other hand, when $Kn \ll 1$, (i.e. $\ell \ll d_p$), the probability that surrounding gas molecules strike the particle surface is high, and the surrounding gas affects the behavior of the particles through a drag force. In this case, the gas surrounding the particle can be treated as a fluid continuum and the drag force acting on the particle surface can be calculated from Stokes' law [$F_D = 3\pi\mu d_p(\vec{v_p} - \vec{v_f})$, where F_D is the drag force, μ is the fluid viscosity and $\vec{v_p}$ & $\vec{v_f}$ are the velocity of the particle & the surrounding fluid, respectively]. For air at sea level, ℓ is approximately 70 nm, and hence for fine/ultrafine particles, Kn cannot be taken as one of these two extremes. In this case, the behavior of the surrounding gas can be still treated as a continuum, but a slip correction factor needs to be introduced to adjust the drag force given by the limiting Stokes' relationship (i.e., the corrected drag force is equal to F_D/C_s). The Cunningham slip correction factor[61] C_s is given by,

$$C_s = 1 + (2\ell/d_p)[A_1 + A_2 \exp(-A_3 d_p/\ell)] \quad (1)$$

Where $A_1 = 1.257$, $A_2 = 0.400$, and $A_3 = 0.55$ are empirically determined constants[67,223]. C_s and related particle transport properties are tabulated in Table 1. The Einstein-Stokes

equation for the diffusion coefficient of a sphere also has to be adjusted to account for slip; i.e., $D = k_B T_{abs} C_s / (3\pi\mu d_p)$, where k_B is Boltzmann's constant and T_{abs} is the absolute temperature.

Particle size distribution

A cloud of equal-sized particles is called a monodisperse aerosol. However, particles in the air we breathe span an extremely large size range, and constitute what is known as a polydisperse aerosol. The physical characteristics of polydisperse aerosols are usually described by their particle size distribution.

The distribution of particle size within a polydisperse aerosol is typically skewed (Fig. 1). This is because a large portion of particles are formed from the breakup of large particles into smaller ones[87] or from the growth (i.e., through certain types of agglomeration) of small particles to larger ones[105]. To characterize such a skewed distribution, there are at least 3 values to consider; the mean (the arithmetic average particle diameter of the distribution), the median (the particle diameter that divides the frequency distribution in half; 50% of the particles have a larger diameter, and the other 50% of the particles have a smaller diameter); and the mode (the value that occurs most frequently in a distribution). The standard measure of skewness is given by the third moment about the mean, normalized by the standard deviation to the third power. When the mean, mode and median all coincide, the skewness is zero; this does not imply symmetry of the distribution, but all symmetric distributions exhibit zero skewness. As shown below, there are several advantages to analyzing symmetric distributions.

Skewed distributions seen in aerosol distributions are often well approximated by lognormal distributions. These are distributions of particles sizes whose logarithms are normally distributed (i.e. Gaussian, Fig. 2)[288]. Note that this is not just a conversion of the abscissa from a linear scale to a logarithmic scale, because the bin widths used to define the histograms are correspondingly changed. In this lognormal representation, the median of the particle size is now equal to the geometric mean of the particle sizes, and the spread of the curve can be conveniently expressed by the geometric standard deviation (σ_g). [The geometric mean is defined as the m^{th} root of the product of m terms. The logarithm of the geometric mean is equal to the arithmetic mean of the logarithms.]

The cumulative frequency of the particle size distribution is the frequency or probability of the occurrence of a particle size less than a given value; this is a sigmoid-shape curve (Fig. 3). Note that there are no bin width questions for cumulative distribution functions, so this issue does not arise. Further, if the cumulative frequency is plotted on the probability scale, one obtains a straight line (Fig. 4). This plot is useful because the geometric mean as well as the geometric standard deviation of lognormal particle size distribution can be readily obtained graphically (see Fig. 4 legend for further details).

The above is a graphical representation of particle size distribution. The underlying mathematical representation is based on normal probability distribution functions for logarithms. Further detailed, excellent, discussions on this topic can be found elsewhere[106,108,284].

Particle shape

The shape of a particle affects its aerodynamic and diffusive behavior; thus, it is one of the important factors determining particle transport and deposition in the lung. Whereas a particle's shape is largely conditioned by how it formed, changes in particle shape may occur after formation because of crystallization, hydration, agglomeration, etc. Liquid droplets form perfect spherical shapes due to surface tension. Highly non-spherical particles include straight or curly fibers as well as complex-shaped agglomerated cluster of particles.

The transport behavior of only a few irregularly-shaped particles, such as the ellipsoid (e.g. a prolate spheroid, like a rugby ball), and the oblate spheroid (disk-shaped), may be described mathematically[e.g., 110,137]. In general, a mathematical description of the transport behavior of irregularly-shaped particles is not possible; thus, the influence of the particle's irregular shape on its behavior is taken into account empirically through a parameter called, the dynamic shape factor. This factor is the ratio of the resistance of a given particle to that of a spherical particle having the same volume. Shape factors for various particles are listed in Hinds (1983, on page 52) or Silverman et al., (1971, on page 12).

Particle density

The density of a particle plays an important role in its transport and deposition (see later sections). Because density is an intensive property, the density of a particle remains the same as that of the original material unless the particle undergoes surface oxidation or hydration (hygroscopcity will be discussed in the next subsection). Many particles agglomerate to form larger particles. In this case, the bulk density is defined as the mass of the component particles making the agglomerate divided by the total volume occupied, which includes particle volume and inter-particle void volume. Thus, the bulk density of an agglomerate of particles is not an intensive property as it depends on how the constituent particles are arranged in the agglomerate[284].

Particle composition, surface characteristics and charge

A particle's core composition and its surface characteristics are important factors for how the particle interacts with the lung tissue after deposition. This will be briefly discussed in the last section. If a particle carries a net electrical charge on its surface and is traveling in an electrical field, the following factors have to be taken into account. If the electrical force, $\vec{F_e}$, and the drag force on the particle are balanced locally in the gas, the steady electrical migration velocity, $\vec{v_e}$, can be expressed as $\vec{v_e} = \vec{F_e}/f_{ric}$, where f_{ric} denotes a friction coefficient (discussed in detail in the next section). The particle flux, $\vec{J}$, due to simultaneous effects of diffusion and migration in the electrical force field, can be expressed by summing the two effects as $\vec{J} = -D\nabla n + \vec{v_e}n$, where n is particle number concentration, D is particle diffusivity (discussed in detail later), and ∇ is the gradient operator. Substituting $\vec{J}$ in $\partial n/\partial t = -\nabla \cdot \vec{J}$, the expression is rewritten as the equation of conservation of particles in the presence of an external electrical force field as, $\partial n/\partial t = \nabla \cdot D\nabla n - \nabla \cdot \vec{v_e}n$. Solutions to this equation for constant D and $\vec{v_e}$ are given by Carslaw and Jaeger (1959).

Nucleation, Condensation, Evaporation, and Hygroscopicity

Nucleation, condensation, evaporation, and hygroscopicity are all processes resulting from molecular transfer between the particle (or droplet) and the surrounding gas. In the case of a liquid droplet, the vapor of the liquid (often water) plays an important role in these processes. The partial pressure of a vapor (the pressure which the vapor would have if it alone occupied the volume) is directly related to the concentration of that liquid vapor in a volume of gas; the ratio of the partial vapor pressure to the saturation vapor pressure, called the saturation ratio S_R, plays a critical role in all of the processes mentioned above.

Under the conditions when $S_R > 1$ (i.e., supersaturation), the size of a droplet grows by condensation of vapor on its surface. The rate of growth depends on the rate of the arrival of vapor molecules at the droplet surface. While it is governed by the kinetic theory of gases when the diameter of the droplet is smaller than the mean free path ℓ of the surrounding gas, the rate of arrival of vapor molecules is governed by the rate of molecular diffusion to the droplet surface (see "coagulation" below) when the diameter of the droplet exceeds ℓ. Under the conditions where $S_R < 1$ (i.e., unsaturated), evaporation (i.e., the reverse process of condensation) occurs; more vapor molecules leave a droplet's surface than arrive, causing a shrinkage of the droplet's size. The initial formation of a particle from vapor by condensation is called nucleation (nucleated condensation). This process is usually facilitated by the presence of small particles, which serve as nucleation sites.

In the respiratory tract, relative humidity (*RH*), which is equal to S_R in the case of water vapor, substantially changes due to an increase in respiratory air temperature and humidification from the nose (or mouth) to the lung. Accordingly, inhaled particles with hydrophilic surfaces, such as sodium chloride particles, may grow in size and change their density by adsorbing water vapor from the warm and humid environment along the respiratory tract. Furthermore, because the size and density of the particles are the major factors in determining the deposition and the distribution of particle deposition, the hygroscopic growth of hydrophilic particles is an important factor to consider[93,97,134-136,150,151,228]. Hygroscopic growth strongly depends on the longitudinal profile of *RH*, which depends on temperature, along the upper airways and tracheobronchial tree.

Determining the longitudinal air temperature profile, and subsequently the *RH* profile is not straightforward. Estimates of how quickly and at what airway generation the particle-laden inspired air reaches a temperature of 37°C and a relative humidity of 99.5% are generally difficult to make because they depend on the mode of breathing (nasal vs. mouth breathing) as well as on the type of breathing pattern (hyperpnea during exercise vs. quiet breathing at rest). Numerous studies of this topic have been reported. In general, while during quiet breathing, in particular during nose breathing, most of the heat exchange between the inspired air and airway walls takes place in the upper airways and *RH* reaches saturation at the trachea or the main-stem bronchi in inspiration. Conversely, in the case of hyperpnea, in particular during mouth breathing, the temperature and *RH* of incoming air may not reach body conditions until many airway generations below the trachea. Further detailed, excellent, discussions on this topic can be found elsewhere[e.g., 69,155,156,218,219,290,306].

Coagulation

Whereas the processes discussed above (e.g., condensation, evaporation, etc.) involve mass transfer between a particle and the surrounding gas molecules, coagulation is an inter-particle phenomenon. That is, it is a process in which particles collide with one another and adhere to form a larger particle. As a result, the particle size distribution shifts towards larger sizes, and the particle number concentration decreases. In the case of solid particles, this process is called agglomeration.

One of the simplest processes of particle coagulation is when a cloud of equal-sized particles collide due to Brownian motion. This is an idealized case, but it can be described mathematically and provides us with a useful benchmark of the coagulation process as shown below.

The motion of a Brownian particle of radius R under steady-state conditions can be written in spherical coordinates as $D\frac{1}{r^2}\frac{d}{dr}\left(r^2\frac{dn}{dr}\right)=0$, where D denotes the Brownian diffusion coefficient, r the radial coordinate, and n denotes the local number concentration of the particles. The boundary conditions are that at large distance ($r\rightarrow\infty$), n approaches the bulk number concentration (n_c), and at the radius of the sphere of influence of the test particle ($r = 2R$ shown as a dotted line in Fig. 5), the free particle concentration vanishes (n=0). Integrating the above equation subject to these boundary conditions, the number concentration is expressed as $n = n_c\,[1\text{-}(2R/r)]$.

Since the flux of particles arriving at the surface of the sphere of influence of the test particle is $D(\partial n/\partial r)_{r=2R} = Dn_c/2R$, the rate at which particles arrive at the surface is $D(4\pi r^2\,\partial n/\partial r)_{r=2R.} = 8\pi DRn_c$. Since there are N_c test particles in a unit volume, the number concentration of test particles is also n_c, and hence the rate at which particles collide is $8\pi DRn_c^2$. The coefficient ($8\pi DR$) is known as the Brownian coagulation coefficient. The most important point to emphasize here is that the coagulation coefficient scales with the size of the particles. As the particle size grows, this scaling remains, with a weak dependence of the prefactor on particle size.

Particle Transport

The most successful description of the motion of a spherical particle of diameter d_p and mass m_p in the surrounding gas has been through the separation of the influence of the gas phase into additive effects; treating the gas as a fluid continuum; and modeling the molecular effects as random collisions of gas molecules. These ideas lead to the Langevin equation[47].

$$m_p\frac{d\vec{v}_p}{dt}=-f_{fric}(\vec{v}_p-\vec{v}_f)+m_p\vec{g}+\vec{F}(t) \quad (2)$$

This stochastic differential equation represents Newton's second law. The equation states that the mass times the acceleration (left hand side) is equal to the resultant of all forces acting on the particle (right hand side). The first of these forces represents the viscous drag

force due to the motion of the particle (particle velocity, v_p) relative to the motion of the surrounding fluid, v_f, here taken as a fluid continuum. The friction coefficient $f_{ric} = 3\pi\mu dp/C_s$, where μ is fluid viscosity, is assumed to be governed by Stoke's law[137] corrected by the Cunningham factor, C_s, (see Particle Size Section) to account for the small particle "slip" through the fluid molecules. The second force is gravitational, $m_p g$. The third force is stochastic, a random force, $F(t)$, that is characteristic of Brownian collisions[47,221] of the surrounding fluid molecules with the particle.

The motion of small particles under Brownian force

When small particles are considered (say, $d_p < 0.5\ \mu m$), several terms in Eq. 2 may be neglected. First, the gravity term $m_p g$ is insignificant. Second, the time scales in the situation relevant to our interest are much longer than the particle momentum relaxation times $\tau_{mom} = m_p C_s/3\pi\mu d_p$, which are on the order of micro or pico seconds for ultrafine particles in air. This implies that the accelerative term (the left hand side of Eq. 2) may also be neglected. With these approximations, the particle motion is simple Brownian, where the impulsive motions due to random collisions with gas particles at temperature T_{abs} are damped by the viscous drag. This leads to simple diffusion of the particles, with a diffusivity given by Einstein's expression for the diffusion coefficient $D = k_B T_{abs}\ C_s/3\pi\mu d_p$, where k_B is Boltzmann's constant and T_{abs} is absolute temperature. Note that, whereas the size (and also the shape) of the particle (d_p) is critical in determining the diffusion coefficient, D, interestingly, D does not depend on the density (ρ_p) of the particles. It is also important to notice here that the diffusion coefficient of aerosol particles is, in general, significantly smaller than that of the typical respiratory gases. For instance, the diffusivity of an aerosol particle of 10 or 100 nm diameter is approximately, $D = 10^{-4}$ to 10^{-6} cm^2/sec, respectively, which is 2 to 4 orders of magnitude smaller than molecular diffusivity of O_2 and CO_2.

Velocity, v_p, and position, r_p, of a particle can be obtained directly by integrating the governing equation with respect to time[47,88,124]. A Monte Carlo approach to integrating the equation, combined with conditional probability and eigensystem analysis considering the stochastic behavior of a particle as a Markov process[47], was used to simulate the behavior of submicron particles in the pulmonary acinus[308].

This type of analysis can be extended to the case where the length scales are sufficiently large that the particle position distribution can be approximated by a continuum of particles, with local concentration n. In this case, the problem reduces to the combined effects of simple convection through interaction with the local fluid velocity v_f and the intrinsic diffusivity D. This leads to the convection-diffusion transport equation for the particle concentration, which in non-dimensional form is given by

$$Sr\frac{dn}{dt} = \frac{1}{Pe}\nabla^2 n - \vec{v}_f \cdot \nabla n \quad (3)$$

where the Strouhal number, $Sr = L/TV$ is a measure of the unsteadiness of the flow (L is a characteristic length scale, such as bronchial, acinar, or alveolar diameter; V is a characteristic velocity, such as mean flow velocity; and T is a characteristic time scale, such

as breathing period). The Péclet number, $Pe = LV/D$ is a measure of the strength of convective over diffusive transport. In the distal lung in healthy human respiration at rest, the Strouhal number is much less than unity and hence lung flow is essentially quasi steady; this is not true in the more proximal airways, especially during exercise. Note, however, that even when $Sr \ll 1$, convection may not be neglected. This is because the Péclet number for nano-size particles is in the range 10^3 to 10^8 throughout the conducting airways and is » 1 for most of the acinus (Table 2) indicating that even in the lung periphery convection dominates the transport of nano-size particles. This in turn means that fluid velocity cannot be neglected, and all three terms in Eq. 3 must be considered. With respect to boundary conditions, to the extent that particles that actually contact any epithelial surface always "stick", and do not subsequently reaerosolize, this condition can be expressed as a Dirichlet boundary condition (i.e., $n = 0$ on the conduit surface).

The motion of large particles under a Gravitational Force field

When particles are relatively large (say, $d_p > 0.5\ \mu m$), for which the Brownian random term (the 3rd term on the right hand side of Eq. 2) may be ignored, the Langevin equation (Eq. 2) can be significantly simplified because the resulting diffusive behavior is negligible. The governing stochastic differential equation becomes an ordinary deterministic differential equation and thus its solution for a given initial condition becomes deterministic. The reduced Langevin equation can be nondimensionalized as,

$$Stk\frac{d\vec{v}^*_p}{dt*} = -(\vec{v}^*_p - \vec{v}^*_f) + \frac{V_g}{\bar{V}}\vec{g}* \quad (4)$$

where $\vec{v}^*_p (= \vec{v}_p/\bar{V})$ and $\vec{v}^*_f (= \vec{v}_f/\bar{V})$ are the dimensionless particle velocity and carrier gas velocity, respectively; t^* is a dimensionless time given by $t^* = tV/L$; $\vec{g}^*$ is a dimensionless gravitational acceleration given by $\vec{g}^* = \vec{g}/|\vec{g}|$ where $|\vec{g}|$ is scalar gravitational acceleration. Equation 4 shows that particle motion is governed by two nondimensional groups: the Stokes number, $Stk(=\rho_p d_p^2 \bar{V}/18\mu L)$, which expresses the ratio of inertial force to viscous drag force, and $V_g/\bar{V}$, the ratio of terminal settling velocity $V_g(=\rho_p d_p^2 |\vec{g}|/18\mu)$ to $\bar{V}$, which expresses the relative importance of gravity to viscous drag. The ratio of Stk and $V_g/\bar{V}$, $[Stk/(V_g/\bar{V}) = \bar{V}^2/L|g|]$, shows the relative importance of inertial to gravitational forces on particle motion. The inertial term is significantly more important than the gravity term in larger conducting airways; by contrast, the gravity term becomes dominant in smaller airways and the acinus (Table 2).

The motion of medium size-range particles

When particles are in the medium-size range (say, $d_p \approx 0.5\ \mu m$), they are too large for significant Brownian transport, and too small for significant inertial or gravitational crossing of streamlines. In this case the only surviving term in Eq. 2 is $-f_{ric}(\vec{v_p} - \vec{v_f})$ which when equated to zero implies that the particles simply follow the local gas velocity field. The resulting transport thus requires an accurate description of the surrounding gas flow patterns. Importantly, this also implies that to the extent that the gas velocity field is reversible during

cyclic breathing, so too is the particle velocity and hence displacement; this is kinematic reversibility, in which there is no net transport over a breathing cycle. A considerable body of research has been dedicated to the study of respiratory fluid mechanics, and velocity fields in particular, in nasal flow[e.g., 37,83,86,111,202,204,278,340,] large airway conducting airway flow[e.g., 8,183,206,317], and acinar fluid mechanics[e.g.,65,125,143-145,192,193,310,314,315]. These topics will be discussed in more detail later in this chapter.

Particle Deposition

Four major deposition mechanisms in the respiratory system for spherical particles are discussed here. They are turbulent deposition, inertial impaction, gravitational sedimentation, and diffusional deposition. The deposition mechanisms for non-spherical particles, particularly fibrous particles such as asbestos, are important for certain disease etiologies; the deposition mechanisms for those special cases have been extensively reviewed elsewhere, including references of basic theory and mechanisms[e.g., 49,110,137,282] and application to the respiratory system[e.g., 5,6,41].

Turbulent deposition

The precise nature of the flow in the upper airways (i.e., nasal cavity and oropharyngeal airway) is still an open question but it is likely to contain turbulence at some point in the breathing cycle. Thus, mixing and deposition due to turbulence need to be addressed.

Much research has been carried out on the nature of turbulence, and into the mathematical description and numerical simulation of turbulent flows. Despite this body of work, turbulence remains relatively poorly understood. Nonetheless, the practical effects of turbulence; such as increased flow resistance and enhanced heat transfer rates, are routinely encountered in our daily lives. The characteristic of turbulence of most interest here is the increased levels of mixing and transport, particularly in the cross-stream direction, exhibited by turbulent flows. The increase level of flow resistance mentioned above is due to an enhanced level of cross-stream transport of momentum caused by the turbulent velocity fluctuations. Providing certain general conditions are met, there is a direct correlation between momentum transfer and mass transfer by the turbulence. Hence, compared to laminar flows, turbulent flows can be expected to have increased levels of particle deposition.

In the 1990s, a series of studies on particle deposition in turbulent duct flow was done by a group led by Ahmadi[e.g.,48,205,289]. While flow in the upper airways may not be well modeled by steady flow in a duct, the results of these studies have general relevance to particle deposition in upper airways of the lung. For instance, Chen & Ahmadi (1997) considered deposition of particles in the range 0.01-100 μm and found that deposition was a complex function of particle size. Results were given in terms of a non-dimensional particle relaxation time $\tau^+ = (\rho_p/\rho_f) d_p^2 (\rho_f u*/\mu)^2 C_s/18$, where ρ_f is the fluid density and $u*$ is the friction velocity (a measure of the strength of the turbulence). For small values of τ^+; that is, submicron particles, deposition increased with decreasing τ^+. Conversely, for large values of τ^+; that is, particles with diameters measured in the tens of microns, deposition increased with increasing τ^+. This implies that there is a middle range of particles ($0.05 < \tau^+ < 0.1$) for

which deposition was at a minimum. Similar results had been previously found by others[e.g.,246,328]. It is of interest to note that the shape of the deposition curve found by Chen & Ahmadi (1997) is reminiscent of the curve for total particle deposition in the lung given by Heyder et al. (1986).

Inertial deposition

Because the diffusion coefficient D (= $k_B T_{abs}\, C_s/3\pi\mu d_p$) is inversely proportional to particle size, the effects of Brownian motion can be neglected for large particles, say, larger than 1 μm in diameter. However, as the size of the particle increases, the momentum relaxation time $\tau_{mom}(=\rho_p d_p^2 C_s/18\mu)$ rapidly increases; the inertia terms (the left hand side of Eq. 2) cannot be ignored from the governing equation. The effects of the particle's inertia on its behavior can be easy seen as follows. Suppose, for instance, that a particle enters a stationary fluid with some initial velocity $v_{p,0}$ in the x direction. The particle will travel a finite distance before coming to rest. The motion of the particle in the stationary fluid can be expressed as $m_p(dv_p/dt) = -f_{ric}\, \vec{v_p}$. The solution of this equation gives the velocity and displacement as $v_p = v_{p,0}\, exp(-\, t/\tau_{mom})$ and $x = v_{p,0}\ \tau_{mom}\ [1\text{-}exp(-\, t/\tau_{mom})]$, respectively. The distance traveled by the particle before coming to rest (as $t \to \infty$) is called the stop-distance and is given by $v_{p,0}\ \tau_{mom}$. It will be recognized that the dimensionless ratio of the stop distance to the characteristic length (L) of the system is proportional to the Stokes number, $Stk\left(=\rho_p d_p^2\, C_s \overline{V}/18\mu L\right)$, which plays an important role in determining inertial deposition.

When the surround fluid is not stationary and the flow streamlines are not rectilinear, an analytical solution of the governing equation (Eq. 4) is difficult and rarely tractable; only a few solutions are known. One such solution is for the case of a Stokesian particle approaching a stagnation point in the flow. The equation of motion for the particle along a stagnation streamline may be described by $Stk \cdot d\vec{v}^*_p/dt * = -(\vec{v}^*_p - \vec{v}^*_f)$ with $\vec{v}^*_f$ being the linearized flow field in the region near the stagnation point. Friedlander (1977) gives a nice explanation of an analytical approach to this problem, which yields the concept of the critical Stokes number, Stk_{crit}. He concluded that in order for inertial deposition to occur, the Stokes number, Stk, needs to be above a critical value given by $Stk_{crit} = 1/4b$ (where b is a dimensionless constant, which depends on the shape of the body or collector on which the stagnation point exists) and Stk_{crit} represents a lower limit for inertial impaction.

Airflow patterns in the respiratory tract are complex and highly curvilinear, and since analytical solutions are generally not possible; numerical approaches are often employed. Usually, the airflow velocity field, v_f, is first solved. Then, applying v_f, the deterministic second-order differential equation of the particle motion (Eq. 4) is solved with given initial conditions (velocity and position) and Dirichlet boundary conditions. This results in a description of the behavior (velocity and position) of the particle as a function of time[e.g., 106, 237,309,338].

Gravitational deposition

Gravitational sedimentation is the most effective deposition mechanism in the small airways for micron-size particles that manage to pass through the nasopharynx and the large

conducting airways. Because the conducting airways may be basically viewed as a collection of quasi-rigid pipes (with bifurcating connections) and the airflow, especially in small airways, is typically laminar, an analytical solution of gravitational deposition of particles from laminar flows in a horizontal pipe of diameter L_{dia} is a useful benchmark[108,256] for the role played by particle size (d_p) in gravitational deposition. In these works, a deposition efficiency, DE, is defined by Fuchs (1964), and is found to be related to a single dimensionless parameter $\varepsilon = 3V_gL/4L_{dia}\bar{V}$ that incorporates the effect of the terminal settling velocity V_g, through the relationship

$$DE = \frac{2}{\pi}\left[2\varepsilon\sqrt{1-\varepsilon^{2/3}} - \varepsilon^{1/3}\sqrt{1-\varepsilon^{2/3}} + \arcsin\left(\varepsilon^{1/3}\right)\right] \quad (5)$$

We note that V_g is proportional to the square of the particle size for a given density of the particle (see The Motion of Large Particles Under a Gravitational Force Field *Section*), quantifying the importance of particle size for gravitational deposition. Several variations of the above analytical solution exist, such as gravitational deposition in an inclining/declining laminar pipe flow[147,320] and gravitation deposition in an oscillatory laminar pipe flow[186]. Tsuda et al (1994b) and Darquenne & Paiva (1996) applied a similar approach to predict numerically gravitational deposition in an acinar airway to estimate the deposition of micron-size particles in the pulmonary acinus.

It is important to note that although these analytical solutions may be employed as a useful reference point in the study of gravitational deposition of particles in the airways, there are several serious limitations. First, because the respiratory tract is a bifurcating network, solutions valid for long straight channels cannot be directly applied. Deposition boundary layers must be re-established in each airway when airflows enter new generations. Similarly, because each airway duct is angled from the preceding one, the airflow changes direction at each generation. Hence, the flow streamlines in real airways are curvilinear, which is substantially different from the rectilinear case dealt with in straight pipe flow. Although the effects of curvilinearity on gravitational deposition have to be evaluated on a case-by-case basis, Tsuda et al. (1994b) show that gravitational cross-streamline motion near the alveolar opening depends on the coupled effects of curvature of gas streamlines and duct orientation relative to gravity, highlighting the importance of the detailed convective flow pattern for particle motion.

Gravitational deposition from a stationary fluid in randomly oriented cylindrical pipes with identical diameters (L_{dia}) was analyzed by Heyder (1975) to estimate deposition of micron-size particles in the human small airways and the airways of the respiratory zone during breath holding. In particular, gravitational deposition, *DE*, after a breath hold time t_{BH} in a cylindrical pipe whose axis lies at an angle β relative to the horizontal, is given by

$$DE(\gamma,\beta) = 1 - \frac{2}{\pi}\left[\arccos(\gamma\cos\beta) - \gamma\cos\beta\left(1-\gamma^2\cos^2\beta\right)^{1/2}\right. \quad (6)$$

Where $\gamma = V_g\, t_{BH}/L_{dia}$ is the dimensionless sedimentation parameter. Now, for a system of randomly oriented pipes, the differential probability of finding a pipe with inclination angle β in space is $\cos\beta\, d\beta$. Hence, the average deposition for an ensemble of uniformly randomly oriented pipes is given by

$$DE(\gamma) = \int_0^{\pi/2} DE(\gamma, \beta)\cos\beta\, d\beta.$$

The complement to particle deposition *DE* is particle recovery, *RC* = 1 - *DE*, that is, the fraction of particles still airborne after a breath hold maneuver (and that can potentially be exhaled). It is useful to know that the measurement of $RC(\gamma)$ as a function of breath hold time (or the dimensionless sedimentation parameter, γ) can be used to estimate the effective airway diameter (*EAD*) of randomly oriented airways at a certain lung depth, V_{depth}. In fact, this noninvasive method of airway morphometry has long been suggested in the field as a potentially useful lung function test[18,30,197,244,245,267,335]. The measurement of *RC* in the human lung[e.g.,112] shows that *RC* decreases exponentially with time, which is consistent with Heyder's model for $\gamma < 0.6$. An evaluation of the above integral gives an approximate expression for retention as

$$RC(\gamma) = \exp(-4\gamma/\pi) \quad (7)$$

This demonstrates that the slope of the exponential recovery function is determined by the terminal sedimentation velocity of the particles (V_g) and the diameter of the pipes (L_{dia}). The numerical factor $4/\pi$, is consistent with the initial slope of Heyder's model $(dRC/d\gamma)_{\gamma=0}$. This suggests that *RC* is initially dominated by the particle recovery from randomly oriented small airways, where the initial gravitational deposition is expected to occur during a breath hold. Finally, therefore, the effective airway diameter (*EAD*) at lung depth V_{depth} can be estimated from the time derivative of Eq. 7 as,

$$EAD(V_{depth}) = \frac{-4V_g}{\pi\, d(\ln RC)/dt} \quad (8)$$

Diffusional deposition

Diffusion is an important mechanism for the deposition of submicron particles in the small airways and in the pulmonary acinus. Similar to the case discussed above, the theoretical analysis of diffusional deposition in steady laminar pipe flow may provide a useful benchmark in capturing some of the essential physics of diffusional deposition in the presence of flow, although it does not deal with the complex geometry of the actual airway morphology. Particle number concentration, *n*, in a fully-developed laminar pipe flow subject to a radially uniform particle concentration distribution at its inlet can be expressed as the following Graetz series solution[159]

$$n(Gz, r*)=C_1 e^{\lambda_1 Gz} S_1(r*)+C_2 e^{\lambda_2 Gz} S_2(r*)+C_3 e^{\lambda_3 Gz} S_3(r*)+\ldots\ldots \quad (9)$$

where $Gz = x/d\,Pe$ is the Graetz number, which expresses axial distance from the inlet, normalized by pipe diameter d and the particle Péclet number; $r^* = r/d$ is normalized radial position. The coefficients C_i are used to satisfy the entrance conditions; λ_i are eigenvalues corresponding to the radial eigenvectors or modes, $S_i(r^*)$. The first three values of C_i, λ_i and $S_i(r^*)$ (for the case of a uniform inlet concentration) are given in Table 3.

Although the Graetz solution has been re-analyzed and re-reported[e.g.,121,157] and is often used to estimate diffusional deposition in the lung[e.g.,2,85,153,264], its limitations need to be appreciated. First of all, because the respiratory tract is not a simple straight pipe, the direct use of the Graetz solution for the case of lung deposition and issues associated with this crude assumption (e.g. the fixed inlet concentration profile assumption violates the successively changing profile at each bifurcation) can only be taken as giving a qualitative description of the actual deposition. Second, the nature of the Graetz series needs to be carefully analyzed. The physical meaning of the Graetz analysis can be illustrated by examining the numerical analysis performed by Tsuda et al. (1994a). They treated a straight non-alveolated duct, and an alveolated duct modeled as a collection of repeating unit cells. A conditional probability analysis was performed in each unit cell, using Eq. 9 discretized for each unit cell ($x = KL_{cell}$, where L_{cell} is the axial length of the unit cell, and K = 1, 2, …. indexes the cells. The unit-cell-based Graetz solution becomes

$$n(K, r*)=C_1(\bar{\lambda}_1)^K[S_1(r*)]+C_2(\bar{\lambda}_2)^K[S_2(r*)]+C_3(\bar{\lambda}_3)^K[S_3(r*)]+\ldots\ldots \quad (10)$$

Where $\bar{\lambda}_i = \exp(\lambda_i L_{cell}/dPe)$, i = 1, 2, ….. are the unit-cell based eigenvalues corresponding to radial eigenvectors, $S_i(r^*)$. Eq. 10 shows that the particle concentration profile after traversing K unit cells, $n(K, r^*)$, can be written as a weighted sum of eigenfunctions or modes (i.e., shapes of radial distribution). The weights $C_i(\bar{\lambda}_i)^K$ progressively decay as powers of the corresponding eigenvalues, which in turn represent a "survival" rate of each mode per unit cell.

Because all $\bar{\lambda}_i < 1$ (see Table 3), all modes decay. Furthermore, those modes with smaller $\bar{\lambda}$ decay faster. Therefore, the fully developed shape will be given by the eigenfunction corresponding to the maximum eigenvalue $\bar{\lambda}_1$ given in Table 3. In other words, for large K, the first term in Eq. 10 dominates and approximates to $n(K, r^*)$. The deposition process can then be considered to have reached a fully developed (stationary) phase that is independent of the details of the entrance conditions. In this case, the normalized radial concentration profile is proportional to S_1, and the deposition rate per unit cell is given by $1 - \bar{\lambda}_1$.

While the eigensystem analysis demonstrates that as K increases (i.e. proceeding axially past more and more unit cells), the shape of the radial concentration profile approaches S_1 it does not follow that this profile is meaningful. This is because two processes are happening simultaneously. The first is the progression of the radial distribution of particle density toward S_1, which is approached with a rate given by $\bar{\lambda}_2/\bar{\lambda}_1$. The second is that the absolute number of particles itself is decaying with a rate given by $\bar{\lambda}_1$. Thus, there is a race between

the particles' profile approaching fully developed shape and the particles themselves being lost entirely. If $\bar{\lambda_1} > \bar{\lambda_2}/\bar{\lambda_1}$, then particles are lost more slowly than the rate at which the profile approaches stationarity, and one may say that a meaningful stationary phase exists. Conversely, if $\bar{\lambda_1} < \bar{\lambda_2}/\bar{\lambda_1}$, then particles are lost faster than the shape decays to S_1 and the fully developed profile, although mathematically valid, is physically irrelevant, as there are negligible surviving particles conforming to that distribution.

Particle Transport and Deposition in the Respiratory Tract

Equipped with a general understanding of particle behavior gained from the material in previous sections, we are now in a position to discuss particle transport and deposition in the respiratory tract. Particle deposition in the human respiratory tract is most often plotted with respect to particle diameter (see Fig. 6). The family of rather complicated curves in Fig. 6 indicates that while particle size is one of the most important determinants of deposition, other factors are significant, including specific sites within the respiratory tract and level of ventilation from basal to exercise. For instance, total deposition is high at both ends of the size spectrum; above ∼1 μm, gravitational sedimentation and inertial impaction are effective; below ∼0.1 μm, diffusional deposition becomes the major mechanism for deposition.

The curves of regional deposition [extrathoracic (upper airways), bronchial (conducting airways), alveolar (including acinar airways)] show very complicated patterns and are strongly size dependent. This is an indication of the substantial role played by the local airway geometry, the associated fluid mechanics, and the kinetics of the particles in determining particle transport and deposition. The breathing pattern and route (e.g. nose breathing during sleeping or mouth breathing during heavy exercise) also play significant roles[191], highlighting again the influence of the local geometry of the respiratory tract and the associated airflow fluid mechanics. Although both total and regional deposition are low in the medium size range of particles (between 0.1 μm and 1 μm), intrathoracic deposition is still appreciable (considering we breathe ∼20,000 times a day); moreover, many important aerosol particles, such as particulates in cigarette smoke, belong to this medium size category. In what follows, we divide our discussion into three regional areas (upper, conducting, and acinar airways), according to the nature of the anatomy of the respiratory tract and the associated fluid mechanics, and discuss aerosol transport and deposition for each region in detail.

Upper airways

The upper airways comprise the nostrils, nasal cavity, pharynx (throat), and larynx (voice box). As humans naturally breathe through the nose, unless strenuously exercising, we will mainly consider this pathway except for the case of inhalation therapy. We note that many mammals, and newborn human infants, are obligate nose breathers[60].

Geometry and fluid mechanics

The nasal passageway is divided into two roughly symmetrical parts by the septum. Air enters the nostril and is then directed into the nasal cavity via the nasal valve. The flow area

within the nasal airways is at its smallest at the nasal valve and hence it is at this site that the air velocity is at its highest. The geometry of the nasal cavity is characterized by narrow passageways, or meatus, formed by the conchae, or turbinates. There are three turbinates on each side of the septum: the inferior, middle and superior turbinates. The parts of the nasal cavity passageways associated with the three turbinates are termed the inferior, middle and superior meatus. The shape of the cross-sectional area of the turbinates and meatus changes considerably with axial direction. The superior meatus is shorter than the other two and is the site of the olfactory region. Most of the flow passes through the middle and inferior meatus. The airstreams from the nasal cavities turn sharply as they combine in the nasopharynx, the beginning of the throat. The pharynx ends at the triangular opening created by the vocal folds of the larynx. A more detailed description of the anatomy of the nasal cavity is given elsewhere in this Handbook series.

The surface of the nasal cavity is kept moist by the mucus membrane, at body temperature due to the high degree of vascularization, and its area is sufficient to ensure that the air reaching the lower airways is essentially completely saturated and at body temperature. Another function of the nose that is affected by the fluid mechanics in the nasal cavity is that of olfaction. Only a small portion of the flow reaches the olfactory region and the flow velocity in this area is relatively low. Doorly et al. (2008) point out that despite a vast amount of research on nasal cavity flow, it is still unclear whether the flow is laminar, turbulent, or transitional. It would appear that the flow may become unstable at certain locations (for instance, in the vicinity of the middle meatus) but whether these instabilities develop into full turbulence is still an open question[83]. As the air leaves the nasal cavity and enters the pharynx, secondary cross-stream flows are created by the curved nature of the airway. Also, as the back of the tongue forms part of the pharyngeal-airway wall, the flow cross-sectional area in this region is a function of the local pressure. Hence, the possibility exists of airway collapse due to a failure of the relevant muscles to stabilize properly the collapsible part of the airway[262]. The flow leaves the upper airways and enters the trachea though the larynx. The cross-sectional area of the larynx is the smallest in the respiratory tract, and hence the flow velocity is highest here.

Further details of the air-conditioning aspects of the human nasal cavity can be found in Elad et al. (2008). More details of nasal fluid mechanics in general, including an extensive list of in vitro and computational fluid dynamics studies (CFD), are given in Doorly et al. (2008). As in most areas of fluid mechanics, CFD studies of nasal airflow are becoming ever more popular[e.g., 111,204].

Deposition in the upper airway

The hairs in the nostrils, acting as a filter for large particles, are the first line of defense in keeping particulate matter from being drawn into the lungs. The mucus layer and cilia that line the narrow passageways of the nasal cavity also act to trap particles. Particles can reach the mucus layer either by Brownian motion, by their own inertia, or by gravitational settling, depending on their mass and size.

Wang et al. (2009), in a numerical study, found that nano-sized particles were fairly evenly distributed throughout the nasal cavity. Conversely, the majority of micron-sized particles

were deposited near the nasal valve region, but some were deposited on the septum wall in the turbinate region. Also, the deposition patterns of micron-sized particles in the left and right cavities were different, especially in the turbinate region, which shows the influence of small differences in flow geometry for particles in this size range.

The deposition of particles in the olfactory region, particularly those in the nano-size range, has received much attention of late[e.g.,216,238]. This is because particle translocation along the olfactory nerves, which circumvents the blood-brain barrier, is considered to be the shortest and most direct path to the brain. In a recent review, Dhuria et al. (2010) discuss the use of this route for delivering therapeutics directly to the central nervous system.

Many studies[e.g.,17,23,50,107,165,166,281,283] have found that inertial particle deposition increases with particle mean diameter and airflow rate, which can be expressed in terms of the impaction parameter (*IP*): $IP = d_a^2 Q$, where d_a is the particle aerodynamic diameter and Q is the volumetric airflow rate. The aerodynamic diameter is the diameter of a sphere of unit density ($1 g/cm^3$) that has the same gravitational settling velocity as the mean settling velocity of the particle in question. An extensive list of numerical and experimental studies of inertial particle deposition in the nasal cavity can be found in Liu et al. (2010).

Conducting airways

The geometry of the conducting airways is characterized by dichotomous branching. The conducting airways start at the trachea, which feeds the two main stem bronchi; each bronchus feeds a pair of smaller bronchi. The conducting airways end at the terminal bronchioles, which are followed by the transitional bronchioles where alveoli (air sacs) first appear. On average, the terminal bronchioles are located at the fifteenth generation below the trachea (see other chapters by Butler and Tsuda; Verbanck et al.; Tawhai et al.; and Suki et al. in this Handbook series).

Conducting airway flows

In the trachea, the airflow Reynolds number, *Re* (based on the mean flow velocity and airway diameter) is typically less than 2000, which would indicate that the flow is laminar. However, the air actually enters the trachea through the narrow passageway formed by the vocal folds. The sudden narrowing of the airway at the larynx causes the flow to accelerate and enter the trachea as a jet[e.g.,32]. The jet's *Re* is above that which turbulence can be expected. Thus, in the trachea there is a mixture of turbulent, transitional and laminar flow. Kamm et al. (1986) found that the influence of an oscillating turbulent jet was felt for up to 20 diameters downstream of the jet orifice, a distance much larger than the length of the trachea. Li & Ahmadi (1995) and Lin et al. (2007), among others, confirmed, through numerical simulation, that the influence of the laryngeal jet reaches down to the main stem bronchi. As *Re* is relatively high in the conducting airways; i.e., inertia dominates the flow process, the flow velocity profile is not parabolic at the entrance to each daughter duct. The bifurcating nature of the conducting airways promotes secondary, Dean-type, flows due to the change in direction from parent to daughter ducts. It should be pointed out that the flow profile in the region of the bifurcation is different for inspiration and expiration and this has been shown to produce enhanced axial dispersion in dye tracer clouds[271]. A survey of recent

flow studies in conducting airways can be found in Kleinstreuer and Zhang (2010). Also, in another section of this handbook, Tawhai et al. (2010) discuss in detail the mechanics of gas flow in the respiratory system.

Deposition in the conducting airways

In the first few generations of the conducting airways, where the airflow is likely to be turbulent (see above), particle deposition from turbulent flows needs to be considered. As mentioned in the Turbulent Deposition Section, a group led by G. Ahmadi performed a series of studies describing the behavior of aerosols in turbulent flow[e.g.48,289,337]; these studies are highly relevant to the understanding of particle deposition in the portion of the conducting airways They found that the deposition rate of particles in turbulent pipe flow followed a curve similar to Fig. 6. That is, deposition increased with an increase in particle size, for large particles, and also increased with a decrease in particle size, for smaller particles. Readers interested in more detail can consult the recent work of Guha (2008) in which he reviews the state of the art on transport and deposition of particles in turbulent and laminar flow.

Due to inertial effects, micron-sized particles tend to deposit in the conducting airways due to impaction, particularly at the site of the carinal ridges of the bifurcations. The first systematic experimental work on deposition in the bifurcating airways was reported by Kim and his group for both inspiratory and expiratory flow in single bifurcation tube models[171,172]. They studied the effects of branching angle, asymmetry of branching pattern and flow division on deposition. Later, they extended their experimental study for a three generation sequentially branching airway model and showed that the effects of upstream flow patterns on deposition in the downstream generations[176]. These results have been used extensively to validate mathematical and CFD models for aerosol transport in the conducting airways. Recently, Balásházy et al. (2003), for instance, proposed a local deposition-enhancement factor to demonstrate preferential sites of particle deposition at the bifurcation carina. In addition, particles are also brought close to, and deposit on, the airway surface in the entrance regions of the daughter ducts due to the secondary flows[e.g.,158]. Thus micron-sized particles are heterogeneously deposited on the surface of the airways[e.g.,173,175,177,179,232,317]. Bennett and Brown (2005) suggested that the number of particles deposited per unit surface area (i.e., deposition density) might be an important parameter in terms of cell response. Deposition density is generally much higher in the conducting airways than that in the parenchyma, although the total number of particles deposited is much smaller in the conducting airways than in the parenchyma. Kim and his group measured surface dose in the airways vs. the alveolar region in human subjects using a bolus aerosol delivery method for micron-sized particles[173,175] and for ultrafine particles[178]. Detailed mathematical analysis of regional airway deposition and surface dose has been reported for various inhalation conditions with different size particles and breathing patterns[51]. For nano-sized particles, Zhang et al. (2005) demonstrated that deposition tends to be more evenly distributed over the airway compared to the case of micron-sized particles, but higher surface concentration were still found in the bifurcation regions. A more detailed discussion of deposition in the conducting airways can be found in Kleinstreuer and Zhang (2010).

The experimental study of aerosol deposition along the conducting airways is generally difficult for two reasons. 1) Unless a very careful shallow breathing technique is employed, it is extremely difficult to restrict deposition to just the conducting airways because the volume of the conducting airways (i.e., anatomical dead space) is small[e.g.,19,189,226,336]. Most inhaled particles quickly enter the lung parenchyma; this makes it difficult to distinguish particle deposition in the conducting airways from that in the parenchyma in, for instance, three-dimensional tomographic imaging. 2) The extent of asymmetry is large in the conducting airways[e.g.,226]; this makes analyses difficult on an airway generation basis. Despite these difficulties, three-dimensional visualization of particle deposition and retention in the conducting airways is probably one of the most instructive experimental approaches, and therefore often attempted by performing radionuclide imaging[e.g.,100,101,272]. Two types of 3D tomographic imaging are frequently performed; they are single photon emission computer tomography (SPECT) and positron emission tomography (PET), where technetium-99m and fluorine-18 or carbon-11 are commonly used as radiotracers, respectively. A rough estimation of regional deposition, such as central vs. peripheral lung, may be possible from the obtained 3D tomographic data[e.g.,254]. Combining magnetic resonance imaging (MRI), which does not pose an additional radiation burden, anatomical information together with particle deposition may be obtained[e.g.,98,99]. The distribution of particle deposition along the conducting airways in diseased lungs is different from that in healthy lungs (discussed more in Particle Deposition in the Diseased Lung). This difference has important implications not only for the etiology of air pollutant effects but also for the optimization of inhalation therapeutic strategies and, not surprisingly, a considerable body of research has been devoted to this topic[e.g.,21,91,96,173,177,180,225,265,268,272].

Finally, it is worth noting that most of the current understanding of the detailed distribution of particle deposition in the conducting airways comes from numerical predictions. Such studies use powerful CFD software and are often combined with realistic airways model obtained from MRI or CT images. Nonetheless, even today's robust CFD codes are not perfect. By their nature, CFD solutions are approximate. How well the prediction agrees with the exact solution is a function of grid density, among other things. However, multi-generational airway models require large grids and adequate grid refinement may not always be possible. Also, further approximation is required when the flow under consideration is turbulent or in transition (from laminar to turbulent flow, or vice versa). There is today no complete theory of turbulence (or transition) and all current turbulence models have their deficiencies. Thus, predictions of flow and deposition in the trachea and main bronchi are particularly difficult, due to the need to model adequately the turbulent laryngeal jet. Thus, results from such predictions should be viewed with some caution. Another potential problem area is the specification of boundary conditions. This is particularly true of the distal end of the model over exhalation; i.e., it is not clear how the flow and particle transport distal of the conducting airways should be taken into account. At the proximal end, it is imperative that the laryngeal jet is modeled accurately. For instance, Xi et al. (2008) showed that including the laryngeal jet in deposition computations reduced the deposition at the main carina. Nevertheless, only one turbulence model was used in this study and hence the effects of the approximations used in the turbulence model on the predicted distributions are unknown. On the influence of turbulence models, Parker et al. (2008), in simulating

particle transport in turbulent pipe flow; that is, a much simpler flow than considered here, found that certain types of turbulence models were generally unsuitable for aerosol deposition simulations.

Pulmonary acinus

More than 90% of the lung volume belongs to the region for gas exchange known as the pulmonary acinus. As noted above in Fig. 6, the majority of fine and ultrafine particles manage to pass through the nasopharynx and conducting airways, successfully penetrate deep into the lungs and, potentially, deposit in the acinus. The rate of particle deposition is not constant throughout the acinus because the flow pattern changes considerably from the acinar entrance to its termination. The change in flow pattern is a result of a combination of the unique geometry of the acinus and associated acinar fluid mechanics. Also, particles of different sizes have different deposition distribution patterns because a particle's intrinsic motion due to inertia, gravitational sedimentation, and diffusion is largely governed by its size. We begin this section with a discussion of acinar geometry.

Acinar geometry

Because the major task of the lung is gas exchange, the pulmonary acinus is the dominant portion of the lung and the air channels in this region of the lung are alveolated, where gas exchange with the blood takes place. The pulmonary acinus is defined to start from the airway on which the first alveolus appears[323]. The first portion of the acinus, just beyond the terminal bronchioles, forms the transitional zone between the conducting airways and the gas exchange region. In humans and primates, the transitional zone consists of a few generations of partially alveolated ducts called respiratory bronchioles, while in rodents the transition from terminal bronchioli to the gas exchange region is more abrupt with, at most, one generation of partially alveolated bronchioles[16,266,316]. Because of the abrupt increase in the cross-sectional area of the airways in this region of the acinus, there is a sudden change in fluid mechanics; the particle-laden airflow rapidly decelerates and becomes dominated by viscous forces. As we will describe in detail below, chaotic mixing is expected to be most effective in this region[145,269,310,314] and this has important implications for particle deposition in this region.

Deeper into the acinus, beyond the respiratory bronchioles, the air channels are fully alveolated. According to Haefeli-Bleuer and Weibel (1988), there are, on average, six more generations of airways beyond the transitional zone. These units of the pulmonary zone are called subacini. The volume of each acinus, of which most of the volume belongs to the subacini, is on average about 187mm^3 at total lung capacity (TLC). There are roughly 30,000 acini in the human lung with over 10,000 alveoli in each acinus[131]. According to Haefeli-Bleuer and Weibel's measurements, the diameter of the central channel in the human acinus falls from 500 μm to 270 μm, and the depth and width of a typical alveolus is approximately 250 μm. Thus, the characteristic length scale of the human alveolus is a few hundred microns. The longitudinal path length of the acinus (i.e., the distance along the ducts from the transitional bronchiole to the alveolar sacs) averages 8.8 mm. These are important dimensions to keep in mind when considering aerosol transport and deposition. For instance, over one breathing cycle, a 0.1 μm particle travels a distance equivalent to only

a small fraction of the alveolar depth by its own diffusive intrinsic motion. This highlights a remarkable difference between the behavior of aerosol particles and that of highly diffusive respiratory gas molecules in the pulmonary acinus (see "Transport of gases between the environment and alveoli – theoretical considerations" chapter in this handbook series[39]. More details and comprehensive discussion of acinar geometry can be found elsewhere in the handbook chapter.

Several groups have used rigid-walled, alveolated-duct, CFD models to study aerosol transport[e.g.,63,64,307,308]. All such geometric models consist of a central channel and surrounding dead-end air pockets (see Fig. 7 *middle* for example). While these are highly simplified models, they capture one of the most essential features of acinar flow; namely, a relatively strong central channel flow passing by numerous terminating side pockets, or alveoli, in which the flow is almost quiescent but slowly rotating. These models were used to illustrate the importance of alveolated geometry on acinar fluid mechanics and consequently on aerosol deposition therein. However, it must be noted that these rigid-walled models do not have the other essential feature of alveolar airways; namely, the rhythmical expansion and contraction of the whole alveolated structure associated with tidal breathing.

The first alveolated duct CFD model with non-rigid walls for studying aerosol transport was developed by Tsuda et al. (1995). The geometry of the alveolated duct was the same as the original alveolated shape[308,309] but in this model the walls expanded and contracted in a sinusoidal manner, with 25% volume excursion. Although there is a view that the size of the alveoli does not change significantly during the breathing period, and that the expansion of the ducts essentially accounts for the tidal volume[e.g.,181,286], a majority of the available experimental evidence shows that during normal breathing, alveoli and alveolar ducts expand and contract in a manner roughly consistent with geometric similarity, namely all dimensions, apart from septal thickness, scale approximately as the 1/3 power of lung volume[3,117,118,222,324]. A 3D alveolated duct model with moving walls was created by Haber et al., (2000, 2003) (Fig. 7 right). Recently, several new 3D alveolar models with moving walls have been developed[10,25,62,65,192,193,201,298].

It has also been recognized that, due to space-filling considerations, alveoli cannot be spherical despite the fact that the truncated sphere is the most commonly used model geometry. Fung (1988) was among the first to propose a space filling structure, constructed from order-2 polyhedra, which matched reasonably well the available morphometric data. In a series of articles, Denny and Schroter (1995, 2000, 2006) used a similar model and finite element analysis to study the mechanical properties of the acinar parenchyma. The flow models of Sznitman et al. (2009) and Kumer et al. (2009, 2011) also use similar space-filling model geometries. However, there is some evidence that the precise shape of the alveolus does not affect greatly the resulting flow and transport in the alveolus[145].

Recently, a finite element-based realistic 3D model of the pulmonary acinus, which can be readily used for subsequent computational analyses; such as fluid dynamics, has been constructed by Tsuda et al. (2008a). Stereologically well-characterized rat lung samples[305] were imaged using high-resolution synchrotron radiation-based X-ray tomographic

microscopy (TOMCAT, Swiss Light Source, Paul Scherrer Institut, Villigen, Switzerland). A stack of 1,024 images (each slice: 1024 × 1024 pixels) with resolution of 1.4 μm^3 per voxel were generated and a part of the acinus was reconstructed after 3D rendering with appropriate segmentation (Fig. 8). Using the 3D finite element shell concept, the air-tissue boundary can be reconstructed (Fig. 9). Once the acinus (or alveoli) is reconstructed in 3D, the target region (e.g., an alveolus) can be viewed from any arbitrary angle (see Fig. 9, *middle*), including from behind the object (Fig. 9, *middle right*), something not easily achievable otherwise. The 3D object can be cut into half (Fig. 9, bottom) and also be sliced to make 2D sections in any orientation with any slab thickness (not shown here) and there is no limitation to the number of times the sectioning process can be repeated. Furthermore, since the target region can be viewed in any chosen angle and an internal view is possible, it is possible to fly through the structure to gain an internal view of the conduit once the 3D reconstructed structure is electronically available.

Acinar fluid mechanics

In the study of acinar fluid mechanics, there are several remarkable features of the lung that need to be considered. First, the rapid increase of the total cross-sectional area of the airways along the bronchial tree leads to a sharp decrease in linear air velocity with each generation. Therefore, under normal breathing conditions, the Reynolds number (*Re*) of acinar airflow (based on duct diameter) is usually much less than unity (see Table 2); airflow momentum is largely governed by the interaction of pressure drops and viscous forces in the alveolated region of the lungs. There is only one entry/exit pathway (i.e., the trachea) through which air enters and leaves the lung, and at the level of the acinus, the same ducts are used for both inhalation and exhalation. This means that at the end of each half breathing cycle the airflow has to come to a stop and reverse. A significant amount of air generally remains in the lung at the end of exhalation. The reversing nature of the airflow and the appreciable amount of residual air in the lung implies that for acinar aerosol deposition to occur the particle-laden incoming airflow needs to mix with residual air in the viscous flow regime.

However, due to the classical idea of "reversibility" of viscous flow[66,302], the possibility of flow-induced mixing in the acinus had been theoretically excluded; it had been long considered that airflow in the gas exchange region of the lung was simple and perfectly kinematically reversible[68,322]. Based on this line of thought, therefore, it had been considered that mixing between tidal air and alveolar residual air must be solely due to intrinsic motion of particles, such as diffusion or inertia/gravitation-mediated cross-streamline motion[68]. However, Heyder et al.'s seminal work (1988) showed that unlike respiratory gas molecules (e.g., O_2 or CO_2), the intrinsic motion of aerosol particles is much too small to account for acinar mixing observed in their bolus experiments (Fig. 10). With these two opposing views, therefore, until the mid-1990s', there was a significant gap between the theoretical understanding of aerosol mixing in the pulmonary acinus[e.g.,66,68,322] based on rigorous classical fluid mechanics theory[e.g.,302] and experimental observations[e.g.,149,275].

In 1995, Tsuda et al. (1995) challenged the classical theoretical view by demonstrating that acinar flow, even though it is basically viscous in nature, can be complex; in particular, it

can be chaotic due to the unique features of the alveolar flow structure. This theoretical finding of a new phenomenon furthermore yields that chaotic acinar flow can lead to substantial kinematically irreversibility, consistent with experimental observations. The essential feature of the flow structure, which allows acinar flow to be chaotic, is the occurrence of rotational flow inside the alveolar cavity (Fig. 11). This will be explained in detail in what follows.

Origin of chaos—When the ductal flow passing by an alveolar opening is sufficiently strong, the flow within the alveolar cavity forms a large recirculation region (Fig. 11), characterized by a spectrum of frequencies (f_1), of purely fluid mechanical origin. By contrast, there is an externally imposed frequency of breathing (f_2) determined by the central nervous system and the consequent action of the respiratory pump muscles, both diaphragmatic and intercostal.

It is important to note that the alveolar recirculation frequency spectrum is *intrinsic* to the system, dependent on the depth/shape of the alveolus, the aperture size of alveolar opening, and the strength of the duct flow; it represents a family of frequencies dependent on the location in the alveolar cavity relative to the center of the recirculation (Fig. 11 *top left*). For instance, the recirculation frequency f_1 will be relatively small on orbits that lie very close to the alveolar wall, where the flow is slow; the frequency f_1 is greater closer to the center of the alveoli, where the flow is faster and the orbit length is shorter. The interplay between the fluid dynamical spectrum and the external breathing cycle is a critical determinant of the onset, location of, and consequences of recirculation-induced mixing and potential chaos.

The behavior of a particle depends on the interaction of the fluid dynamical spectrum, characterized by intrinsic frequency f_1 of an individual recirculation path and the breathing frequency f_2. In particular, when the two frequencies are resonant (i.e. between that of a particular alveolar recirculation orbit and the breathing cycle), there is the potential that chaos can ensue, and thus, particles in the acinus may behave chaotically. In other words, the ratio f_1 / f_2 dictates whether or not, and where a particle will follow a chaotic path [Fig. 12, also see Tsuda, Laine-Pearson & Hydon (2011)].

A crucial factor required to trigger chaos is that the system needs to be perturbed, even infinitesimally. Contrary to kinematically reversible idealized alveolar flow systems, as suggested in the past[68] –referred to as a strictly “unperturbed system” (Fig. 12 left), in the more realistic situation of cyclically expanding and contracting lungs there are many sources of perturbations (Fig. 12 right), including non-zero Reynolds number effects[143,144,310], small but persistent geometric hysteresis[125,127,222] and wall movement[143,196,310]. These observations strongly suggest that chaos is likely to be present in real lungs.

Chaotic flow in the acinus—When air flow in an alveolus contains rotational components (Fig. 13 *Left*), computer simulations show that the Poincaré map (i.e., location of a fluid particle at the beginning of every cycle) exhibits highly complex chaotic patterns (Fig. 13 *Right*). It is noted that the critical flow feature here is the occurrence of alveolar recirculating flow; chaotic mixing can occur regardless of whether alveolar walls are moving[125,143,310] (Fig. 12) or stationary[144] (Fig. 14).

The intensity of chaotic mixing depends on the strength of the recirculation in the alveoli. Hence, chaotic mixing is most effective where the alveolar flow is most vigorously rotating. Tsuda et al. (1995) have shown that the feature of flow patterns in the individual alveoli, whether or not the flow rotates in an alveolus, is largely determined by the ratio Q_A/Q_D, where Q_A is the flow entering the alveolus and Q_D is the flow passing by the alveolar opening. The parameter (Q_A/Q_D) depends on the location of the alveolus within the acinar airway tree. Since Q_A is roughly constant throughout the acinus due to approximate geometric similarity in alveolar expansion, the value of this parameter depends largely on the value of Q_D. At any local site in the acinar tree, Q_D is proportional to the time rate of change of parenchymal air volume distal to that site. The strength of recirculation[310] increases with decreasing Q_A/Q_D; i.e., recirculation flow within the alveolar cavity (Fig. 11) is strongest at the acinar entrance. Hence, chaotic mixing is expected to be most effective in this region.

Furthermore, because the lung expands and contracts roughly in a geometrically similar fashion[3,117,118,222,324], Q_A/Q_D is simply a function of lung geometry. Specifically, Q_A/Q_D is equal to the ratio, V_A/V_D, where V_A is the volume of the alveolus at a particular site and V_D is gas volume distal to that site. Finally, it should be noted that *Re* and Q_A/Q_D are both functions of V_D, and are thus linked through V_D. However, *Re* has little effect on the flow in the alveolus, as it is predominately Stokes flow. Conversely, the flow structure occurring in the alveolus is almost exclusively controlled by the value of Q_A/Q_D.

Visualization of chaotic flow—To demonstrate experimentally how inhaled tidal air and residual alveolar gas kinematically interact, Tsuda et al. (2002) developed a new flow visualization technique. They ventilated excised rat lungs with ultra-low viscosity polymerizable fluids of two colors [one color (blue) representing tidal fluid, and the other (white) the residual fluid] under very low Reynolds number flow conditions. Ventilation was halted at predetermined time points in the ventilatory cycle, allowing the fluids to polymerize. The detailed convective flow patterns were preserved in the casts; these patterns were examined on lung sections by light microscopy.

After only one breathing cycle, remarkably complicated stirring patterns emerged on transverse cross-sections of the airways (Fig. 15). Stretch-and-fold patterns – a hallmark of chaos[4,243,300] – of the two-color interface were observed throughout many airway generations. Spatial correlation analysis performed on the patterns of transverse cross-sectional images further revealed 1) these observed stretch-and-fold patterns were fractal with a fractal dimension of 1.1; 2) the fractal nature of these mixing patterns was invariant throughout the tracheobronchial tree.

These findings may be interpreted as follows. During inspiration, as the lungs expand, the front of the tidal fluid also expands, and by the end of the inspiration the tidal front is enormously stretched, entering multiple pathways (2^{23} distal acinar ducts for human lungs[323]), sampling millions of alveolar spaces. Note that there exist numerous recirculations within the alveoli (Fig. 11 bottom). During expiration, the stretched tidal front contracts, approximating the contraction of the lungs and merging into the single trachea. However, because the acinar flow is not exactly kinematically

reversible[38,65,125,143,192,193,304,310,311], each fluid element does not retrace its original inspiratory path, but rather ends up at a location which can be substantially different from its initial position. The presence of recirculation (Fig. 11) implies that alveolar flow can produce chaotic dynamics when it is perturbed (see Fig. 12-14). It is well known that the iteration of chaotic trajectories is often manifested in fractal geometries[215,291], consistent with the observations (Fig. 15). Importantly, the fact that the observed fractal patterns persist over many airway generations with nearly the same fractal dimension suggests that this mixing originates deep in the lung rather than in the central airways.

To quantify the extent of mixing in the acini, Tsuda et al. (2002) also examined the time evolution of mixing patterns on transverse cross-sections of acinar airways. After one cycle (N =1, Fig. 16), most of the acinar airways appeared predominantly white, with microscopic traces of blue. After 2 or 3 cycles, however, a large amount of tidal (blue) fluid appeared on the cross-sectional images (N =2,3, Fig. 16), indicating that substantial net axial transport had occurred along the bronchial-acinar tree. The cross-sectional images of acinar airways showed clearly delineated interface patterns with both blue and white fluids being stretched and folded. After 4 cycles, the clarity of the interface patterns had largely disappeared, and the previously clear blue/white patterns changed into smeared and mixed bluish-white uniformity (N =4, Fig. 16).

It is important to note that this temporal evolution of convection patterns is fundamentally different from that predicted by the classical theory based on kinematically reversible fluid flow. To illustrate the importance of this observation in terms of aerosol transport and deposition, let us consider the following experiment. Suppose there are two systems: one is a kinematically reversible system (Fig. 17, left panel) and the other is a system with stretch-and-fold convection (Fig. 17, right panel). Now, a Brownian tracer is introduced into both systems, and the evolution of relevant diffusive and convective length scales is tracked in both systems. In the kinematically reversible system, there is no net convective transport; mixing is therefore characterized by a diffusion distance δ, which increases with time t very slowly, typically like $\sqrt{Dt}$, where D is the tracer diffusivity (Fig. 17, middle left panels). Significant mixing only occurs when δ, becomes of the order of L, the fixed system size, which in our case is a typical alveolar dimension (a few hundred microns (Weibel, 1986)). For fine aerosol particles, this process would be extremely slow (Fig. 17, bottom left panel) because of the low diffusivities of the fine aerosols. By contrast, in the system with stretch-and-fold convection, the two processes, diffusion and convection, interact. First, the diffusion length scale δ, initially increases as $\sqrt{Dt}$, but asymptotically reaches a constant value of $\sqrt{D/\alpha}$, where α is the stretching rate. Importantly, however, the length scale over which diffusion must operate to effect mixing is no longer fixed at the system size L, but due to convective folding, decreases exponentially with cycle number N, expressed as f^{-N}, where f is a characteristic cycle-by-cycle folding factor (Fig. 17, middle right panel). In this interaction, mixing is initially very slow, but suddenly increases after a few cycles when the rapidly decreasing folded scales Lf^{-N} become comparable to the asymptotically constant value of diffusion length scale δ (Fig. 17, bottom right panel). This phenomenon –a sudden increase in mixing which can be described by an equivalent entropy burst[38] – is a characteristic feature of chaotic mixing[4,243,300], and is quantified by the folding factor, f.

To determine the folding factor in real acini, Tsuda et al. (2002) performed two-dimensional spectra analysis on mixing patterns of approximately 50 acinar airways for each of *N*=1, 2, 3, and 4. They obtained the folding factor, *f*, of 2.3 This means that the length scales over which the complexity of the convective flow patterns is evolving are decreased by more than half at every breath, and the complexity of the pattern itself more than doubles at each breath. This is a fundamentally different process from those described in past based on the classical kinematically reversible acinar flow theory. This is an exponentiating phenomenon, which in consequence implies that only a modest number of breaths are required to ensure that the mixing lengths become sufficiently small for true diffusive and irreversible mixing to take place, even for very low diffusible aerosols.

Particle Deposition in the Pulmonary Acinus

There is no doubt that a majority of fine particles (e.g., $PM_{2.5}$, particulate matter of size less than 2.5 micron) deposit deep in the lung[79,82,115,153,312] Such particles have negligible inertia when inhaled in slow, deep breaths; thus they pass through the nasal/conducting airways without depositing and penetrate deep into the acinus[29]. If there is vigorous mixing between the particle-laden tidal airflow and the alveolar residual air, and sufficient time for deposition, then a significant portion of the particles are likely to deposit in the acinus. [The counter example is that large, heavy particles inhaled in rapid, shallow breaths (e.g., panting) would deposit in the large airways and at airway bifurcations.]

While it is well known that fine particles deposit in the lung periphery, the details of their distribution pattern along the acinus is less well known. This is because the acinus is in general hard to access, and even if this were not true, it would be difficult to pinpoint the deposition site within the complex, tortuous structure of the acinar tree. However, using a combination of elaborate tissue sampling and tissue histology, Pinkerton et al. (2000) visualized deposition patterns along the airway paths from the trachea down to the acinus in human autopsy specimens. Although they found little evidence of particle deposition in the larger conducting airways (generations 2–6), they observed great accumulations of particles in the acinus, especially in the entrance region (the highest retention in the first, second, and third respiratory bronchioles in that order). In fact, it has been repeatedly demonstrated that the proximal area of the acinus –a few generations beyond the terminal bronchioles -- is the primary site of lung injury after exposure to airborne pollutants[54,58,59,122,138,182,236,257,269,329]. Churg and Brauer (2000) reported that long-term accumulation of submicron-size particles were found at the entrance of the acinus, at typically 25-100 times higher concentrations than in the main stem bronchi. Lung tissues in the transitional zone are likely to respond to particle insults in a more complex fashion than in other parts of the lung because bronchiolar and alveolar epithelial cells interdigitate in this zone[258,259] and are of different phenotypes.

The heterogeneous distribution of particle deposition observed experimentally in the level of the entire acinar tree is likely a result of the change in alveolar flow patterns along the acinus. The preferentially high deposition in the proximal region of the acinus, which forms the transitional zone between the conducting airways and the gas exchange region, can be predicted by the chaotic mixing theory described above. In the last few years, attempts have

been made to combine experimental and numerical analyses. To this end, Haberthür et al. (2010) recently developed a wide field scanning protocol for the synchrotron radiation-based X-ray tomographic microscope, and using this, succeeded in imaging and reconstructing a section of rat lung parenchyma containing 2-3 acini in 3D at a voxel size of 1.48 micron. This protocol will enhance the size of previous computational analyses of acinar flow and particle kinetics in a realistic 3D acinar tree geometry (see *Top Middle & Right* panels of Fig. 10) using a combination of skeletonization techniques[129] and a finite element-based 3D modeling technique[313].

The distribution of particle deposition within an alveolus was measured by Zeltner et al., (1991). They found that in the hamster lung, particles tended to deposit at the alveolar septa tips but that, later, particles moved from the septa tips to the interior of the alveoli. While the redistribution of particles after deposition is not within the scope of this chapter, the observation of initial deposition site, which is consistent with early finding[31], is highly relevant here. First, it should be noted that, unlike the conducting airways, the acinar ducts have no discernable wall; rather, the ducts are formed by a collection of septal tips (see Fig. 7 left). Second, particle-laden tidal bulk airflow (Q_D) travels through the central channel, and the flow entering each alveolus (Q_A) comes from a thin annular area of the central bulk flow coincident with the acinar wall. Third, the fluid that enters the alveolus passes very close to the proximal tip of the alveolar opening, and flow between the central duct and an expanding (or contracting) alveolus occurs through a narrow channel near the distal end of the alveolar opening[145]. The preferentially high deposition at the tip of the alveolar septa found experimentally can be explained by these three facts. This preferential deposition may have biological consequence. The tips of the alveolar septa form the entrance rings of the alveolar duct and are rich with contractile elements[76,324]. This morphological arrangement might be strategically important in keeping the optimal shape and size of the alveolus in response to biological demand[104,187,327]. The preferential deposition of particles on the alveolar entrance rings might tip the balance of biological homeostasis (e.g., equilibrium of the gas-liquid interface). In this regard, the total amount of particles deposited, as well as the deposition density (i.e., surface dose) is likely to be important. Many computational flow models with expanding-and-contracting alveolar walls predict this highly heterogeneous initial particle deposition within an alveolus[65,125,126,143,192,310].

Special Issues

We have so far discussed the essential properties and physics of aerosol particles, as well as the general principles underlying their transport and deposition in the lung. In this penultimate section, we will discuss some more specific topics of particle deposition in the lung relevant to respiratory physiology.

Particle deposition in the postnatal developing (infant) lung

From birth to adulthood, human lungs undergo dramatic structural changes, not only in size, but also in the internal architecture of the acinus. At birth, the acinus consists of wide and smooth-walled saccular airspaces (Fig. 18 *upper left*). Rapid structural alveolation takes place in the first few years after birth, followed by a slow and gradual increase in alveolar size that ends in late childhood. Detailed analyses on the postnatal changes of parenchymal

ultrastructure, which have been performed in rats[33-36], show that the rapid structural alveolation in early postnatal development is achieved by the formation of *new septa* (denoted *secondary septa*) from shallow indentations (denoted *primary septa*) lining the saccules and transitory ducts present at birth. When bulk alveolation wanes, lung development enters the stage of microvasculature remodeling and septal thinning (several months to 2-3 years in humans)[332,333]. After the completion of microvascular maturation and septal thinning (Fig. 18 *upper right*), the shape of the alveoli and the structure of the acinus resemble those of the adult lung but at a smaller scale [after ∼3 years in humans[332,333]]. The lung volume also rapidly increases during this period. There is no doubt that structural alveolation is a major event during postnatal lung development.

The pattern of breathing (tidal volume, breathing frequency) is another major determinant of particle deposition, and both tidal volume and breathing frequency in the postnatal developing lungs are different from those in adults[229]. According to Mortola's allometric power-law expression, tidal volume and breathing frequency are scaled as the 1.01 and -0.09 power of body mass, respectively, during postnatal lung development. This is because the metabolic rate (reflected in O_2 consumption and CO_2 production) per body weight in children is generally higher than that in adults, which is reflected in higher minute ventilation (the product of tidal volume and breathing frequency) per body weight in children than in adults.

Because the aerosol deposition process is strongly dependent on acinar duct geometry and breathing pattern, and the lung structure and breathing pattern are dramatically changing during the different stages of postnatal development, transport and deposition (the amount and its distribution) of inhaled particles must be commensurately age-dependent. Based on current knowledge, we can predict the following. As the acinar airways are wide, relatively smooth, and saccular in the newborn, we can expect that the inhaled air enters the acinar airways along axial pathways like a narrow tongue. This is because the viscous nature of the flow retards the air near the walls but leaves the air near the center line of the ducts relatively unhindered. Hence, the residual air forms an annular barrier between the particle-laden air and the acinar surface. As the airways are relatively smooth, we expect that the incoming air travels to the periphery relatively undisturbed. This leads to a situation in which particle deposition in the newborn acinus occurs at a relatively low rate but uniformly over the entire acinar tree. As the acinus develops, secondary septa grow and alveoli are formed (Fig. 18, right, top). At some point in this development, Q_A/Q_D starts to play an important role in determining alveolar flow patterns. Specifically, when the alveoli become sufficiently deep the flow starts to rotate; particularly, in alveoli in the entrance region, where Q_A/Q_D is lowest (Fig. 18, right, bottom)[144,145,310,314] Rotational flow enhances particle deposition through the generation of chaotic mixing: the more energetic the rotational flow the more deposition. Hence, deposition would be enhanced more in the proximal region, where the rotation is the strongest. By contrast, alveolar flow in the distal alveoli is largely radial and without rotation due to a large Q_A/Q_D ratio (Fig. 18, right, bottom), resulting in reduced deposition. This leads to the situation that as the acinus becomes alveolated, the distribution of particle deposition would become heterogeneous with preferentially higher deposition in the entrance region of the acinus.

Overall, it is thus clear that the developing lung is not simply a miniature version of the adult lung, neither in structure (e.g. airway wall geometry) nor in functions (e.g. breathing pattern). Therefore a simple application of linear extrapolation of adult exposure/dose relationships to infants based on body mass ratio alone would lead to an incorrect prediction of particle deposition in infants. Changes in lung anatomy and breathing patterns associated with growth and development need to be critically considered when assessing particle exposure/dose in infants[279]. Finally, note that particle transport and deposition phenomena in young children (i.e., no infants) are discussed in many other papers, such as Foos et al. (2008).

Particle deposition in the diseased lung

Lung diseases that affect particle deposition can be grouped into two broad categories: those affecting the conducting airways; such as asthma and chronic bronchitis; and those affecting acinar septa; such as emphysema and pulmonary fibrosis. However, co-morbidities are common. One example, presenting particularly in smokers, is chronic obstructive pulmonary disease (COPD), which is a variable mixture of chronic bronchitis and emphysema. Many lung diseases are either caused, or exacerbated, by inhaling airborne particulate matter such as cigarette smoke. In 2006, it was estimated that in the United States alone there were nearly 23 million cases of asthma and over 12 million cases of COPD (CDC, 2006).

Asthma and chronic bronchitis are characterized by inflammation and narrowing of the bronchial airways. In most cases, therapeutics for alleviating the symptoms of these diseases are administered in the form of inhaled aerosolized particles. It can be expected that the characteristics of the flow and particle transport in the affected airways will be different from those in the healthy lung. For example, narrowing of the airways will tend to produce higher flow velocities, which in turn will lead to enhanced inertial deposition of particles at bifurcations, due to impaction. Further, the narrowed airways will restrict the amount of particle-laden air that can reach the acinus. Experimental evidence of how the pattern of aerosol deposition in the lung is affected by asthma as well as by chronic bronchitis has been reported both in a rodent model[297] and in human subjects [e.g.,20,24,199]. Kim & Kang (1997) showed that particle deposition is greater in patients with obstructive airways disease such as asthma and COPD. As the degree of airways obstruction increases, particle deposition also increases in almost a linear fashion and the deposition pattern becomes more heterogeneous, revealing hot spots with remarkably high local dose levels. This is an important aspect of lung deposition in patients with obstructive airways disease. A group led by Kim also studied aerosol deposition in large animals (e.g., sheep and dogs) by challenging bronchoconstricting agents in different fashions. Specifically, they used IV infusion or aerosol challenge to the whole lung or the partial lung and reported that deposition was increased in the obstructed lungs but the degree of increase was variable, depending on the type of obstructions induced[167,170]. Kim and his group also investigated the effects of excessive mucus on airflow and aerosol transport. They reported that the mucus layer in the airways may not always present as a static layer but can exhibit wave motion for certain combinations of airflow velocity and mucus viscoelasticity; this is a classic gas-liquid interaction, which can cause a marked increase in aerosol deposition[168,169]. Harkema et al. (2004) studied a rat model of human asthma and chronic bronchitis and found that particles

were preferentially retained in allergic airways. Further, Venegas et al. (2005) showed that in asthmatic lungs there can exist clusters of severely restricted terminal bronchioles alongside areas in which the terminal bronchioles exhibit normal flows. They note that this could lead to reduced effectiveness of inhaled bronchodilators as the areas of the lung that need the therapeutic effect of these drugs most are the least likely to receive it. In fact, as they also note, preferentially dilating the already well-ventilated areas of the lung could actually exacerbate the situation.

COPD sufferers usually have reduced FEV_1 (forced expiratory volume in one second) and it has been shown[154,252] that the depth of particle penetration decreases with a decrease in FEV_1. However, it has also been shown[e.g.,194] that patients with COPD can increase peripheral particle penetration if their FEV_1 is increased through bronchodilation. This is presumably because dilating the central airways reduces the flow velocities in these airways, and hence deposition at bifurcations by impaction is reduced. Thus more particles are available to be transported peripherally. However, there is evidence that continued exposure to airborne pollutants increases the severity of many lung diseases. For instance, Hogg & van Eeden (2009) concluded that the lung's natural response to airborne particulate matter may account for the acute exacerbation of COPD in the elderly.

Pulmonary fibrosis is one of a group of conditions known as interstitial lung diseases. These diseases are characterized by a decrease in gas diffusion capacity across the air-blood barrier and, of more importance to the current discussion, an increased rigidity of the septal tissue. Estimates of the prevalence of idiopathic pulmonary fibrosis in the United States range from 14 to 63 per 100,000[92,263]. It is probable that the increase in parenchymal rigidity results in changes in the flow and particle kinetics in the alveoli. Indeed, Sweeney et al. (1983, 1987) studied the deposition of particles in hamster lungs and concluded that local decreases in compliance caused by fibrosis alter regional ventilation and particle retention.

Other lung pathologies include those associated with mechanical ventilation of premature infants; e.g. bronchopulmonary dysplasia (BPD). Tepper et al. (1986) showed that infants with BPD have abnormal functional airway growth and decreased expiratory flow reserve. While, more recently, management procedures and understanding of BPD have improved, a new form of this disease has emerged[26]. One characteristic of this new BPD is alveoli that are larger than normal, which results in a reduction in the overall surface available for gas exchange[11]. Moreover, lungs of long-term ventilated infants have been found to have parenchymal air-exchanging volumes twice are large as normal[70]. In a recent review of BPD, Baraldi et al. (2009) concluded that there is increasing evidence that early lung function abnormalities leads to suboptimal respiratory function later in life. Inhaled therapeutics for the treatment of lung injury is particularly attractive for infants as it avoids such barriers to therapeutic efficacy as poor gastrointestinal absorption and first-pass metabolism in the liver[194]. Unfortunately, the mechanics of air flow and particle transport in the postnatally developing lung are currently poorly understood. Due to the small scale of the acinar airways, and obvious ethical constraints, it is impossible to measure air flow and particle deposition in the developing human lung in vivo. Thus future progress in determining the appropriate dosage of inhaled therapeutics, as well as quantifying the risk of

exposure to pollutants, in the pediatric population is likely to come from computational and animal studies.

Animal models

The geometry and kinematics (anatomy and motion) of the upper, conducting, and acinar airways is one of the major determinants of aerosol transport and deposition in the respiratory tract. Difficulties in measuring these features in humans has led to a large portion of current research on particle deposition in the lung being based on animal models (primarily mouse, rat, rabbit, dog, pig, and sheep). This raises the important question of how to scale results from animal models to implications about the basic processes of aerosol deposition in human lungs.

The issue of body size was specifically addressed by McMahon et al. (1977). They simultaneously exposed five different species (mouse, hamster, rat, rabbit, dog) of very different body size to particles (0.78μm in median aerodynamic diameter) and measured the retention of the aerosol in the respiratory tract immediately after a 30-min exposure, as well as their ventilation parameters. The results showed that while the total deposition (the amount of particles deposits), which depends primarily on ventilation per body weight, was quite different among the species studied, deposition efficiency (percent of total particles inhaled which actually deposit) in the lung was essentially independent of body size. This result can be explained theoretically by the law of dynamic similitude; i.e., two flows of different magnitudes have similar behaviors if certain non-dimensional parameters are the same in both cases. In the case of many mammals, including humans, the range of airflow Reynolds number does not vary significantly among species or over body mass. To the extent that the Reynolds number is the dominate parameter determining deposition efficiency, the similarity of flow dynamics would imply a similar concordance of deposition efficiencies across the species studies by McMahon et al. (1977).

The above results have to be viewed with some caution because there are, obviously, substantial differences in the anatomy of the respiratory tract between humans and other animals. The geometries of the upper airways (nasal cavity, oropharyngeal airway) of most animals (except primates) are substantially different from that of humans, thus non-primate animal models present serious difficulties in scaling upper airway deposition results to humans. At the level of intrathoracic airway branching patterns, while the human bronchial tree mainly represents dichotomous branching, some animals, such as rodents, have a monopodial branching structure. However, at the acinar level, the structure of the pulmonary acinus of many mammals is morphologically very similar. Therefore, while animals with a monopodial branching structure may not be suitable for the study of particle deposition in the conducting airways of the human lung, those animals can still be used for the study of acinar deposition in the human lung. This is particular true for studies of submicron particle deposition, as such particles tend to deposit in the acinus.

Differences in lung function (lung volumes, airway conductances, etc.) between human and animal models and how these might affect particle deposition comparisons also need to be considered. However, some of these issues are of secondary importance. For example, during normal breathing in healthy humans, the distribution of ventilation is dominated by

downstream lung compliance, with only little influence of airway conductance[241,307]. Therefore, the distribution of particle-laden tidal air among various regions of the lung (lobes, acini) and consequently the distribution of particle deposition within the acinus, are controlled by the way in which the acinar volume expands. As the structure and dynamic behavior of the pulmonary acinus of mammals are similar, this argues in favor of the use of animal models as surrogates for the human acinus. On the other hand, certain features of lung volumes do not easily scale between species. For example, in normal humans, functional residual capacity (FRC) defined as end expiratory lung volume, is essentially equal to relaxation volume; this is substantially different in small rodents, where end expiratory volumes are dynamically determined, and relaxation volumes are rarely achieved.

Expired Aerosols

Not only are the lungs depositories of inhaled particles; they can also be the source of aerosols[7,90,113,161,214,247]. These particles are called bioaerosols, and include pathogenic particles that may spread infectious diseases[84,94,253]. There are basically two areas in the respiratory tract where bioaerosols can be generated. One is in trachea and the other is at the level of the small airways. The former is usually associated with cough, which generates an extremely high velocity expiratory airflow and as a result, a part of a mucous layer is torn from the tracheal walls and polydisperse droplets are entrained. This mechanism is reviewed extensively by Clarke et al. (1970) and Leith et al. (1986). The latter phenomenon; i.e., the generation of bioaerosols in small airways, is the topic of this section. In contrast to turbulent flows or high Reynolds number flows occurring in the trachea, airflow in the small airways is relatively slow. What possible mechanisms are responsible in producing bioaerosols at the level of small airways?

Under normal breathing conditions, especially at low lung volumes, some of the small airways may be occluded by airway surface liquid[45,164,210,211,242]. In engineering terms, this is known as Rayleigh instability or the elastrocapillary instability problem; that is, a tube, whose inner walls are lined with a viscous liquid layer, becomes occluded by forming a liquid meniscus[132,133,140,141,162,227]. During the inspiratory phase, these closed airways reopen as the lungs start to inflate. Importantly, this airway reopening occurs in an abrupt and avalanche fashion[293] –the phenomenon is recognized as crackle sounds during lung inflation. In late 80's, J. D. Brain and J. Heyder hypothesized that this abrupt reopening of small airways may generate fine aerosol droplets (personal communication). Gebhart et al. (1988) tested this hypothesis by measuring the concentration of submicron (0.4μm) particles in the exhaled air. They found that 1) the concentration of expired particles increased with increased tidal volume and was highest when inspiration started at the closing or residual volume, 2) the particle concentration decreased following breath-holding, 3) all particles were expired from the level of small airways. These data are consistent with the abrupt opening of occluded peripheral airways as a mechanism of generation of these particles.

Recently, Malasheko et al. (2009) demonstrated how particles are generated when menisci collapse using a computational model. They showed that when the capillary number, *Ca* (which is a dimensionless number expressing the ratio of hydrodynamic shear forces to surface tension at a gas-liquid interface) increases above a critical value (e.g., *Ca* =1 in Fig.

19 for instance), a meniscus traveling in a tube diminishes in thickness ($0.0 < t < 0.05$sec in Fig. 19). When both sides of a thinning meniscus meet (at $t = 0.055$ sec), the tube pops open to create an air passage. At that abrupt transition (at $t = 0.06$ sec), a number of small droplets are formed. In other words, liquid menisci occlusions, which may be present inside small airways especially at low lung volume, may disintegrate into small droplet during early inspiration.

In the past, the generation and transport of bioaerosols has not attracted as much attention as the mechanics of aerosol deposition. This situation has changed recently with renewed interest in such topics as the transmission of infectious diseases. As our understanding of this important area of aerosol mechanics is incomplete, we can expect further expansion of research in this area.

Drug delivery

Inhalation therapies can be divided into two groups. The first is classical, targeting the local treatment of lung disease; the second is a more recent development of systemic therapies achieved through aerosolized drugs delivered via the lung surface.

Treatment of local lung disease—Inhalation of medications has been widely used as the first-line therapy for the treatment of such respiratory diseases as asthma, bronchitis, cystic fibrosis, and chronic obstructive pulmonary disease (COPD). The advantages of such inhalation therapy over systemic drug therapy are numerous: 1) high local drug concentration can be achieved at the site of disease, 2) drug effects can be rapid, 3) systemic side-effects can be minimized, and 4) therapeutic efficacy is higher than that of systemic therapy because drug barriers such as poor gastrointestinal absorption are bypassed. The efficacy of inhalation therapy for lung disease largely depends on the optimization of topical dosing and its distribution within the lung. To achieve this optimization, it is critical to first identify where the site of action should be and to manage targeting drug deposition specifically to those sites in the respiratory tract.

As an example, the β_2 adrenergic receptors, which relax smooth muscle if activated, are present throughout the lung, including airway smooth muscle, epithelium, vascular smooth muscle, submucosal glands, as well as the lung parenchyma[13,15,44,213]. Inhaled β_2-agonists, such as aerosolized micron-size salbutamol, is the most effective bronchodilator in asthma and COPD. Similarly, because the respiratory tract is heavily innervated by the vagus nerve, cholinergic receptors, which cause bronchoconstriction if activated, are present in all airways with a higher density in the smooth muscle of large airways as well as airway epithelium and submucosal glands[14,212]. Therefore, aerosolized anticholinergics, such as ipratropium bromide, are effective bronchodilators of airways. Inhalation of anti-inflammatory drugs, such as corticosteroids, are also used for the treatment of asthma and COPD. Target sites of anti-inflammatories are the glucorcorticoid receptors, which every cell type including inflammatory cells in the lung expresses[1,42,188]. Further detailed, excellent, discussions on this topic can be found elsewhere[e.g.,15,81,194,195,331].

Pulmonary drug delivery for systemic therapy—Due to the enormously large surface area and extremely thin air-blood barrier of the lung (less than 1μm), the lung is not

only the target organ but also an ideal port of entry for the systemic drug therapy[251]. The advantages of systemic drug therapy via the pulmonary route over that via oral or intravenous injection routes are as follows[40,194,249]. 1) The lung surface provides a low enzymatic environment for the systemic absorption of medication; many peptides such as insulin cannot be taken orally due to degradation in the gastrointestinal tract; 2) because the entire cardiac output passes through the lung, drug particles deposited on the lung surface are in very close proximity to a large volume of blood and hence the potential is high for a large portion of the particles to be absorbed directly into the bloodstream; 3) pulmonary drug delivery is noninvasive.

To achieve high drug efficacy and to avoid mucociliary clearance operating in the conducting airways, systemic drug particles generally need to deposit deep in the alveolar region of the lung. In this regard, the size of the drug particles plays a crucial role; submicron particles dominantly deposit in the pulmonary acinus[312]. Even after successfully depositing in the lung parenchyma, these fine particles still have several barriers to overcome; they need to avoid being engulfed by alveolar macrophages, which patrol the alveolar surfaces and keep them clean and sterile; the particles have to submerge into the alveolar surface liquid layer to make contact with the epithelial surface (the liquid layer can sometimes be thicker than the size of particles); and the particles then have to translocate through the epithelium, interstitium, basement membrane, and endothelium before being absorbed into the bloodstream. Again, the size of the particle is a critical factor for these processes[190,194]. For instance, macromolecles < 40 kDa (5-6nm in diameter) inhaled into the airways or nano-size (quantum dot) particles <6 nm in diameter instilled in the lung periphery[52] appear in the blood within minutes. Insulin (5.7 kDa, 2.2nm) peaks in the blood 15-60 min after inhalation[142,160,200]. Choi et al (2010) showed that particles between 6 nm to 34 nm appear in mediastinal lymph nodes much less than 30 minutes in the rat, while no particles larger than 34 nm appeared at draining lymph nodes within the first one hour.

Drug delivery system—Regardless of whether the drug delivery is aimed at the treatment of topical lung disease or for systemic delivery, an appreciable number of drug particles must pass through the oropharyngeal region and deposit in the lung to achieve good therapeutic efficacy. Facilitated by recent rapid improvement and development of new inhaler devices, the deposition efficiency of drug aerosols in the lung has been increased significantly[80]. Three main types of drug delivery systems currently used are nebulizers, metered-dose inhalers (MDI), and dry-powder inhalers (DPI)[74,81,195]. Although poor delivery efficiency is one of the most notable disadvantages of nebulizers compared to the other systems, they have been used for many years, especially in a hospital setting, because of their ability to aerosolize most drug solutions in large quantities without the requirement of the patient having to learn a specific inhalation technique. They are, therefore, often used in pediatric clinics, as well as for patients who are physically unable to use other devices.

The MDI is currently the most widely used portable inhaler device. The device emits a drug aerosol, which is driven by a propellant, such as Hydrochlorofluorocarbons (HCFC), through a nozzle. Because of the high velocity and the relatively large (micron) size of the aerosol, a large portion of emitted particles is lost at the back of the throat by impaction[235]; only the small remaining portion of the dose manages to enter the intrathoracic airways and

is deposited in the lung[235]. However, by synchronizing with inspiratory flow, coordinating hand-mouth inhalation maneuvers, using an accessory spacer device, breathing slow and deep, as well as applying breath hold techniques, the deposition efficiency can be improved[233,235,240].

The DPI is a propellant-free breath-activate inhaler, designed to avoid 1) the difficulties of inhalation maneuvers, which are required for the appropriate use of the MDI, and 2) the use of CFC (propellant used in some MDIs), a gas that depletes the atmosphere's ozone layer, and which has been banned throughout the world. The DPI, driven by patient's quick and forceful inhalation, entrains powder from the device[234]. The powder, which contains medication, breaks-up into aerosol particles due to vigorous (e.g., turbulent) airflow in the powder container[57,89] and subsequently a small drug aerosol is delivered into the lung.

There are many other important issues, such as drug particle type (e.g., liposome, porous particles), bioavailability, etc. that should be discussed for the optimization of inhalation drug therapy. However, they are beyond the scope of this chapter. Excellent detailed discussions on these topics can be found elsewhere[e.g.,27,81,102,194,195,251,251].

Ambient particulate pollutant and particle toxicology

Ambient air contains many different types of pollutant components, such as chemicals, particles, and biological materials. This chapter deals with particulate matter (PM) - solid or liquid matter suspended in the air. During the last few decades, both cohort and time-series epidemiology studies show a strong association between premature mortality and excess morbidity and ambient pollutant PM exposure[79]. Needless to say, there is an overwhelmingly strong link between the exacerbation of lung diseases, such as asthma and bronchitis, and high ambient concentration of PMs[270,277], and there is now evidence that the adverse health effects of PMs go beyond the lung[82,115]. An example is the epidemiological evidence of the link between cardiovascular diseases and ambient PM exposure[120,198,292] The widely cited Harvard Six City study demonstrates the increased prevalence of cardiovascular diseases in areas where ambient particle level were higher[56,78]. The overall adverse health effects of particulate pollution are clearly seen by the fact that the reduction in air pollutants over the last 20 years was accompanied by a 15% increase in overall life expectancy[270]. Further references are available elsewhere[e.g.,119,207,224,255,276,285].

Finally, the current US regulations of ambient PMs are listed as follows. Under the authority of the Clean Air Act, the United States Environmental Protection Agency (USEPA) established the National Ambient Air Quality Standards (NAAQS). In the mid-80's, the USEPA began regulating the ambient concentration of particulate matter whose aerodynamic diameter is less than 10 μm (PM_{10}) because particles in this size range are thought to be, in large part, responsible for the health threat due to air pollution. Particles larger than 10 μm tend not to reach the respiratory part of the lung. Current US law requires that the 24-hour average concentration of PM_{10} must not exceed 150 μg per cubic meter more than once per year on average over 3 years. In the 90's, ambient concentration of even smaller particulate matter, whose aerodynamic diameter is less than 2.5 μm ($PM_{2.5}$), became regulated. This is because accumulated evidence suggests that finer particles (smaller than PM_{10}) are more of a health threat because they are likely to penetrate deep into the gas

exchange region of the lungs. Annual arithmetic mean concentration of $PM_{2.5}$ and 24-hour average concentration of $PM_{2.5}$ are now regulated not to exceed 15μg/m^3 and 35μg/m^3, respectively, on average over 3 years.

Summary and Future Directions

How inhaled particles interact with the lung has been the subject of intense research for many years. As described in the Introduction, there are two sequential causative relationships; exposure-to-dose and dose-to-response. The nature of the former relationship is conditioned by the physical characteristics of the inhaled particles (discussed in Particle Characteristics), the transport and deposition mechanics in a conduit in general (Particle Transport and Particle Deposition, respectively), and in the respiratory tract in particular (Particle Transport and Deposition in the Respiratory Tract). The "exposure-to-dose" relationship was briefly discussed for specific cases (e.g., age-, disease-dependent) in Special Issues.

Although the biological response to a deposited particle is beyond the scope of this chapter, deposition significantly conditions the subsequent biological response because the former relationship sets the initial conditions for the latter relationship. For instance, the lung has two types of defense mechanisms in response to inhaled particles. When particles deposit in the conducting airways, where the epithelium is ciliated and covered by mucus producing goblet cells[326], they are trapped in the mucus layer and pushed up and out into the throat by the continually beating cilia[185,287]. This is called the mucociliary escalator, which is the major clearance mechanism for deposited particles in the conducting airways. Conversely, when particles deposit deep in the gas-exchange regions of the lung, where the epithelium is extremely thin and not ciliated, they are cleared by alveolar macrophages (AMs); AMs engulf particles and keep the lung surface clean and sterile. Therefore, depending on which part in the respiratory tract particles deposit, the clearance response of the lung is completely different.

Concerning the site of particle deposition, it is reasonable, as a first approximation, to divide the respiratory tract into two; the conducting airways and the pulmonary acinus, based on the differences in airway structure, in epithelial characteristics, and in clearance mechanisms. With this division, much attention is currently paid to small particles because they likely penetrate into a deeper part of the lung by virtue of their physical characteristics, deposit and remain in the acinus (in the alveolar epithelium or in AMs) for a long time, and most importantly, cause particle-induced pathogenesis or translocate systemically via the enormously large lung surface.

One area of future development is to devise a technique to locate accurately the site of deposition within the structure of the acinus. As mentioned in Acinar Geometry, according to Haefeli-Bleuer and Weibel (1998), the human pulmonary acinus is well approximated by a 9-generation bifurcating structure on average; the first few generations below the terminal bronchioles are partially alveolated (called transitional bronchioles, including respiratory bronchioles) and the remaining approximately 6 generations, on average, are fully-alveolated (called the subacinus). To locate a particle deposited on the septal wall of a

specific alveolus in the acinar tree, it is necessary to have both a global scale (millimeter-scale) locator, which can identify the alveolus of interest with respect to the whole acinus and a local scale (nanometer- or submicron-scale) imaging tool, which can visualize individual particles on the septal wall within the alveolus. To move back and forth across these widely different length-scales, it will be necessary to develop multimodal imaging techniques[129,274] (Fig. 20).

Another topic for future study is the investigation of the fate of very small particles, particularly those whose aerodynamic diameters are less than 100nm. These are the "ultrafine" particles or "nanoparticles", and their importance is just now emerging. Two areas in the respiratory tract are of particular interest; the olfactory region and the pulmonary acinus. As remarked in Upper Airways, nanoparticles may have a direct route to the brain via the olfactory nerves[75,216,238]. With respect to the pulmonary acinus, there are several reasons for the recent trend. 1) Because of their small size, these particles may be able to escape the body's natural defense system. Indeed, it has been shown that the phagocytic ability of AMs is less effective for ultra-small particles compared to larger, micron-size, particles, and hence a larger number of nano-size particles escapes from being engulfed by AMs[116]. 2) Particles not being engulfed by AMs are likely to make contact with the underlying epithelial layer. Because the surface-to-volume ratio of ultra-small particles is significantly higher than that of larger particles, bio-reactivity (including absorbability in tissue or translocatability into the tissue) of ultra-small particles may be much greater than that of larger particles. 3) Because the size of ultra-small particles is comparable to the size of intracellular components, such as molecules of plasma membrane, DNA molecule, etc., the properties of the particle materials (such as surface charge, surface coating of particles, etc.) may directly interact with the host cellular structure, leading to toxicological or therapeutically beneficial consequences.

In terms of systemic effects of nano-size particles, the mechanisms by which particles translocate through the lung's gas-blood barrier are currently not known[230]. Although the topic is beyond the scope of this chapter, we note that two possibilities are currently being considered and studied extensively[28,46,77,209,217,230,231,280]; specifically, transcellular (e.g., clathrin-, caveolin-, Fc receptor-mediated endocytosis) and pericellular (via tight junction gap, diffusion mediated transport, etc.). Once nanoparticles enter the interstitium, passing through the epithelium, they may either move directly toward the capillary bloodstream via the endothelium or move toward draining lymph nodes via the lymphatic system and then move to the bloodstream[52]. In any event, once particles are in the bloodstream, they can circulate anywhere in the body.

As the topic covered in this chapter covers many fields (e.g., aerosol physics, engineering, biology and physiology) over a wide range of length scales (from centimeter as an organ level to nanometer as an interaction between nanoparticles and intracellular components), further improvement of our basic understanding towards particle transport and deposition in the lung necessarily requires multidisciplinary and multiscale research. With the ever-increasing rapidity of advances in experimental techniques and equipment together with similar developments in computational power and numerical techniques we can expect much progress in the near future.

Acknowledgments

We thank Dr. Dolovich for her useful discussion. This work was supported by National Heart, Lung, and Blood Institute Grants HL054885, HL070542, HL094567, and HL074022.

References

1. Adcock IM, Gilbey T, Gelder CM, Chung KF, Barnes PJ. Glucocorticoid receptor localization in normal and asthmatic lung. Am J Respir Crit Care Med. 1996; 154:771–782. [PubMed: 8810618]
2. Anjilvel S, Asgharian B. A Multiple-Path Model of Particle Deposition in the Rat Lung. Fundam Appl Toxicol. 1995; 28(1):41–50. [PubMed: 8566482]
3. Ardila R, Horie T, Hildebrandt J. Macroscopic isotropy of lung expansion. Respir Physiol. 1974; 20:105–115. [PubMed: 4826745]
4. Aref H. Stirring by chaotic advection. J Fluid Mech. 1984; 143:1–21.
5. Asgharian B, Ahmadi G. Effect of Fiber Geometry on Deposition in Small Airways of the Lung. Aerosol Sci Technol. 1998; 29(6):459–474.
6. Asgharian B, Anjilvel S. A multiple-path model of fiber deposition in the rat lung. Toxicol Sci. 1998; 44(1):80–6. [PubMed: 9720144]
7. Aver HE, Willeke K. Particle concentration in exhaled breath. Am Ind Hyg Assoc J. 1988; 49:A156–A158.
8. Balásházy I, Hofmann W. Deposition of aerosols in asymmetric airway bifurcations. J Aerosol Sci. 1995; 26(2):273–292.
9. Balásházy I, Hoffmann W, Heistracher T. Local particle deposition patterns may play a key role in the development of lung cancer. J Appl Physiol. 2003; 94:1719–1725. [PubMed: 12533493]
10. Balásházy I, Hofmann W, Farkas A, Madas BG. Three-Dimensional Model for Aerosol Transport and Deposition in Expanding and Contracting Alveoli. Inhal Toxicol. 2008; 20(6):611–621. [PubMed: 18444013]
11. Baraldi E, Filippone M. Chronic lung disease after premature birth. N Engl J Med. 2007; 357(19): 8. 1946–55.
12. Baraldi E, Carraro S, Filippone M. Bronchopulmonary dysplasia: definitions and long-term respiratory outcome. Early Hum Dev. 2009; 85(10 Suppl):S1–3. [PubMed: 19793629]
13. Barnes PJ, Basbaum CB, Nadal JA, Roberts JM. Localization of β-adrenoreceptors in mammalian lung by light microscopy autoradiography. Nature. 1982; 299:444–447. [PubMed: 6289123]
14. Barnes PJ, Basbaum CB, Nadel JA. Autoradiographic localization of autonomic receptors in airway smooth muscle: marked differences between large and small airways. Am Rev Respir Dis. 1983; 127:758–762. [PubMed: 6305241]
15. Barnes PJ. Distribution of Receptor Targets in the Lung. Proc Am Thorac Soc. 2004; 1:345–351. [PubMed: 16113456]
16. Bastacky J, Hayes TL, von Schmidt B. Lung structure as revealed by microdissection. Am Rev Resp Dis. 1983; 128:S7–S13. [PubMed: 6881714]
17. Becquemin MH, Swift DL, Bouchikhi A, Roy M, Teillac A. Particle deposition and resistance in the noses of adults and children. Eur Respir J. 1991; 4(6):694–702. [PubMed: 1889496]
18. Bennett WD, Smaldone GC. Use of aerosols to estimate mean airspace size in COPD. J Appl Physiol. 1988; 64(4):1554–1560. [PubMed: 3378990]
19. Bennett WD, Scheuch G, Zeman KL, Brown JS, Kim C, Heyder J, Stahlhofen W. Regional deposition and retention of particles in shallow, inhaled boluses: effect of lung volume. J Appl Physiol. 1999; 86(1):168–173. [PubMed: 9887127]
20. Bennett WD, Zeman KL, Foy C, Shaffer CL, Johnson FL, Regnis JA, Sannuti A, Johnson. Effect of aerosolized uridine 5′-triphosphate on mucociliary clearance in mild chronic bronchitis. Am J Respir Crit Care Med. 2001; 164(2):302–306. [PubMed: 11463605]
21. Bennett WD, Brown JS, Zeman KL, Hu SC, Scheuch G, Sommerer K. Targeting delivery of aerosols to different lung regions. J Aerosol Med. 2002; 15(2):179–188. [PubMed: 12184868]

22. Bennett, WD.; Brown, JS. Particulate Dosimetry in the Respiratory Tract. In: Foster; Costa, editors. Air Pollutants and the Respiratory Tract. Marcel Dekker, Inc; NY, NY: 2005.
23. Bennett WD, Zeman KL. Effect of race on fine particle deposition for oral and nasal breathing. Inhal Toxicol. 2005; 17(12):641–648. [PubMed: 16087570]
24. Bennett WD, Almond MA, Zeman KL, Johnson JG, Donohue JF. Effect of salmeterol on mucociliary and cough clearance in chronic bronchitis. Pulm Pharmacol Ther. 2006; 19(2):96–100. [PubMed: 15970448]
25. Berg EJ, Weisman JL, Oldham MJ, Robinson RJ. Flow field analysis in a compliant acinus replica model using particle image velocimetry (PIV). J Biomech. 2010; 43:1039–1047. [PubMed: 20116064]
26. Bhandari A, Bhandari V. Pitfalls, problems, and progress in bronchopulmonary dysplasia. Pediatrics. 2009; 123:1562–1573. [PubMed: 19482769]
27. Bisgaard, H.; O'Callaghan; Smaldone, GC. Lung Biology in Human and Disease. Vol. 162. Marcel Dekker, Inc.; New York: 2002. Drug delivery to the lung.
28. Blank F, Rothen-Rutishauser B, Gehr P. Dendritic cells and macrophages form a transepithelial network against foreign particulate antigens. Am J Respir Cell Mol Biol. 2007; 36:669–677. [PubMed: 17272826]
29. Brain JD, Valberg PA. Deposition of aerosol in the respiratory tract. Am Rev Respir Dis. 1979; 120:1325–1373. [PubMed: 391112]
30. Brand P, Rieger C, Beinert T, Heyder J. Aerosol derived airway morphometry in healthy subjects. Eur Respir J. 1995; 8:1639–1646. [PubMed: 8586115]
31. Brody AR, Hill LH, Adkins B, O'Connonr RW. Chrysotile asbestos inhalation in rats: deposition pattern and reaction of alveolar epithelium and pulmonary macrophages. Am Rew Respir Dis. 1981; 123:670–679.
32. Brouns M, Verbanck S, Lacor C. Influence of glottic aperture on the tracheal flow. J Biomech. 2007; 40(1):165–172. [PubMed: 16403504]
33. Burri PH, Dbaly J, Weibel ER. The postnatal growth of the rat lung I Morphometry. Anat Rec. 1974a; 178(4):711–30. [PubMed: 4592625]
34. Burri PH. The postnatal growth of the rat lung 3 Morphology. Anat Rec. 1974b; 180(1):77–98. [PubMed: 4416419]
35. Burri, PH. Structural aspects of prenatal and postnatal development and growth of the lung. In: McDonald, JA., editor. Lung growth and development. Marcel Dekker; New York: 1997. p. 1-35.
36. Burri PH. Structural aspects of postnatal lung development - alveolar formation and growth. Biol Neonate. 2006; 89(4):313–22. [PubMed: 16770071]
37. Bush ML, Frederick CB, Kimbell JS, Ultman JS. A CFD-PBPK hybrid model for simulating gas and vapor uptake in the rat nose. Toxicol Appl Pharmacol. 1998; 150(1):133–145. [PubMed: 9630462]
38. Butler JP, Tsuda A. Effect of convective stretching and folding on aerosol mixing deep in the lung, assessed by approximate entropy. J Appl Physiol. 1997; 83(3):800–9. [PubMed: 9292466]
39. Butler, JP.; Tsuda, A. Transport of gases between the environment and alveoli – theoretical considerations. In: Fredberg, J.; Sieck, G.; Gerthoffer, W., editors. Handbook of Physiology, Respiratory Physiology Section. 2010. Amer Physiol Soc
40. Byron PR, Patton JS. Drug delivery via the respiratory tract. J Aerosol Med. 1994; 11:197–219.
41. Cai FS, Yu CP. Inertial and interceptional deposition of spherical particles and fibers in a bifurcating airway. J Aerosol Sci. 1988; 19:679–688.
42. Carroll N, Cooke C, James A. The distribution of eosinophils and lymphocytes in the large and small airways of asthmatics. Eur Respir J. 1997; 10:292–300. [PubMed: 9042623]
43. Carslaw, HS.; Jaeger, JC. Conduction of heat in solids. Oxford Univ Press; 1959.
44. Carstairs JR, Nimmo AJ, Barnes PJ. Autoradiographic visualization of β-adrenoceptor subtypes in human lung. Am Rev Respir Dis. 1985; 132:541–547. [PubMed: 2864008]
45. Cassidy KJ, Halpern D, Ressler BG, Grotberg JB. Surfactant effect in model airway closure experiment. J Appl Physiol. 1999; 87:415–427. [PubMed: 10409603]

46. Cedervall T, Lynch I, Lindman S, Berggard T, Thulin E, Nilsson H, Dawson KA, Linse S. Understanding the nanoparticle-protein corona using methods to quantify exchange rates and affinities of proteins for nanoparticles. Proc Natl Acad Sci U S A. 2007; 104:2050–2055. [PubMed: 17267609]
47. Chandrasekhar S. Stochastic problems in physics and astronomy. Rev Modern Physics. 1943; 15:1–91.
48. Chen Q, Ahmadi G. Deposition of Particles in a turbulent pipe flow. J of Aerosol Sci. 1997; 28(55):789–796.
49. Chen YK, Yu CP. Sedimentation of Fibers from Laminar Flows in a Horizontal Circular Duct. Aerosol Sci Technol. 1991; 14(3):343–347.
50. Cheng KH, Cheng YS, Yeh HC, Guilmette RA, Simpson SQ, Yang YH, Swift DL. *In vivo* measurements of nasal airway dimensions and ultrafine aerosol deposition in the human nasal and oral airways. J Aerosol Sci. 1996; 27:785–801.
51. Choi J, Kim CS. Mathematical analysis of particle deposition in human lungs: An improved single-path transport model. Inhal Toxicol. 2007; 19:925–939. [PubMed: 17849277]
52. Choi HS, Ashitate Y, Lee JH, Kim SH, Matsui A, Insin N, Bawendi MG, Semmler-Behnke M, Frangioni JV, Tsuda A. Rapid Translocation of Nanoparticles from the Lung Airspaces to the Body. Nature Biotechnology. 2010; 28(12):1300–1303.
53. Churg A, Brauer M. Ambient atmospheric particles in the airways of human lungs. Ultrastruct Pathol. 2000; 24(6):353–61. [PubMed: 11206332]
54. Churg A, Brauer M, Avila-Casado MdC, Fortoul TI, Wright JL. Chronic exposure to high levels of particulate air pollution and small airway remodeling. Environ Health Perspect. 2003; 111:714–718. [PubMed: 12727599]
55. Clarke SW, Jones JG, Olive DR. Resistance to two-phase gas-liquid flow in airways. J Appl Physiol. 1970; 29(4):464–471. [PubMed: 5459914]
56. Committee on the Medical Effects of Air Pollutants. Cardiovascular disease and air pollution. Department of Health. 2006
57. Concessio NM, VanOort MM, Knowles MR, Hickey AJ. Pharmaceutical dry powder aerosols: correlation of powder properties with dose delivery and implications for pharmacodynamic effect. Pharmaceut Res. 1999; 16:828–834.
58. Craighead JE, Abraham JL, Churg A, Green FHY, Kleinerman J, Pratt PC, Seemayer TA, Vallyathan V, Weill H. The pathology of asbestos-associated diseases of the lungs and pleural cavities: diagnostic criteria and proposed grading scheme. Arch Pathol Lab Med. 1982; 106(1): 544–596. [PubMed: 6897166]
59. Craighead JE, Kleinerman J, Abraham JL, Gibbs AR, Green FHY, Harley RA, Ruttner JR, Vallyathan V, Juliano EB. Diseases associated with exposure to silica and non-fibrous silicate minerals. Arch Pathol Lab Med. 1988; 112:673–720. [PubMed: 2838005]
60. Crelin, E. The Human Vocal Tract: Anatomy, Function, Development and Evolution. Vantage Press; New York: 1987.
61. Cunningham E. On the velocity of steady fall of spherical particles through fluid medium. Proc Roy Soc A. 1910; 83:357–365.
62. Dailey HL, Ghadiali SN. Fluid-structure analysis of microparticle transport in deformable pulmonary alveoli. J Aerosol Sci. 2007; 38:269–288.
63. Darquenne C, Paiva M. Two- and three-dimensional simulations of aerosol transport and deposition in alveolar zone of human lung. J Appl Physiol. 1996; 80(4):1401–1414. [PubMed: 8926273]
64. Darquenne C. Heterogeneity of aerosol deposition in a two-dimensional model of human alveolated ducts. J Aerosol Sci. 2002; 33:1261–1278.
65. Darquenne C, Harrington L, Prisk GK. Alveolar duct expansion greatly enhances aerosol deposition: a three-dimensional computational fluid dynamics study. Philos Transact A Math Phys Eng Sci. 2009; 367(1896):2333–2346.
66. Davidson MR, Fitz-Gerald JM. Flow patterns in models of small airway units of the lung. J Fluid Mech. 1972; 52:161–177.

67. Davies CN. Definitive equations for the fluid resistance of spheres. Proc Phys Soc. 1945; 57:259–270.
68. Davies CN. Breathing of half-micron aerosols II Interpretation of experimental results. J Appl Physiol. 1972; 32:601–611. [PubMed: 5064587]
69. Daviskas E, Gonda I, Anderson SD. Mathematical modeling of heat and water transport in human respiratory tract. J Appl Physiol. 1990; 69(1):362–372. [PubMed: 2394658]
70. De Paepe ME, Mao Q, Powell J, Rubin SE, DeKoninck P, Appel N, Dixon M, Gundogan F. Growth of pulmonary microvasculature in ventilated preterm infants. Am J Respir Crit Care Med. 2006; 173:204–211. [PubMed: 16210670]
71. Denny E, Schroter RC. The Mechanical Behavior of a Mammalian Lung Alveolar Duct Model. ASME J Biomech Eng. 1995; 117:254–261.
72. Denny E, Schroter RC. Viscoelastic Behavior of a Lung Alveolar Duct Model. ASME J Biomech Eng. 2000; 122:143–151.
73. Denny E, Schroter RC. A Model of Non-Uniform Lung Parenchyma Distortion. J Biomech. 2006; 39:652–663. [PubMed: 16439235]
74. Derom, E.; Thorsson, L. Factors affecting the clinical outcome of aerosol therapy, Drug delivery to the lung. In: Bisgaard, H.; O'Callaghan; Smaldone, GC., editors. Lung Biology in Human and Disease. Vol. 162. 2002. p. 143-171.Chap. 5
75. Dhuria SV, Hanson LR, Frey. WH Intranasal delivery to the central nervous system: mechanisms and experimental considerations. J Pharm Sci. 2010; 99(4):1654–73. [PubMed: 19877171]
76. Dickie R, Wang YT, Butler JP, Schulz H, Tsuda A. Distribution and quantity of contractile tissue in postnatal development of rat alveolar interstitium. Anat Rec. 2008; 291(1):83–93.
77. Dickie R, Cormack M, Kreyling WG, Semmler-Behnke M, Tsuda A. Deep pulmonary lymphatics in immature lungs. J Appl Physiol. 2009; 107(3):859–863. [PubMed: 19556455]
78. Dockery DW, Pope CA, Xu XP, Spengler JD, Ware JH, Fay ME, Ferris BG, Speizer FE. An association between air-pollution and mortality in 6 United States cities. N Engl J Med. 1993; 329:1753–1759. [PubMed: 8179653]
79. Dockery DW. Health effects of particulate air pollution. Ann Epidemiol. 2009; 19(4):257–263. [PubMed: 19344865]
80. Dolovich MB. New propellant-free technologies under investigation. J Aerosol Med. 1999; 12(Suppl 1):s9–s17. [PubMed: 10623341]
81. Dolovich MB, Dhand R. Aerosol drug delivery: developments in device design and clinical use. Lancet. 2011; 377(9770):1032–1045. [PubMed: 21036392]
82. Donaldson, K.; Borm, P. Particle toxicology. CRC Press. Taylor & Francis; New York: 2007.
83. Doorly DJ, Taylor DJ, Schroter RC. Mechanics of airflow in the human nasal airways. Respir Physiol Neurobiol. Nov 30; 2008 163(1-3):100–10. [PubMed: 18786659]
84. Edwards DA, Man JC, Brandt P, Katstra JP, Sommerer K, Stone HA, Nardell E, Scheuch G. Inhaling to mitigate exhaled bioaerosols. Proc Natl Acad Sci USA. 2004; 101:17383–17388. [PubMed: 15583121]
85. Egan MJ, Nixon W. A model of aerosol deposition in the lung for use in inhalation dose assessments. Radiat Prot Dosim. 1985; 11:507.
86. Elad D, Wolf M, Keck T. Air-conditioning in the human nasal cavity. Respir Physiol Neurobiol. 2008; 163(1-3):121–7. [PubMed: 18565805]
87. Epstein B. The mathematical description of certain breakage mechanisms leading to the logarithmic-normal distribution. J Franklin Institute. 1947; 244(6):471–477.
88. Ermak DL, Buckholz H. Numerical integration of the Langevin equation: Monte Carlo simulation. J Comp Physiol. 1980; 35:169–182.
89. Everard ML, Devadason SG, Le Souef PN. Flow early in the inspiratory manoeuver affects the aerosol particle size distribution from a Turbuhaler. Respir Med. 1997; 91:624–628. [PubMed: 9488896]
90. Fairchild CI, Stampfer JF. Particle concentration in exhaled breath. Am Ind Assoc J. 1987; 48:948–949.

91. Fazzi P, Borsò E, Albertelli R, Mariani G, Giuntini C. The use of combined single photon emission computed tomography and X-ray computed tomography to assess the fate of inhaled aerosol. Q J Nucl Med Mol Imaging. 2009; 53(4):428–436. [PubMed: 19174757]
92. Fernández Pérez ER, Daniels CE, Schroeder DR, St Sauver J, Hartman TE, Bartholmai BJ, Yi ES, Ryu JH. Incidence, prevalence, and clinical course of idiopathic pulmonary fibrosis: a population-based study. Chest. 2010; 137(1):129–37. [PubMed: 19749005]
93. Ferron GA. The size of soluble aerosol particles as afunction of the humidity of the air Application of the human respiratory tract. J Aerosol Sci. 1977; 8:251–267.
94. Fiegel J, Clarke R, Edwards DA. Airborne infectious disease and the suppression of pulmonary bioaerosols. Drug Discov Today. 2006; 11(1-2):51–57. [PubMed: 16478691]
95. Filipovic, N.; Haberthür, D.; Henry, FS.; Milasinovic, D.; Nikolic, D.; Schittny, J.; Tsuda, A. Am J Respir Crit Care Med. New Orleans: 2010. Recirculation identified in a 3D alveolar duct reconstructed using synchrotron radiation based X-ray tomographic microscopy. abstr
96. Finlay WH, Stapleton KW, Chan HK, Zuberbuhler P, Gonda I. Regional deposition of inhaled hygroscopic aerosols: in vivo SPECT compared with mathematical modeling. J Appl Physiol. 1996; 81(1):374–383. [PubMed: 8828688]
97. Finlay WH. Estimating the type of hygroscopic behavior exhibited by aqueous droplets. J Aerosol Med. 1998; 11(4):221–229. [PubMed: 10346665]
98. Fleming JS, Halson P, Conway J, Moore E, Nassim MA, Hashish AH, Bailey AG, Holgate ST, Martonen TB. Three-dimensional description of pulmonary deposition of inhaled aerosol using data from multimodality imaging. J Nucl Med. 1996; 37(5):873–877. [PubMed: 8965167]
99. Fleming JS, Conway JH, Holgate ST, Moore EA, Hashish AH, Bailey AG, Martonen TB. Evaluation of the accuracy and precision of lung aerosol deposition measurements from planar radionuclide imaging using simulation. Phys Med Biol. 1998; 43(8):2423–2429. [PubMed: 9725617]
100. Fleming JS, Conway JH. Three-dimensional Imaging of aerosol deposition. J Aerosol Med. 2001; 14(2):147–153. [PubMed: 11681647]
101. Fleming J, Conway J, Majoral C, Tossici-Bolt L, Katz I, Caillibotte G, Perchet D, Pichelin M, Muellinger B, Martonen T, Kroneberg P, Apiou-Sbirlea G. The use of combined single photon emission computed tomography and X-ray computed tomography to assess the fate of inhaled aerosol. J Aerosol Med Pulm Drug Deliv. 2011; 24(1):49–60. [PubMed: 21166585]
102. Flotte TR, Laube BL. Gene Therapy in Cystic Fibrosis. Chest. 2001; 120(3 Suppl):124S–131S. [PubMed: 11555567]
103. Foos B, Marty M, Schwartzj, Bennett W, Moya J, Jarabek AM, Salmon AG. Focusing on Children's Inhalation Dosimetry and Health Effects for Risk Assessment: An Introduction Children's Inhalation and Risk Assessment. J Toxic Environ Health Part A. 2008; 71:149–165.
104. Fredberg JJ, Stamenovic D. On the imperfect elasticity of lung tissue. J Appl Physiol. 1989; 67(6):2408–2419. [PubMed: 2606848]
105. Freidlander SK, Wang CS. The Self-Preserving Particle Size Distribution for Coagulation by Brownian Motion. J Colloid and Interface Sci. 1966:22L126–132.
106. Friedlander, SK. Smoke, Dust, and Haze. New York: Wiley; 1977.
107. Fry FA. Black A Regional deposition and clearance of particles in the human nose. J Aerosol Sci. 1973; 4:113–124.
108. Fuchs, NA. The mechanics of aerosols. Oxford: Pergamon Press; 1964.
109. Fung YC. A Model of the Lung Structure and Its Validation. J Appl Physiol. 1988; 64:2132–2141. [PubMed: 3391912]
110. Gallily I, Eisner AD. On the Orderly Nature of the Motion of Nonspherical Aerosol Particles I Deposition from a Laminar Flow. J Colloid Interface Sci. 1979; 68(2):320–337.
111. Garcia GJ, Rhee JS, Senior BA, Kimbell JS. Septal deviation and nasal resistance: an investigation using virtual surgery and computational fluid dynamics. Am J Rhinol Allergy. 2010; 24(1):e46–53. [PubMed: 20109325]
112. Gebhart J, Heyder J, Stahlhofen W. Use of aerosols to estimate pulmonary air-space dimensions. J Appl Physiol. 1981; 51(2):465–76. [PubMed: 7263453]

113. Gebhart J, Anslem A, Heyder J, Stahlhofen W. The human lung as aerosol particle generator. J Aerosol Med. 1988; 1:196–197. abstr.
114. Gehr P, Bachofen M, Weibel ER. The normal human lung: ultrastructure and morphometric estimation of diffusion capacity. Respir Physiol. 1978; 32:121–140. [PubMed: 644146]
115. Gehr, P.; Heyder, J. Lung biology in health and disease series. Vol. 143. Marcel Dekker; New York: 2000. Particle-Lung Interactions.
116. Geiser M, Casaulta M, Kupferschmid B, Schulz H, Semmler-Behnke M, Kreyling W. The role of macrophages in the clearance of inhaled ultrafine titanium dioxide particles. Am J Respir Cell Mol Biol. 2008; 38(3):371–376. [PubMed: 17947511]
117. Gil J, Weibel ER. Morphological study of pressure-volume hysteresis in rat lungs fixed by vascular perfusion. Respiratory Physiol. 1972; 15:190–213.
118. Gil J, Bachofen H, Gehr P, Weibel ER. Alveolar volume-surface area relation in air and saline-filled lungs fixed by vascular perfusion. J Appl Physiol. 1979; 45(5):990–1001. [PubMed: 511725]
119. Godleski, JJ.; Clarke, RE. Systemic responses to inhaled ambient particles: Pathophysiologic mechanisms and cardiopulmonary effects. In: Gehr, P.; Heyder, J., editors. Particle-Lung Interactions. Marcel Dekker; 1999. p. 577-601.Lung biology in health and disease series
120. Godleski JJ. Responses of the heart to ambient particle inhalation. Clin Occup Environ Med. 2006; 5(4):849–864. [PubMed: 17110296]
121. Gormley PG, Kennedy K. Diffusion from a stream flowing through a cylindrical tube. Proc R Irish Acad. 1949; 52A:163–169.
122. Green, FHY.; Churg, A. Occupational asthma, byssinosis, extrinsic allergic alveolitis and related conditions. In: Churg, A.; Green, FHY., editors. Pathology of Occupational Lung Disease. 2nd. Baltimore, MD: Williams & Wilkins; 1998. p. 403-450.
123. Guha A. Transport and Deposition of Particles in Turbulent and Laminar Flow. Annual Rev Fluid Mech. 2008; 40:311–341.
124. Gupta D, Peters MH. A Brownian dynamics simulation of aerosol deposition onto spherical collectors. J Colloid Interface Sci. 1984; 104:375–389.
125. Haber S, Butler JP, Brenner H, Emanuel I, Tsuda A. Shear flow over a self-similar expanding pulmonary alveolus during rhythmical breathing. J Fluid Mech. 2000; 405:243–268.
126. Haber S, Yitzhak D, Tsuda A. Gravitational deposition in a rhythmically expanding and contracting alveolus. J Appl Physiol. 2003; 95:657–671. [PubMed: 12639848]
127. Haber S, Tsuda A. Cyclic model for particle motion in the pulmonary acinus. J Fluid Mech. 2006; 567:157–184.
128. Haberthür D, Hintermüller C, Tsuda A, Stampanoni M, Schittny JC. Generation of Acinar Skeletons after Synchrotron Radiation Based X-ray Tomographic Microscopy of the Lung Parenchyma. Am J Respir Crit Care Med. 2009a; 179:A3531. abstr.
129. Haberthür D, Semmler-Behnke M, Takenaka S, Kreyling WG, Stampanoni M, Tsuda A, Schittny JC. Multimodal imaging for the detection of sub-micron particles in the gas-exchange region of the mammalian lung. J Phys: Conf Ser. 2009b; 186:012040.
130. Haberthür D, Hintermüller C, Marone F, Schittny JC, Stampanoni M. Radiation dose optimized lateral expansion of the field of view in synchrotron radiation X-ray tomographic microscopy. J Synchrotron Radiation. 2010; 17:1–10.
131. Haefeli-Bleuer B, Weibel ER. Morphometry of the human pulmonary acinus. Anat Rec. 1988; 220(4):401–14. [PubMed: 3382030]
132. Halpern D, Grotberg JB. Surfactant effects on fluidelastic instabilities of liquid-lined flexible tubes: a model of airway closure. J Biomech Eng. 1993; 115:271–277. [PubMed: 8231142]
133. Halpern D, Grotberg JB. Nonlinear saturation of the Rayleigh instability due to oscillatory flow in a liquid-lined tube. J Fluid Mech. 2003; 492:251–270.
134. Hänel G. The real part of the mean complex refractive index and the mean density of sample of atmospheric aerosol particles. Tellus. 1968; 20:371–379.
135. Hänel G. The properties of atmospheric aerosol particles as functions of relative humidity at thermodynamic equilibrium with the surrounding moist air. Adv Geophy. 1976; 19:73–188.

136. Hänel G, Zankl B. Aerosol size and relative humidity: Water uptake by mixtures of salts. Tellus. 1979; 31:478–486.

137. Happel, J.; Brenner, H. Low Reynolds number hydrodynamics. The Hague: Martinus Nijhoff; 1983.

138. Harkema J, Plopper C, Hyde D, St George J, Wilson D, Dungworth D. Response of macaque bronchiolar epithelium to ambient concentrations of ozone. Am J Pathol. 1993; 143:857–866. [PubMed: 8362981]

139. Harkema JR, Keeler G, Wagner J, Morishita M, Timm E, Hotchkiss J, Marsik F, Dvonch T, Kaminski N, Barr E. Effects of concentrated ambient particles on normal and hypersecretory airways in rats. Res Rep Health Eff Inst. 2004; 120:1–68. discussion 69-79. [PubMed: 15543855]

140. Hazel AL, Heil M. Surface-tension-induced buckling of liquid-lined elastic tubes—A model for pulmonary airway closure. Proc R Soc. 2005; 461:1847–1868.

141. Heil M, White JP. Airway closure: surface-tensiondriven non-axisymmetric instabilities of liquid-lined elastic rings. J Fluid Mech. 2002; 462:79–109.

142. Heinemann L, Traut T, Heise T. Time-action profile of inhaled insulin. Diabet Med. 1997; 14:63–72. [PubMed: 9017356]

143. Henry FS, Butler JP, Tsuda A. Kinematically irreversible flow and aerosol transport in the pulmonary acinus: a departure from classical dispersive transport. J Appl Physiol. 2002; 92:835–845. [PubMed: 11796699]

144. Henry FS, Laine-Pearson FE, Tsuda A. Hamiltonian chaos in a model alveolus. ASME J Biomech Eng. 2009; 131(1):011006.

145. Henry FS, Tsuda A. Flow and particle tracks in model acini. ASME J Biomech Eng. 2010; 132(10):101001.

146. Heyder J. Gravitational deposition of aerosol particles within a system of randomly oriented tubes. J Aerosol Sci. 1975; 6:133–137.

147. Heyder J, Gebhart J. Gravitational deposition of particles from laminar aerosol flow through inclined circular tubes. J Aerosol Sci. 1977; 8:289–295.

148. Heyder J, Gebhart J, Rudolf G, Schiller CF, Stahlhofen W. Deposition of particles in the human respiratory tract in the size range 0.005–15 μm. J Aerosol Sci. 1986; 17:811–25.

149. Heyder J, Blanchard D, Feldman HA, Brain JD. Convective mixing in human respiratory tract: estimates with aerosol boli. J Appl Physiol. 1988; 64(3):1273–1278. [PubMed: 3366742]

150. Hickey AJ, Martonen TB. Behavior of hygroscopic pharmaceutical aerosols and the influence of hydrophobic additives. Pharm Res. 1993; 10(1):1–7. [PubMed: 8430044]

151. Hinds, WC. Aerosol Technology. John Wiley and Sons; New York: 1983.

152. Hogg JC, van Eeden S. Pulmonary and systemic response to atmospheric pollution. Respirology. 2009; 14(3):336–46. [PubMed: 19353772]

153. ICRP Publication 66: Human respiratory tract model for radiological protection. A report of a Task Group of the International Commission on Radiological Protection. Ann ICRP. 1994; 24(1-3):1–482.

154. Ilowite JS, Gorvoy JD, Smaldone GC. Quantitative deposition of aerosolized gentamicin in cystic fibrosis. Am Rev Respir Dis. 1987; 136(6):1445–9. [PubMed: 3688646]

155. Ingenito EP, Solway J, McFadden ER Jr, Pichurko BM, Cravalho EG, Drazen JM. Finite difference analysis of respiratory heat transfer. J Appl Physiol. 1986; 61(6):2252–2259. [PubMed: 3804930]

156. Ingenito EP, Solway J, McFadden ER Jr, Pichurko B, Bowman HF, Michaels D, Drazen JM. Indirect assessment of mucosal surface temperatures in the airways: theory and tests. J Appl Physiol. 1987; 63(5):2075–2083. [PubMed: 3693240]

157. Ingham DB. Diffusion of aerosols from a stream flowing through a cylindrical tube. J Aerosol Sci. 1975; 6:125–132.

158. Inthavong K, Choi LT, Tu J, Ding S, Thien F. Micron particle deposition in a tracheobronchial airway model under different breathing conditions. Med Eng Phys. 2010; 32(10):1198–1212. [PubMed: 20855226]

159. Jakob, M. Heat Transfer. Vol. 1. New York: Wiley; 1949. p. 451-464.

160. Jendle JH, Karlberg BE. Intrapulmonary administration of insulin to healthy volunteers. J Intern Med. 1996; 240:93–98. [PubMed: 8810935]

161. Johnson GR, Morawska L. The mechanism of breath aerosol formation. J Aerosol Med Pulm Drug Deliv. 2009; 22(3):229–237. [PubMed: 19415984]

162. Johnson M, Kamm R, Ho LW, Shapiro A, Pedley TJ. The nonlinear growth of the surface-tension-driven instabilities of a thin annular film. J Fluid Mech. 1991; 233:141–156.

163. Kamm RD, Bullister ET, Keramidas C. The effect of a turbulent jet on gas transport during oscillatory flow. J Biomech Eng. 1986; 108(3):266–272. [PubMed: 3747470]

164. Kamm RD, Schroter RC. Is airway closure caused by liquid film instability? Respir Physiol. 1989; 75:141–156. [PubMed: 2711049]

165. Kesavanthan J, Bascom R, Swift DL. The effect of nasal passage characteristics on particle deposition. J Aerosol Med. 1998; 11:27–39.

166. Kesavanathan J, Bascom R, Laube B, Swift DL. The relationship between particle deposition in the anterior nasal passage and nasal passage characteristics. J Aerosol Med. 2000; 13(1):17–23. [PubMed: 10947320]

167. Kim CS, Brown LK, Lewars GG, Sackner MA. Deposition of aerosol particles and flow resistance in mathematical and experimental airway models. J Appl Physiol. 1983; 55(1):154–163. [PubMed: 6885565]

168. Kim CS, Abraham WM, Chapman GA, Sackner MA. Influence of two phase gas liquid interaction on aerosol deposition in airways. Am Rev Respir Dis. 1985; 131:618–623. [PubMed: 3994158]

169. Kim CS, Eldridge MA. Aerosol deposition in the airway model with excessive mucus secretions. J Appl Physiol. 1985; 59:1766–1772. [PubMed: 4077785]

170. Kim CS. Aerosol deposition in the lung with obstructed airways. J Aerosol Med. 1989; 2:111–120.

171. Kim CS, Iglesias AJ. Deposition of inhaled particles in bifurcating airway models: I inspiratory deposition. J Aerosol Med. 1989; 2:1–14.

172. Kim CS, Iglesias AJ, Garcia L. Deposition of inhaled particles in bifurcating airway models: II. expiratory deposition. J Aerosol Med. 1989; 2:15–27.

173. Kim CS, Hu SC, DeWitt P, Gerrity TR. Assessment of regional deposition of inhaled particles in human lungs by serial bolus delivery method. J Appl Physiol. 1996; 81(5):2203–2013. [PubMed: 8941546]

174. Kim CS, Kang TC. Comparative measurement of lung deposition of inhaled fine particles in normal subjects and patients with obstructive airway disease. Am J Respir Crit Care Med. 1997; 155:899–905. [PubMed: 9117024]

175. Kim CS, Hu SC. Regional deposition of inhaled particles in human lungs: comparison between men and women. J Appl Physiol. 1998; 84(6):1834–1844. [PubMed: 9609774]

176. Kim CS, Fisher DM. Deposition characteristics of aerosol particles in sequentially bifurcating airway models. Aerosol Sci Technol. 1999; 31:198–220.

177. Kim CS. Methods of calculating lung delivery and deposition of aerosol particles. Respir Care. 2000; 45(6):695–711. [PubMed: 10894462]

178. Kim CS, Jaques PA. Respiratory dose of inhaled ultrafine particles in healthy adults. Phil Trans Roy Soc London A. 2000; 358:2693–2705.

179. Kim CS, Hu SC. Total respiratory tract deposition of fine micrometer-sized particles in healthy adults: empirical equations for sex and breathing pattern. J Appl Physiol. 2006; 101:401–412. [PubMed: 16849812]

180. Kim CS. Deposition of aerosol particles in human lungs: in vivo measurement and modeling. Biomarkers. 2009; 14(S1):54–58. [PubMed: 19604060]

181. Kitaoka H, Nieman GF, Fujino Y, Carney D, DiRocco J, Kawase I. A 4-dimensional Model of the Alveolar Structure. J Physiol Sci. 2007; 57(3):175–185. [PubMed: 17540054]

182. Kleinerman J, Green F, Harley RA, Lapp L, Laqueur L, Laqueur W, Naeye RL, Taylor G, Wiot J, Wyatt J. Pathology standards for coal worker's pneumoconiosis. (A report of the Pneumoconiosis Committee of the College of American Pathologists.). Arch Pathol Lab Med. 1979; 101:375–431.

183. Kleinstreuer C, Zhang Z, Zheng L. Modeling airflow and particle transport/deposition in pulmonary airways. Respir Physiol Neurobiol. 2008; 163:128–138. [PubMed: 18674643]

184. Kleinstreuer C, Zhang Z. Airflow and particle transport in the human respiratory system. Annual Review of Fluid Mechanics. 2010; 42:301–34.

185. Knowles M, Boucher RC. Mucus clearance as a primary innate defense mechanism for mammalian airways. J Clin Invest. 2002; 109(5):571–577. [PubMed: 11877463]

186. Kojic M, Tsuda A. Gravitational Deposition of Aerosols from oscillatory pipe flows. J Aerosol Sci. 2004; 35(2):245–261.

187. Kojic M, Butler JP, Vlastelica I, Stojanovic B, Rankovic V, Tsuda A. Geometric Hysteresis of Alveolated Ductal Architecture. ASME, J Biomech Eng. 2011; 133(11):111005-1–111005-11.

188. Kraft M, Djukanovic R, Wilson S, Holgate ST, Martin RJ. Alveolar tissue inflammation in asthma. Am J Respir Crit Care Med. 1996; 154:1505–1510. [PubMed: 8912772]

189. Kreyling WG, Blanchard JD, Godleski JJ, Haeussermann S, Heyder J, Hutzler P, Schulz H, Sweeney TD, Takenaka S, Ziesenis A. Anatomic localization of 24- and 96-h particle retention in canine airways. J Appl Physiol. 1999; 87(1):269–284. [PubMed: 10409585]

190. Kreyling WG, Semmler-Behnke M, Möller W. Ultrafine particle-lung interactions: does size matter? J Aerosol Med. 2006; 19(1):74–83. [PubMed: 16551218]

191. Kreyling, WG.; Möller, W.; Semmler-Behnke, M.; Oberdörster, G. Paricle dosimetry: Deposition and clearance from the respiratory tract and translocation towards extra-pulmonary sites. In: Donaldson, K.; Borm, P., editors. Particle toxicology. CRC Press. aylor & FrancisT; New York: 2007. p. 47-74.Chap. 3

192. Kumar H, Tawhai MH, Hoffman EA, Lin CL. The effects of geometry on airflow in the acinar region of the human lung. J Biomech. 2009; 42:1635–1642. [PubMed: 19482288]

193. Kumar H, Tawhai MH, Hoffman EA, Lin CL. Steady streaming: A key mixing mechanism in low-Reynolds-number acinar flows. Phys Fluids. 2011; 23(4):41902.

194. Labiris NR, Dolovich MB. Pulmonary drug delivery Part I: Physiological factors affecting therapeutic effectiveness of aerosolized medications. Br J Clin Pharmacol. 2003a; 56:588–599. [PubMed: 14616418]

195. Labiris NR, Dolovich MB. Pulmonary drug delivery Part II: The role of inhalant delivery device and drug formations in therapeutic effectiveness of aerosolized medications. Br J Clin Pharmacol. 2003b; 56:600–612. [PubMed: 14616419]

196. Laine-Pearson FE, Hydon PE. Particle transport in a moving corner. J Fluid Mech. 2006; 559:379–390.

197. Landahl HD. On the removal of air-borne droplets by the human respiratory tract. I. The lung. Bull Math Biophys. 1950; 12:43–56.

198. Langrish JP, Mills NL, Newby DE. Air pollution: the new cardiovascular risk factor. Intern Med J. 2008; 38(12):875–878. [PubMed: 19120545]

199. Laube BL, Swift DL, Wagner HN, Norman PS, Adams GKI. The effect of bronchial obstruction on central airway deposition of a saline aerosol in patients with asthma. Am Rev Respir Dis. 1986; 133:740–743. [PubMed: 3706880]

200. Laube BL, Georgopoulos A, Adams GKI. Preliminary study of the efficacy of insulin aerosol delivered by oral inhalation in diabetic patients. JAMA. 1993; 269:2106–2109. [PubMed: 8385716]

201. Lee DY, Lee JW. Characteristics of particle transport in an expanding or contracting alveolated tube. J Aerosol Sci. 2003; 34:1193–1215.

202. Lee JH, Na Y, Kim SK, Chung SK. Unsteady flow characteristics through a human nasal airway. Respir Physiol Neurobiol. 2010; 172(3):136–146. [PubMed: 20471501]

203. Leith, DE.; Butler, JP.; Sneddon, SL.; Brain, JD. Cough. In: Fishman, AP., editor. Handbook of Physiology, The Respiratory System. Vol. III. Bethesda, MD: 1986. p. 315-336.Sect. 3Chapt. 20Am Physiol Soc

204. Leong SC, Chen XB, Lee HP, Wang DY. A review of the implications of computational fluid dynamic studies on nasal airflow and physiology. Rhinology. 2010; 48(2):139–145. [PubMed: 20502749]

205. Li A, Ahmadi G. Computer Simulation of Particle Deposition in the Upper Tracheobronchial Tree. Aerosol Sci Technol. 1995; 23:201–223.

206. Lin CL, Tawhai MH, McLennan G, Hoffman EA. Characteristics of the turbulent laryngeal jet and its effect on airflow in the human intra-thoracic airways. Respir Physiol Neurobiol. 2007; 157(2-3):295–309. [PubMed: 17360247]

207. Ling SH, van Eeden SF. Particulate matter air pollution exposure: role in the development and exacerbation of chronic obstructive pulmonary disease. Int J Chron Obstruct Pulmon Dis. 2009; 4:233–43. [PubMed: 19554194]

208. Liu YA, Matida EA, Johnson MR. Experimental measurements and computational modeling of aerosol deposition in the Carleton-Civic standardized human nasal cavity. J Aerosol Sci. 2010; 41(6):569–586.

209. Lynch I, Dawson KA. Protein-nanoparticle interactions. Nano Today. 2008; 3:40–47.

210. Macklem PT, Proctor DF, Hogg JC. Stability of peripheral airways. Respir Phsysiol. 1970; 8:191–203.

211. Macklem PT. Airway obstruction and collateral ventilation. Physiol Rev. 1971; 51:368–436. [PubMed: 4928122]

212. Mak JCW, Barnes PJ. Autoradiographic visualization of muscarinic receptor subtypes in human and guinea pig lung. Am Rev Respir Dis. 1990; 141:1559–1568. [PubMed: 2350099]

213. Mak JCW, Grandordy B, Barnes PJ. High affinity [^{3}H] formoterol binding sites in lung: characterization and autoradiographic mapping. Eur J Pharmacol. 1994; 269:35–41. [PubMed: 7828656]

214. Malashenko A, Tsuda A, Haber S. Propagation and Breakup of Liquid Menisci and Aerosol Generation in Small Airways. J Aerosol Med Pulm Drug Deliv. 2009; 22(4):341–353. [PubMed: 19580367]

215. Mandelbrot, BB. The fractal geometry of nature. Freeman; San Francisco: 1982.

216. Matsui Y, Sakai N, Tsuda A, Tarada Y, Takaoka M, Fujimaki H, Uchiyama I. Tracking the pathway of diesel exhaust particles from the nose to the brain by X-ray florescence analysis. Spectrochimica Acta Part B. 2009; 64:796–801.

217. Maynard A. Nanotechnology:assessing the risks. Nanotoday. 2006a; 1:22.

218. McFadden ER Jr, Denison DM, Waller JF, Assoufi B, Peacock A, Sopwith T. Direct recordings of the temperatures in the tracheobronchial tree in normal man. J Clin Invest. 1982; 69(3):700–705. [PubMed: 7061708]

219. McFadden ER Jr, Pichurko BM, Bowman HF, Ingenito E, Burns S, Dowling N, Solway J. Thermal mapping of the airways in humans. J Appl Physiol. 1985; 58(2):564–570. [PubMed: 3980358]

220. McMahon, TA.; Brain, JD.; LeMott, S. Species differences in aerosol deposition. In: Walton, WH., editor. Inhaled Particles. Vol. IV. Oxford, UK: Pergamon; 1977. p. 23-33.

221. McQuarrie, DA. StatisticaL Mechanics. New York: Harper Row; 1976.

222. Miki H, Butler JP, Rogers RA, Lehr JL. Geometric hysteresis in pulmonary surface-to-volume ratio during tidal breathing. J Appl Physiol. 1993; 75:1630–1636. [PubMed: 8282613]

223. Millikan R. Coefficients of Slip in Gases and the Law of Reflection of Molecules from the Surfaces of Solids and Liquids. Phys Rev. 1923; 21:217–238.

224. Mills NL, Donaldson K, Hadoke PW, Boon NA, MacNee W, Cassee FR, Sandström T, Blomberg A, Newby DE. Adverse cardiovascular effects of air pollution. Nat Clin Pract Cardiovasc Med. 2009; 6(1):36–44. [PubMed: 19029991]

225. Möller W, Felten K, Sommerer K, Scheuch G, Meyer G, Meyer P, Häussinger K, Kreyling WG. Deposition, retention, and translocation of ultrafine particles from the central airways and lung periphery. Am J Respir Crit Care Med. 2008; 77(4):426–32. [PubMed: 17932382]

226. Möller W, Meyer G, Scheuch G, Kreyling WG, Bennett WD. Left-to-right asymmetry of aerosol deposition after shallow bolus inhalation depends on lung ventilation. J Aerosol Med Pulm Drug Deliv. 2009; 22(4):333–339. [PubMed: 19580369]

227. Moriarty JA, Grotberg JB. Flow-induced instabilities of a mucus-serous bilayer. J Fluid Mech. 1999; 397:1–22.

228. Morrow PE. Factors determining hygroscopic aerosol deposition in airways. Physiol Rev. 1986; 66(2):330–376. [PubMed: 3515373]

229. Mortola, JP. Respiratory physiology of newborn mammals: a comparative perspective. The Johns Hopkins University Press; 2001.

230. Mühlfeld C, Gehr P, Rothen-Rutishauser B. Translocation and cellular entering mechanisms of nanoparticles in the respiratory tract. Swiss Med Wkly. 2008a; 138(27-28):387–391. [PubMed: 18642134]

231. Mühlfeld C, Rothen-Rutishauser B, Blank F, Vanhecke D, Ochs M, Gehr P. Interactions of nanoparticles with pulmonary structures and cellular responses. Am J Physiol Lung Cell Mol Physiol. 2008b; 294(5):L817–L829. [PubMed: 18263666]

232. Nazridoust K, Asgharian B. Unsteady-state airflow and particle deposition in a three-generation human lung geometry. Inhal Toxicol. 2008; 20(6):595–610. [PubMed: 18444012]

233. Newman SP. Spacer devices for metered dose inhalers. Clin Pharmacokinet. 2004a; 43(6):349–360. [PubMed: 15086274]

234. Newman SP. Newman SP Dry powder inhalers for optimal drug delivery. Expert Opin Biol Ther. 2004b; 4(1):23–33. [PubMed: 14680466]

235. Newman SP. Principles of Metered-Dose Inhaler Design. RESP CARE. 2005; 50(9):1177–1190.

236. Niewoehner DE, Kleinerman J, Rice DB. Pathologic changes in the peripheral airways of young cigarette smokers. N Engl J Med. 1974; 291(15):755–758. [PubMed: 4414996]

237. Nowak N, Kakade PP, Annapragada AV. Computational fluid dynamics simulation of airflow and aerosol deposition in human lungs. Ann Biomed Eng. 2003; 31(4):374–90. [PubMed: 12723679]

238. Oberdörster G, Sharp Z, Atudorei V, Elder A, Gelein R, Kreyling WG, Cox C. Translocation of inhaled ultrafine particles to the brain. Inhal Toxicol. 2004; 16(6-7):437–445. [PubMed: 15204759]

239. Oberdörster G, Stone V, Donaldson K. Toxicology of nanoparticles: A historical perspective. Nanotoxicology. 2007; 1(1):2–25.

240. O'Callaghan, C.; Wright, P. The metered-dose inhaler. In: Bisgaard, H.; O'Callaghan; Smaldone, GC., editors. Drug delivery to the lung. Vol. 162. Marcel Dekker, Inc; New York: 2002. p. 211-268.Lung Biology in Human and DiseaseChap.7

241. Otis AB, Mckerrow CB, Bartlettra RA, Mead J, Mcilroy MB, Selver-Stone NJ, Radford EP Jr. Mechanical factors in distribution of pulmonary ventilation. J Appl Physiol. 1956; 8(4):427–43. [PubMed: 13286206]

242. Otis DR, Johnson JM, Pedley TJ, Kamm RD. Role of pulmonary surfactant in airway closure: a computational study. J Appl Physiol. 1993; 75:1323–1333. [PubMed: 8226547]

243. Ottino, JM. The Kinematics of Mixing: Stretching, Chaos, and Transport. Cambridge University Press; 1989.

244. Palmes ED. Measurement of pulmonary air spaces using aerosols. Arch Intern Med. 1973; 131:76–79. [PubMed: 4682064]

245. Palmes, ED.; Altshuler, B.; Nelson, N. Deposition of aerosols in human respiratory tract during breath-holding. In: Davies, CN., editor. Inhaled Particles and Vapours. Vol. II. London: Pergamon; 1976. p. 339-347.

246. Papavergos PG, Hedley AB. Particle deposition behavior from turbulent flow. Chem Engng Des. 1984; 62

247. Papineni RS, Rosenthal FS. The size distribution of droplets in the exhaled breath of healthy human subjects. J Aerosol Med. 1997; 10:105–116. [PubMed: 10168531]

248. Parker S, Foat T, Preston S. Towards quantitative prediction of aerosol deposition from turbulent flows. J Aerosol Sci. 2008; 39(2):99–112.

249. Patton JS. Mechanisms of macromolecule absorption by the lungs. Adv Drug Rev. 1996; 19(1):3–36.

250. Patton JS, Fishburn CS, Weers JG. The lungs as a portal of entry for systemic drug delivery. Proc Am Thorac Soc. 2004; 1(4):338–344. [PubMed: 16113455]

251. Patton JS, Byron PR. Inhaling medicines: delivering drugs to the body through the lungs. Nat Rev Drug Discov. Jan; 2007 6(1):67–74. [PubMed: 17195033]
252. Pavia D, Thomson ML, Clarke SW, Shannon HS. Effect of lung function and mode of inhalation on penetration of aerosol into the human lung. Thorax. 1977; 32(2):194–7. [PubMed: 867333]
253. Peccia J, Hernandez M. Photoreactivation in Airborne *Mycobacterium parafortuitum*. Appl Environ Microbiology. 2001; 67(9):4225–4232.
254. Perring S, Summers Q, Fleming JS, Nassim MA, Holgate ST. A new method of quantification of the pulmonary regional distribution of aerosols using combined CT and SPECT and its application to nedocromil sodium administered by metered dose inhaler. Br J Radiol. 1994; 67(793):46–53. [PubMed: 8298874]
255. Peters A, Perz S, Doring A, Stieber J, Koenig W, Wichmann HE. Increases in heart rate during an air pollution episode. Am J Epidemiol. 1999; 150(10):1094–1098. [PubMed: 10568625]
256. Pich J. Theory of gravitational deposition of particles from laminar flows in channels. J Aerosol Sci. 1972; 3:351–361.
257. Pinkerton KE, Green FH, Saiki C, Vallyathan V, Plopper CG, Gopal V, Hung D, Bahne EB, Lin SS, Ménache MG, Schenker MB. Distribution of particulate matter and tissue remodeling in the human lung. Environ Health Perspect. 2000; 108(11):1063–1069. [PubMed: 11102298]
258. Plopper, C. Structural methods for studying bronchiolar epithelial cells. In: Gil, J., editor. Models of Lung Disease: Microscopy and Structural Methods. New York: Marcel Dekker, Inc; 1990. p. 537-559.
259. Plopper, CG.; Ten Have-Opbroek, A. Anatomical and histological classification of the bronchioles. In: Epler, G., editor. Diseases of Bronchioles. New York: Raven Press Ltd; 1995. p. 15-25.
260. Pope CA 3rd, Ezzati M, Dockery DW. Fine-particulate air pollution and life expectancy in the United States. N Engl J Med. 2009; 360:376–386. [PubMed: 19164188]
261. Probstein, RF. Physicochemical Hydrodynamics: An Introduction. New York, NY: John Wiley; 1989.
262. Proctor DF. The naso-oro-pharyngo-laryngeal airway. Eur J Respir Dis Suppl. 1983; 128(Pt 1): 89–96. [PubMed: 6578090]
263. Raghu G, Weycker D, Edelsberg J, Bradford WZ, Oster G. Incidence and prevalence of idiopathic pulmonary fibrosis. Am J Respir Crit Care Med. 2006; 174(7):810–6. [PubMed: 16809633]
264. Robinson RJ, Snyder P, Oldham MJ. Comparison of Particle Tracking Algorithms in Commercial CFD Packages: Sedimentation and Diffusion. Inhal Toxicol. 2007; 19(6-7):517–531. [PubMed: 17497530]
265. Roche N, Chinet T, Huchon G. Ambulatory inhalation therapy in obstructive lung diseases. Respiration. 1997; 64(2):121–130. [PubMed: 9097347]
266. Rodriguez M, Bur S, Favre A, Weibel ER. Pulmonary acinus: geometry and morphometry of the peripheral airway system in rat and rabbit. Am J Anat. 1987; 180(2):143–55. [PubMed: 3673919]
267. Rosenthal FS. Aerosol recovery following breathholding derived from the distribution of chordlengths in pulmonary tissue. J Aerosol Sci. 1989; 20:267–277.
268. Rubin BK. Air and Soul: The Science and Application of Aerosol Therapy. Respir Care. 2010; 55(7):911–912. [PubMed: 20587104]
269. Saldiva PH, Clarke RW, Coull BA, Stearns RC, Lawrence J, Murthy GG, Diaz E, Koutrakis P, Suh H, Tsuda A, Godleski JJ. Lung inflammation induced by concentrated ambient air particles is related to particle composition. Am J Respir Crit Care Med. 2002; 165(12):1610–7. [PubMed: 12070061]
270. Sarnat JA, Holguin F. Asthma and air quality. Curr Opin Pulm Med. 2007; 13(1):63–66. [PubMed: 17133127]
271. Scherer PW, Haselton FR. Convective exchange in oscillatory flow through bronchial-tree models. J Appl Physiol. 1982; 53:1023–1033. [PubMed: 7153112]
272. Scheuch G, Bennett W, Borgström L, Clark A, Dalby R, Dolovich M, Fleming J, Gehr P, Gonda I, O'Callaghan C, Taylor G, Newman S. Deposition, imaging, and clearance: what remains to be done? J Aerosol Med Pulm Drug Deliv Suppl. 2010; 2:S39–57.

273. Schittny, JC.; Burri, PH. Development and growth of the lung. In: Fishman, AP., et al., editors. Fishman's Pulmonary Diseases and Disorders. 4th. McGraw-Hill; New York: 2008. p. 91-114.
274. Schittny, JC.; Haberthür, D.; Semmler-Behnke, M.; Takenaka, S.; Stampanoni, M.; Kreyling, MG.; Tsuda, A. Am J Respir Crit Care Med. New Orleans: 2010. High Resolution 3-dimensional Imaging of Ultrafine Particles in the Lung Parenchyma. abstr
275. Schulz H, Heilmann P, Hillebrecht A, Gebhart J, Meyer M, Piiper J, Heyder J. Convective and diffusive gas transport in canine intrapulmonary airways. J Appl Physiol. 1992; 72:1557–1562. [PubMed: 1592750]
276. Schwartz J. Air pollution and blood markers of cardiovascular risk. Environ Health Perspect. 2001; 109(suppl. 3):405–409. [PubMed: 11427390]
277. Schwartz J. Air pollution and children's health. Pediatrics. 2004; 113(4 Suppl):1037–1043. [PubMed: 15060197]
278. Segal RA, Kepler GM, Kimbell JS. Effects of differences in nasal anatomy on airflow distribution: a comparison of four individuals at rest. Ann Biomed Eng. 2008; 36(11):1870–1882. [PubMed: 18777212]
279. Semmler M, Moeller W, Takenaka S, Schulz H, Tsuda A, Kreyling WG. Is there protection against ultrafine particle deposition in the developing lungs of rats? Am J Resp Critic Care Med. 2005; 171:A236. abstr.
280. Semmler M, Moeller W, Kreyling WG, Schulz H, Takenaka S, Butler JP, Henry FS, Tsuda A. Nanoparticle Delivery in Infant Lungs. Proc Natl Acad Sci USA. 2012; 109(13):5092–5097. [PubMed: 22411799]
281. Shanley KT, Zamankhan P, Ahmadi G, Hopke PK, Cheng YS. Numerical simulations investigating the regional and overall deposition efficiency of the human nasal cavity. Inhal Toxicol. 2008; 20:1093–1100. [PubMed: 18800272]
282. Shapiro M, Goldengberg M. Deposition of glass fiber particles from turbulent air flow in a pipe. J Aersol Sci. 1993; 24(1):65–87.
283. Shi H, Kleinstreuer C, Zhang Z. Modeling of inertial particle transport and deposition in human nasal cavities with wall roughness. J Aerosol Sci. 2007; 38:391–419.
284. Silverman, L.; Billings, CE.; First, MW. Particle size analysis in industrial hygiene. Academic Press; NY: 1971.
285. Sint T, Donohue JF, Ghio AJ. Ambient air pollution particles and the acute exacerbation of chronic obstructive pulmonary disease. Inhal Toxicol. 2008; 20(1):25–29. [PubMed: 18236218]
286. Smaldone GC, Mitzner W, Itoh H. Role of alveolar recruitment in lung inflation: influence on pressure-volume hysterisis. J Appl Physiol. 1983; 55:1321–1332. [PubMed: 6629967]
287. Smith DJ, Gaffney EA, Blake JR. Modelling mucociliary clearance. Respir Physiol Neurobiol. 2008; 163(1-3):178–188. [PubMed: 18439882]
288. Smith JE, Jordan ML. Mathematical and graphical interpretation of the log-normal law for particle size distribution analysis. J Colloid Sci. 1964; 19:549–559.
289. Soltani M, Ahmadi G. Direct numerical simulation of particle entrainment in turbulent channel flow. Phys Fluids. 1995; 7(3):647–657.
290. Solway J, Pichurko BM, Ingenito EP, McFadden ER Jr, Fanta CH, Ingram RH Jr, Drazen JM. Breathing pattern affects airway wall temperature during cold air hyperpnea in humans. Am Rev Respir Dis. 1985; 132(4):853–857. [PubMed: 4051320]
291. Sommerer JC. Fractal tracer distributions in complicated surface flows: an application of random maps to fluid dynamics. Physica D. 1994; 76:85–98.
292. Stone PH, Godleski JJ. First steps toward understanding the pathophysiologic link between air pollution and cardiac mortality. Am Heart J. 1999; 138(5 Pt 1):804–807. [PubMed: 10539808]
293. Suki B, Barabási AL, Hantos Z, Peták F, Stanley HE. Avalanches and power-law behaviour in lung inflation. Nature. 1994; 368(6472):615–618. [PubMed: 8145846]
294. Suki, B.; Bates, JHT.; Frey, U. Complexity and emergent phenomena. In: Fredberg, J.; Sieck, G.; Gerthoffer, W., editors. Comprehensive Physiology, Respiratory Physiology Section. 2011. Amer Physiol Soc, in review

295. Sweeney TD, Brain JD, Tryka AF, Godleski JJ. Retention of inhaled particles in hamsters with pulmonary fibrosis. Am Rev Respir Dis. 1983; 128:138–14. [PubMed: 6191603]
296. Sweeney TD, Brain JD, Leavitt SA, Godleski JJ. Emphysema alters the deposition pattern of inhaled particles in hamsters. Am J Pathol. Jul; 1987 128(1):19–28. [PubMed: 3649192]
297. Sweeney TD, Skornik WA, Brain JD, Hatch V, Godleski JJ. Chronic bronchitis alters the pattern of aerosol deposition in the lung. Am J Respir Crit Care Med. 1995; 151(2 Pt 1):482–8. [PubMed: 7842210]
298. Sznitman J, Heimsch F, Heimsch T, Rusch D, Rösgen T. Three-dimensional convective alveolar flow induced by rhythmic breathing motion of the pulmonary acinus. J Biomech Eng. 2007; 129(5):658–665. [PubMed: 17887891]
299. Sznitman J, Heimsch T, Wildhaber JH, Tsuda A, Rösgen T. Respiratory flow phenomena and gravitational sedimentation in a three-dimensional space-filling model of the pulmonary acinar tree. ASME J Biomech Eng. 2009; 131(3):031010-1–16.
300. Tabor, M. Chaos and IntegrabiZity in NonLinear Dynamics. New York: Wiley; 1989.
301. Tawhai, MH.; Lin, CL.; Hoffman, E. Airway gas flow. In: Fredberg, J.; Sieck, G.; Gerthoffer, W., editors. Handbook of Physiology, Respiratory Physiology Section. 2010. Amer Physiol Soc
302. Taylor, GI. LowReynoldsNumber flow. (16mmfilm). MAEducational Services Inc.; Newton: 1960.
303. Tepper RS, Morgan WJ, Cota K, Taussig LM. Expiratory flow limitation in infants with bronchopulmonary dysplasia. J Pediatr. 1986; 109:1040–6. [PubMed: 3783328]
304. Tippe A, Tsuda A. Recirculating flow in an expanding alveolar model: Experimental evidence of flow-induced mixing of aerosols in the pulmonary acinus. J Aerosol Sci. 2000; 31(8):979–986.
305. Tschanz SA, Makanya AN, Haenni B, Burri PH. Effects of neonatal high-dose short-term glucocorticoid treatment on the lung: a morphologic and morphometric study in the rat. Pediatr Res. 2003; 53:72–80. [PubMed: 12508084]
306. Tsu ME, Babb AL, Ralph DD, Hlastala MP. Dynamics of heat, water, and soluble gas exchange in the human airways: 1. A model study. Ann Biomed Eng. 1988; 16(6):547–571. [PubMed: 3228218]
307. Tsuda A, Kamm RD, Fredberg JJ. Periodic flow at airway bifurcations Part II: Flow partitioning. J Appl Physiol. 1990; 69(2):553–561. [PubMed: 2228865]
308. Tsuda A, Butler JP, Fredberg JJ. Effects of alveolated duct structure on aerosol kinetics: Part I Diffusion in the absence of gravity. J Appl Physiol. 1994a; 76(6):2497–2509. [PubMed: 7928876]
309. Tsuda A, Butler JP, Fredberg JJ. Effects of alveolated duct structure on aerosol kinetics: Part II Gravitational deposition and Inertial impaction. J Appl Physiol. 1994b; 76(6):2510–2516. [PubMed: 7928877]
310. Tsuda A, Henry FS, Butler JP. Chaotic mixing of alveolated duct flow in rhythmically expanding pulmonary acinus. J Appl Physiol. 1995; 79:1055–1063. [PubMed: 8567502]
311. Tsuda A, Otani Y, Butler JP. Acinar flow irreversibility caused by boundary perturbation of reversible alveolar wall motion. J Appl Physiol. 1999; 86(3):977–984. [PubMed: 10066713]
312. Tsuda A, Rogers RA, Hydon PE, Butler JP. Chaotic mixing deep in the lung. Proc Natl Acad Sci. 2002; 99:10173–10178. [PubMed: 12119385]
313. Tsuda A, Filipovic N, Haberthür D, Dickie R, Stampanoni M, Matsui Y, Schittny JC. The Finite Element 3D Reconstruction of the pulmonary acinus imaged by Synchrotron X-ray tomography. J Appl Physiol. 2008a; 105:964–976. [PubMed: 18583378]
314. Tsuda A, Henry FS, Butler JP. Gas and aerosol mixing in the acinus. Respir Physiol Neurobiol. 2008b; 163(1-3):139–49. [PubMed: 18396469]
315. Tsuda A, Laine-Pearson FE, Hydon PE. Why chaotic mixing of particles is inevitable in the deep lung? J Theor Biol. 2011; 286:57–66. [PubMed: 21801733]
316. Tyler WS. Comparative subgross anatomy of lungs. Am Rev Resp Dis. 1983; 128:S32–S36. [PubMed: 6881704]

317. van Ertbruggen C, Hirsch C, Paiva M. Anatomically based three-dimensional model of airways to simulate flow and particle transport using computational fluid dynamics. J Appl Physiol. 2005; 98(3):970–80. [PubMed: 15501925]
318. Venegas JG, Winkler T, Musch G, Vidal Melo MF, Layfield D, Tgavalekos N, Fischman AJ, Callahan RJ, Bellani G, Harris RS. Self-organized patchiness in asthma as a prelude to catastrophic shifts. Nature. 2005; 434(7034):777–82. [PubMed: 15772676]
319. Verbanck, S.; Paiva, M. Gas mixing in the airways and airspaces. In: Fredberg, J.; Sieck, G.; Gerthoffer, W., editors. Comprehensive Physiology, Respiratory Physiology Section. Vol. 1. 2011. p. 835-882.Amer Physiol Soc
320. Wang CS. Gravitational deposition of particles from laminar flows in inclined channels. J Aerosol Sci. 1975; 6:191–204.
321. Wang SM, Inthavong K, Wen J, Tu JY, Xue CL. Comparison of micron- and nanoparticle deposition patterns in a realistic human nasal cavity. Respir Physiol Neurobiol. 2009; 166(3): 142–51. [PubMed: 19442930]
322. Watson EJ. Fluid flow in a model alveolar sac (Appendix). J Appl Physiol. 1974; 37:251.
323. Weibel, ER. Morphometry of the Human Lung. SpringerVerlag/Academic Press; Heidelberg, New York: 1963.
324. Weibel, ER. Functional morphology of lung parenchyma. In: Fishman, AP., editor. Handbook of Physiology, The Respiratory System. Vol. III. Bethesda, MD: 1986. p. 89-111.Sect. 3Chapt. 8Am Physiol Soc
325. Weibel ER, Sapovale B, Filoche M. Design of peripheral airways for efficient gas exchange. Respir Physiol Neurobiol. 2005; 148:3–21. [PubMed: 15921964]
326. Widdicombe JH. Regulation of the depth and composition of airway surface liquid. J Anat. 2002; 201(4):313–318. [PubMed: 12430955]
327. Wilson TA, Bachofen H. A model for mechanical structure of alveolar duct. J Appl Physiol. 1982; 52(4):1064–1070. [PubMed: 7085408]
328. Wood NB. A simple method for the calculation of turbulent deposition to smooth and rough surfaces. J Aerosol Sci. 1981; 12:275–290.
329. Wright JL, Cagle P, Churg A, Colby TV, Myers J. State of the art: diseases of the small airways. Am Rev Respir Dis. 1992; 146:240–262. [PubMed: 1626808]
330. Xi JX, Longest PW, Martonen TB. Effects of the laryngeal jet on nano- and microparticle transport and deposition in an approximate model of the upper tracheobronchial airways. J Appl Physiol. 2008; 104:1761–77. [PubMed: 18388247]
331. Zanen, P.; Laube, BL. Targeting the lungs with therapeutic aerosols, Drug delivery to the lung. In: Bisgaard, H.; O'Callaghan; Smaldone, GC., editors. Lung Biology in Human and Disease. Vol. 162. 2002. p. 211-268.Chap. 7
332. Zeltner TB, Burri PH. The postnatal development and growth of the human lung. II. Morphology. Respir Physiol. 1987; 67(3):269–82. [PubMed: 3575906]
333. Zeltner TB, Caduff JH, Gehr P, Pfenninger J, Burri PH. The postnatal development and growth of the human lung. I. Morphometry. Respir Physiol. 1987; 67(3):247–67. [PubMed: 3575905]
334. Zeltner TB, Sweeney TD, Skornik WA, Feldman HA, Brain JD. Retention and clearance of 0.9-micron particles inhaled by hamsters during rest or exercise. J Appl Physiol. Mar; 1991 70(3): 1137–45. [PubMed: 2032979]
335. Zeman KL, Bennett WD. Growth of the small airways and alveoli from childhood to the adult lung measured by aerosol-derived airway morphometry. J Appl Physiol. 2006; 100:965–971. [PubMed: 16357074]
336. Zeman KL, Wu J, Bennett WD. Targeting aerosolized drugs to the conducting airways using very large particles and extremely slow inhalations. J Aerosol Med Pulm Drug Deliv. 2010; 23(6): 363–369. [PubMed: 20863250]
337. Zhang H, Ahmadi G. Aerosol Particle Transport and Deposition in Vertical and Horizontal Turbulent Duct Flows. J Fluid Mech. 2000; 406:55–80.
338. Zhang L, Asgharian B, Anjilvel S. Inertial and interceptional deposition of fibers in a bifurcating airway. J Aerosol Med. 1996; 9(3):419–430. [PubMed: 10163664]

339. Zhang Z, Kleinstreuer C, Donohue JF, Kim CS. Comparison of micro- and nano-size particle depositions in a human upper airway model. J Aerosol Sci. 2005; 36:211–33.

340. Zhao K, Pribitkin EA, Cowart BJ, Rosen D, Scherer PW, Dalton P. Numerical modeling of nasal obstruction and endoscopic surgical intervention: Outcome to airflow and olfaction. Am J Rhinol. 2006; 20(3):308–316. [PubMed: 16871935]

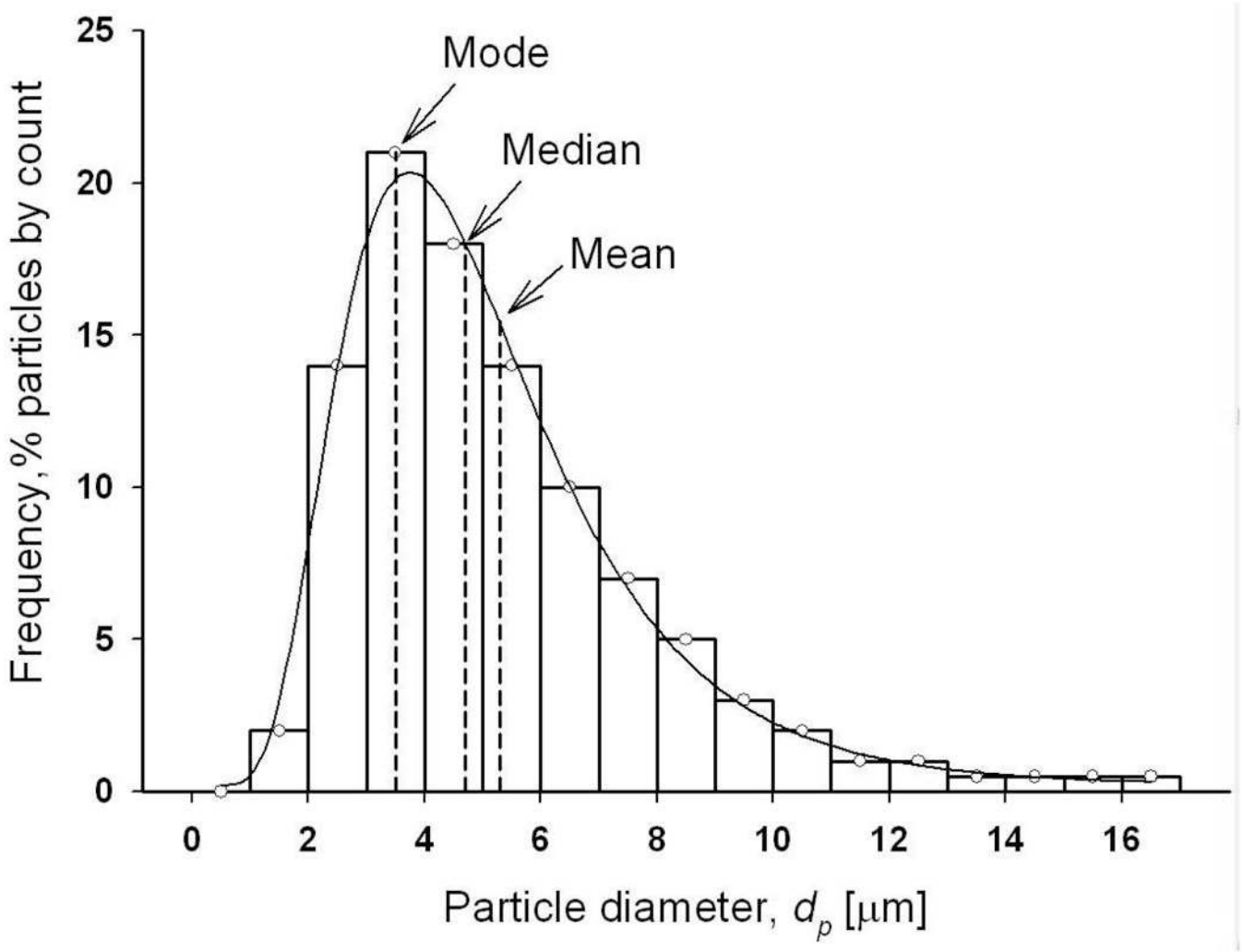

Figure 1.
A Skewed particle size distribution. Re-plotted after Silverman et al. (1971)[284].

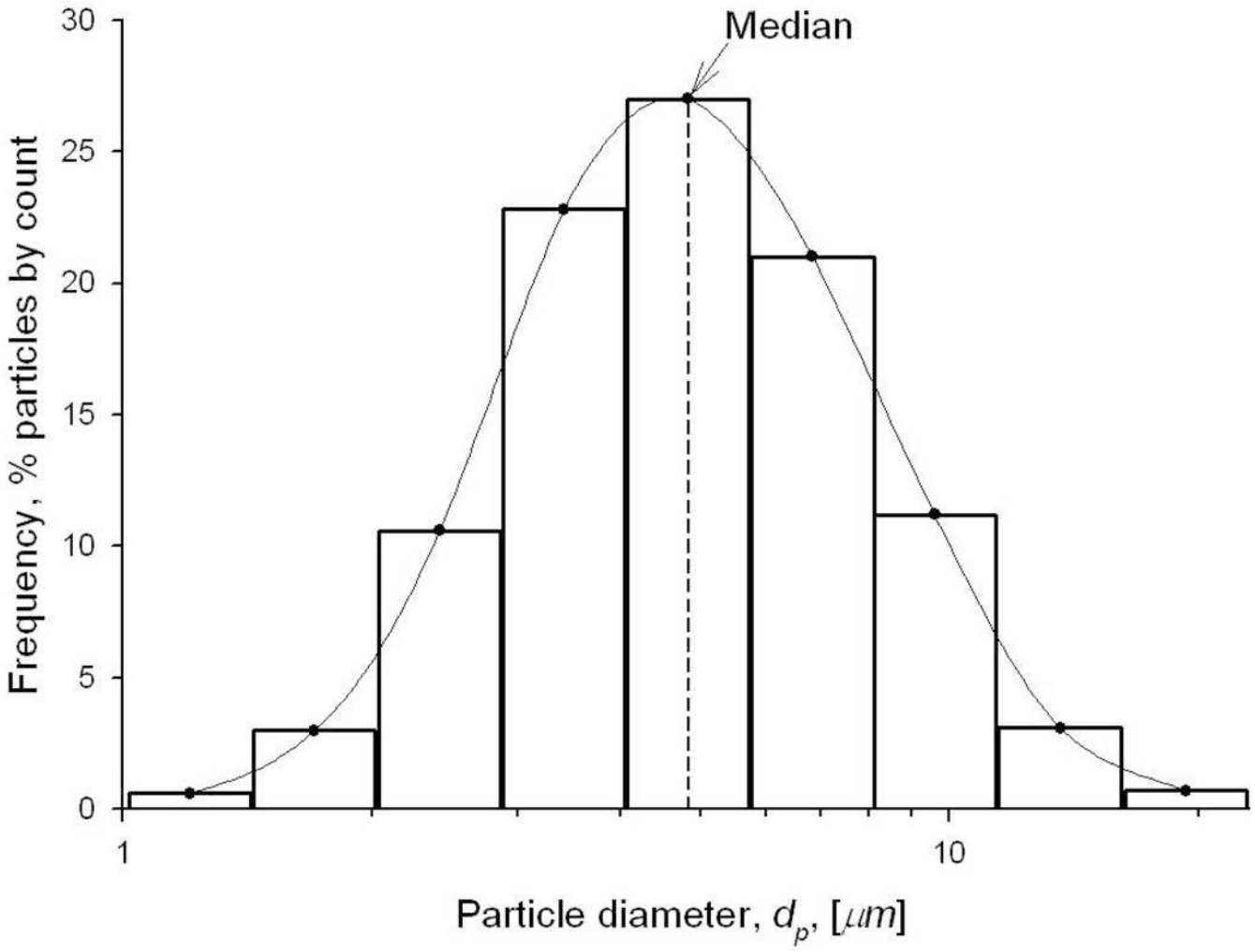

Figure 2.
Lognormal particle size distribution. Re-plotted after Silverman et al. (1971)[284].

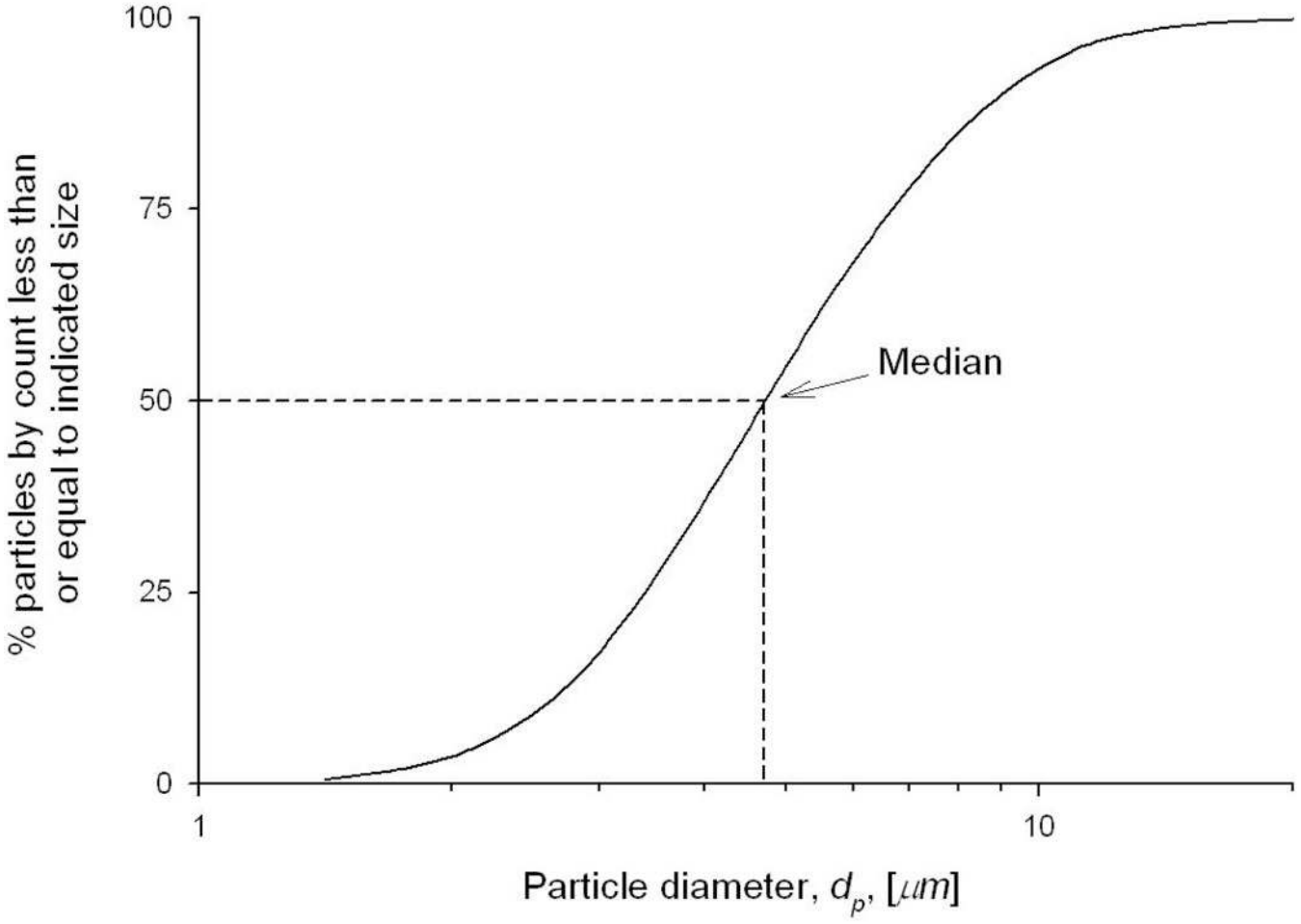

Figure 3.
Cumulative lognormal size distribution. Re-plotted after Silverman et al. (1971)[284].

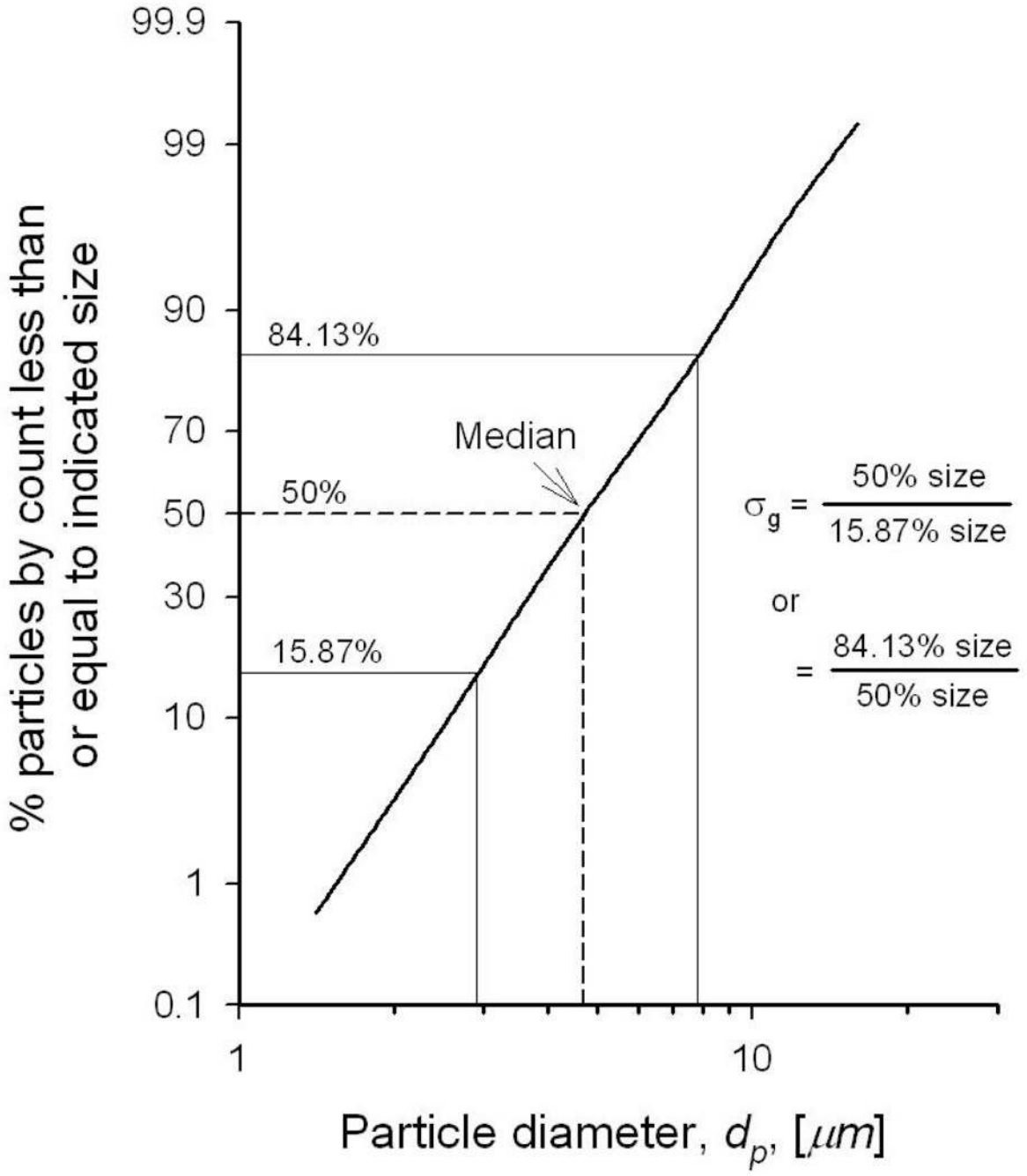

Figure 4.

Cumulative particle size distribution plotted on logarithmic probability graph paper. The spread of the distribution of Fig. 2 or the geometric standard deviation (σ_g), is defined as the ratio of (84.13% size) /(50% size) or (50% size)/(15.87% size). Re-plotted after Silverman et al. (1971)[284].

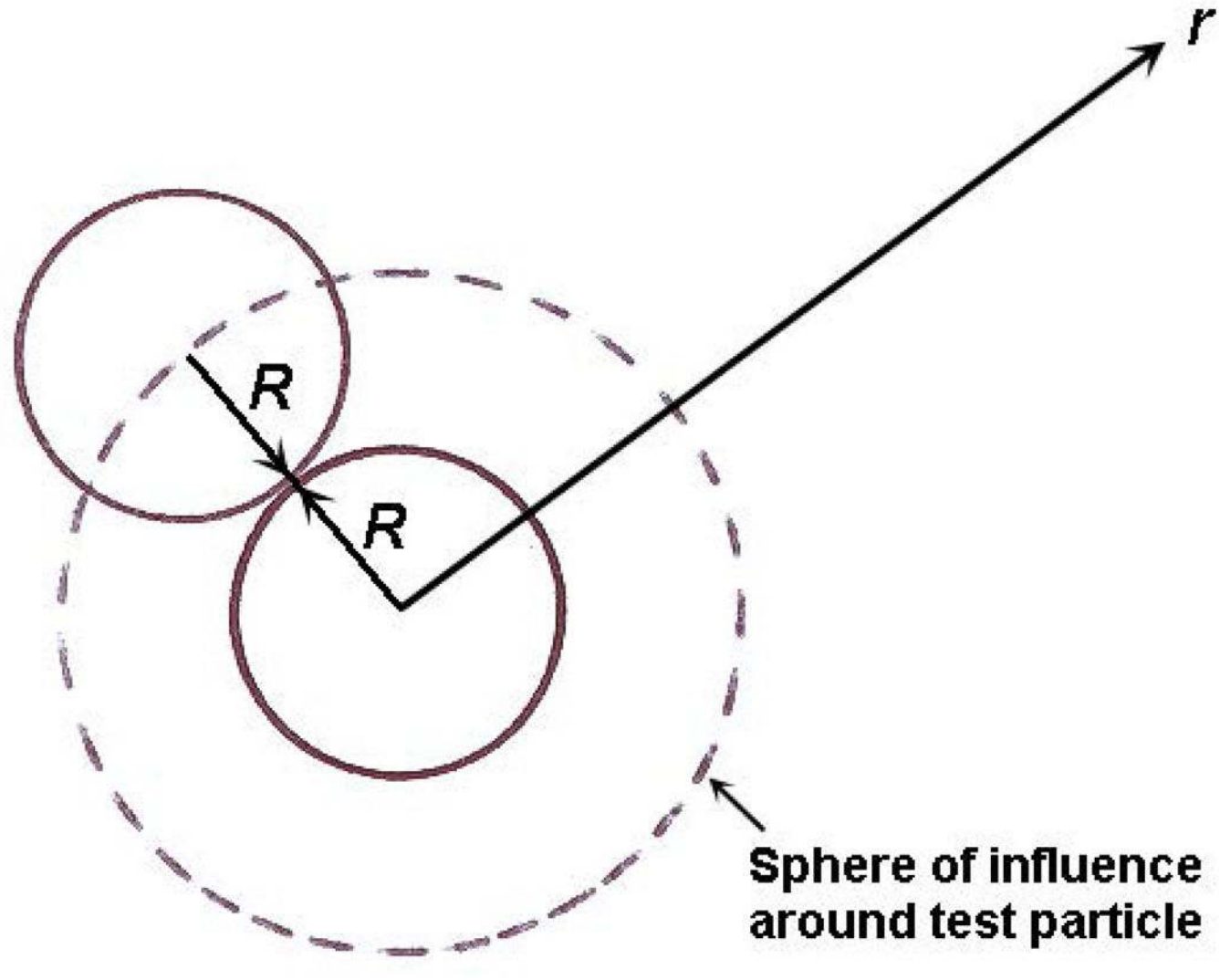

Figure 5.

Smoluchowski's Brownian coagulation. Sphere of influence around test (fixed) particle of radius *R* in collision with moving particles of the same radius *R*. Once particles collide, perfect adhesion is assumed. Modified after Probstein (1989)[261].

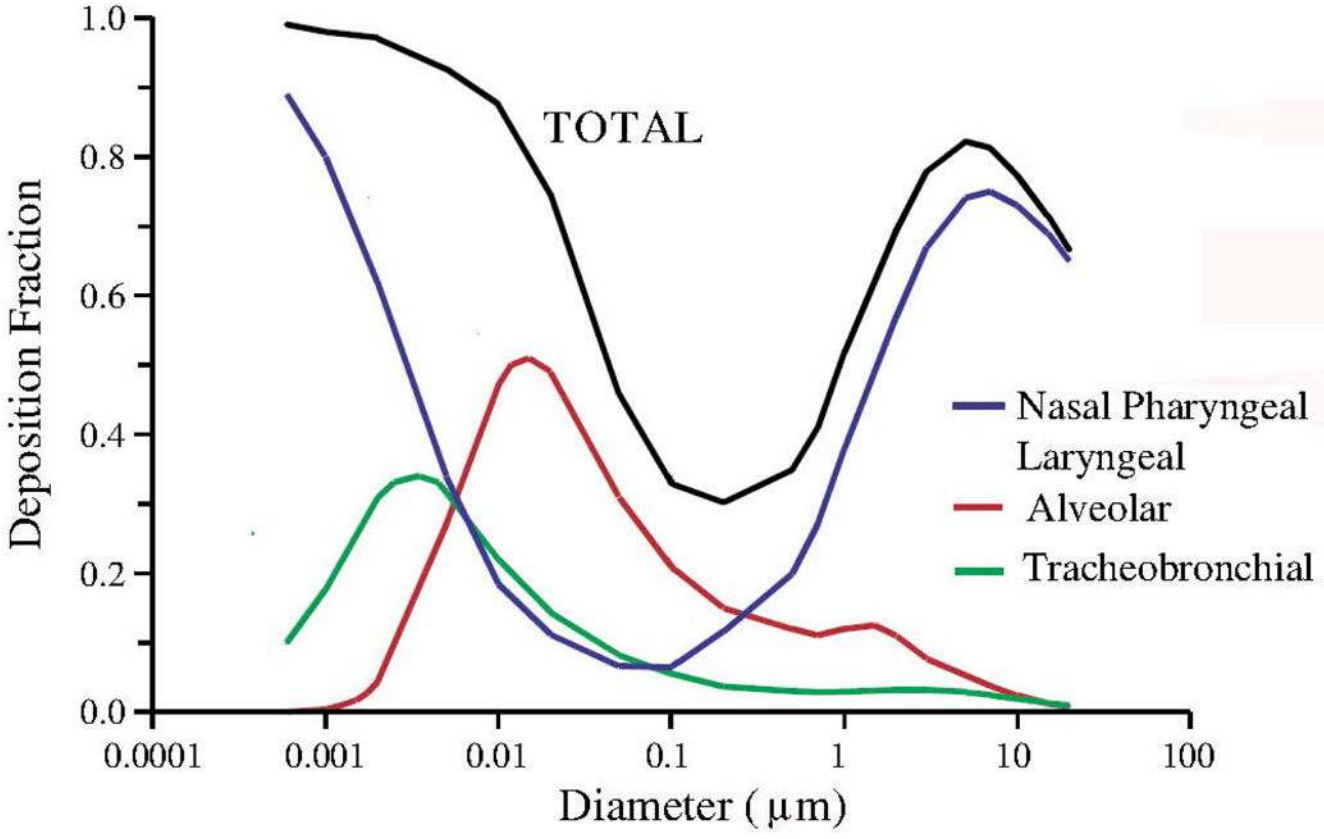

Figure 6.

Total particle deposition in the human respiratory tract and corresponding fractions in the extrathoracic, bronchial, and alveolar region according to ICRP Publication 66 (1994)[153]. Data are shown for two different breathing scenarios: exposure during sleeping (nose breathing), and exposure during heavy exercise (mouth breathing). Adapted from Oberdörster, et al. (2007)[239].

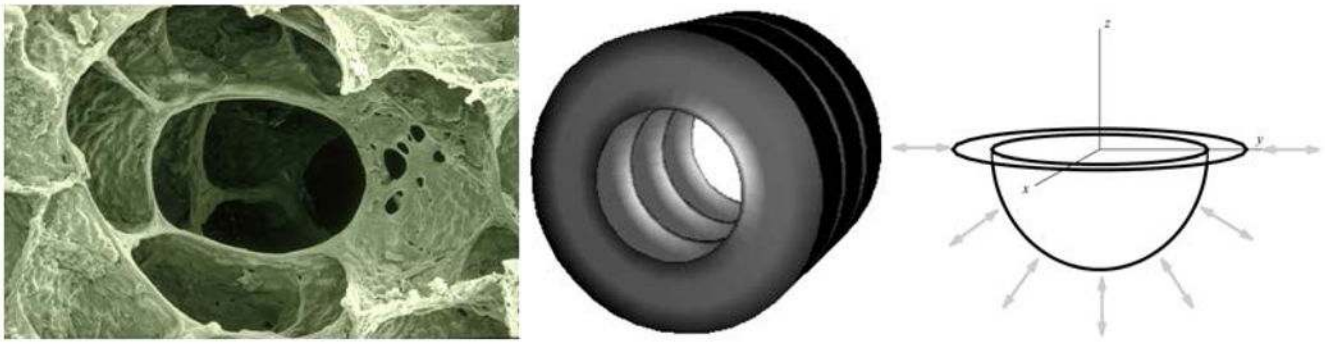

Figure 7.

Alevolar duct. *Left*: Scanning electron micrograph of an alveolar duct surrounded by alveoli. From Gehr et al. (1978)[114], by permission. *Middle*: An axisymmetric alveolated duct model (i.e., a computationally 2D but physically 3D model) used in Tsuda et al. (1994a,b)[308,309]. *Right*: Rhythmically expanding and contracting 3D alveolar duct model used in Haber et al. (2000[125], 2003[126]).

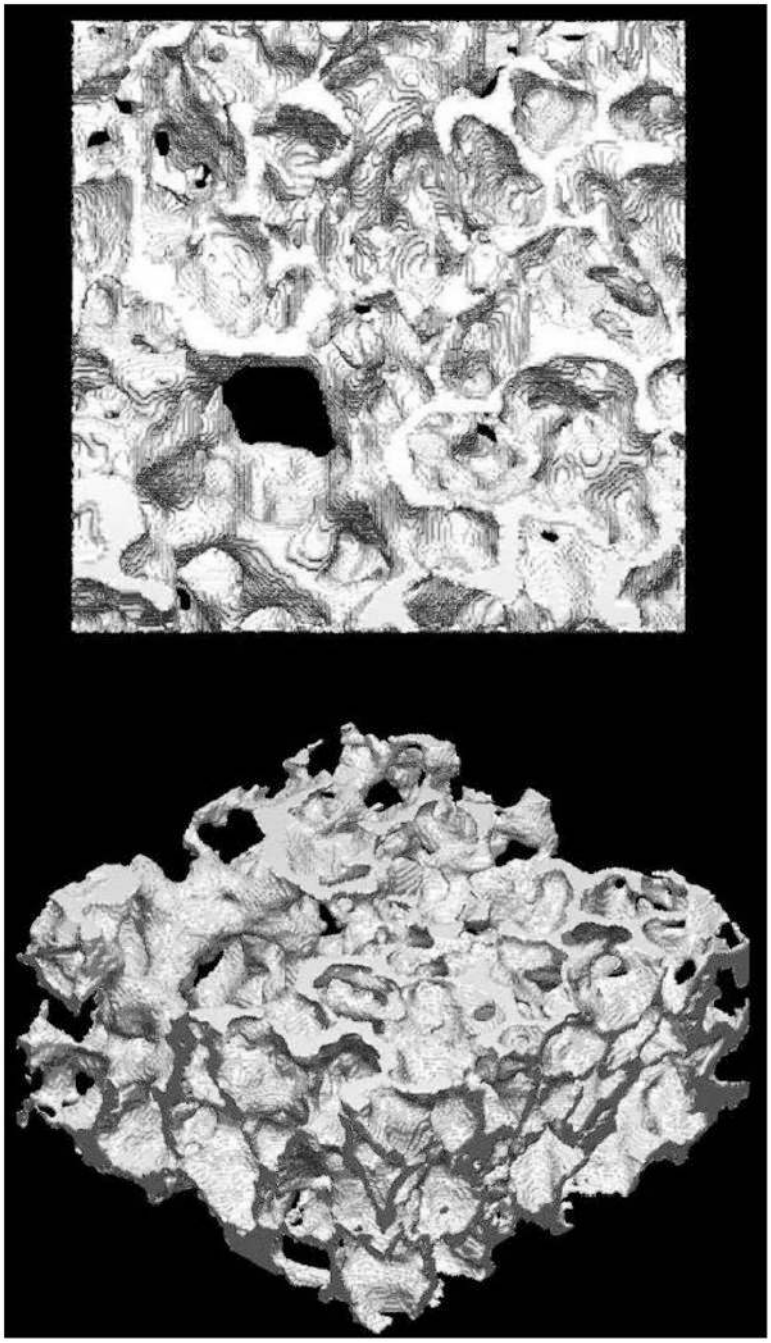

Figure 8.
Three dimensional reconstruction of the parenchyma tissue imaged by synchrotron X-ray tomography. *Upper*: top view. *Lower*: side angle view. From Tsuda et al. (2008a)[313].

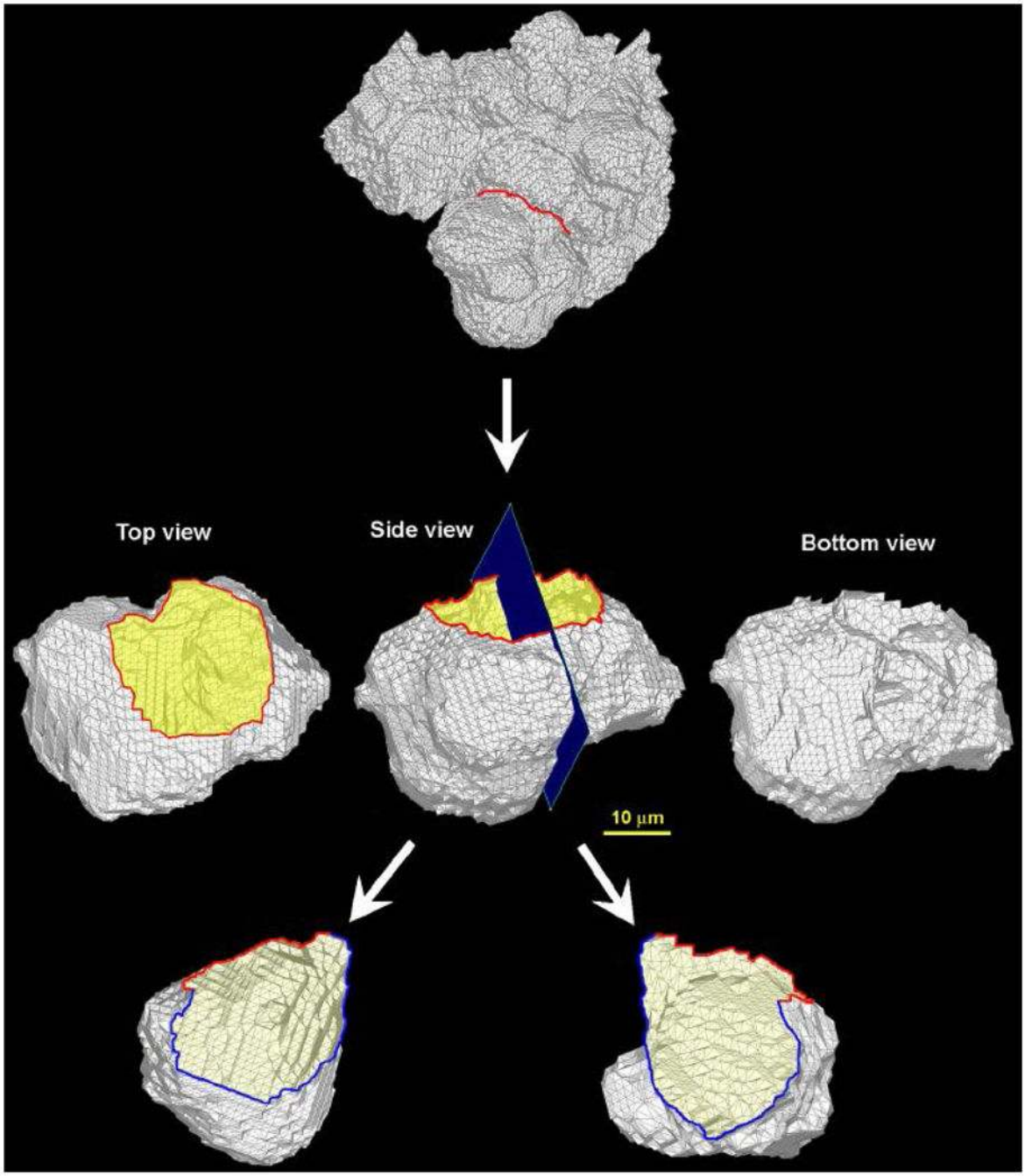

Figure 9.

3D finite element shell model of an alveolus viewed from different angles. *Top*: Region of interest. *Middle*: top view (*left*); side view (*middle*); bottom view (*right*). *Bottom*: alveolar inside views (*left* and *right*). From Tsuda et al. (2008a)[313].

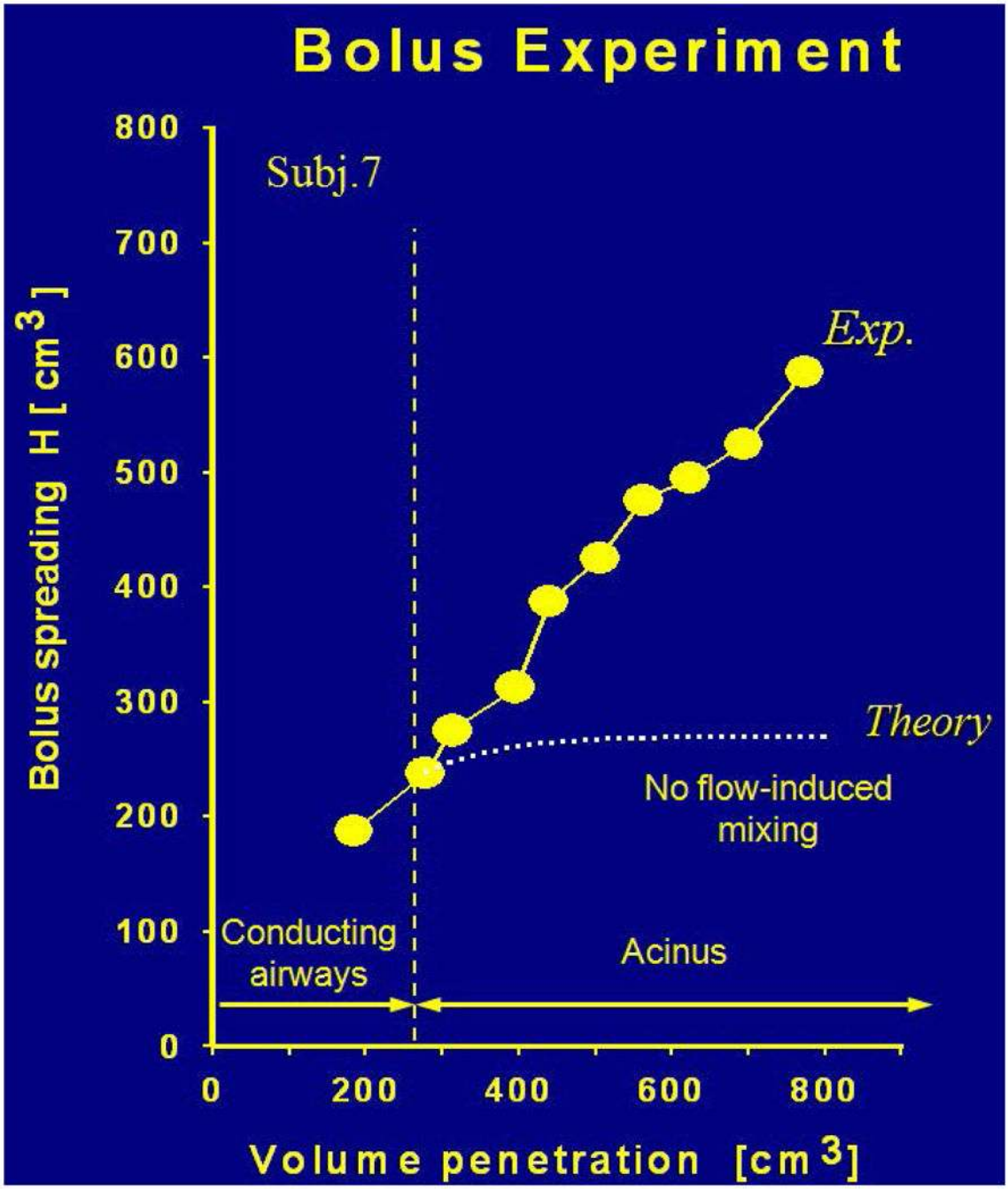

Figure 10.
Heyder et al.'s seminal work (1988)[149]. The presence of kinematical irreversibility in the acinus was demonstrated experimentally.

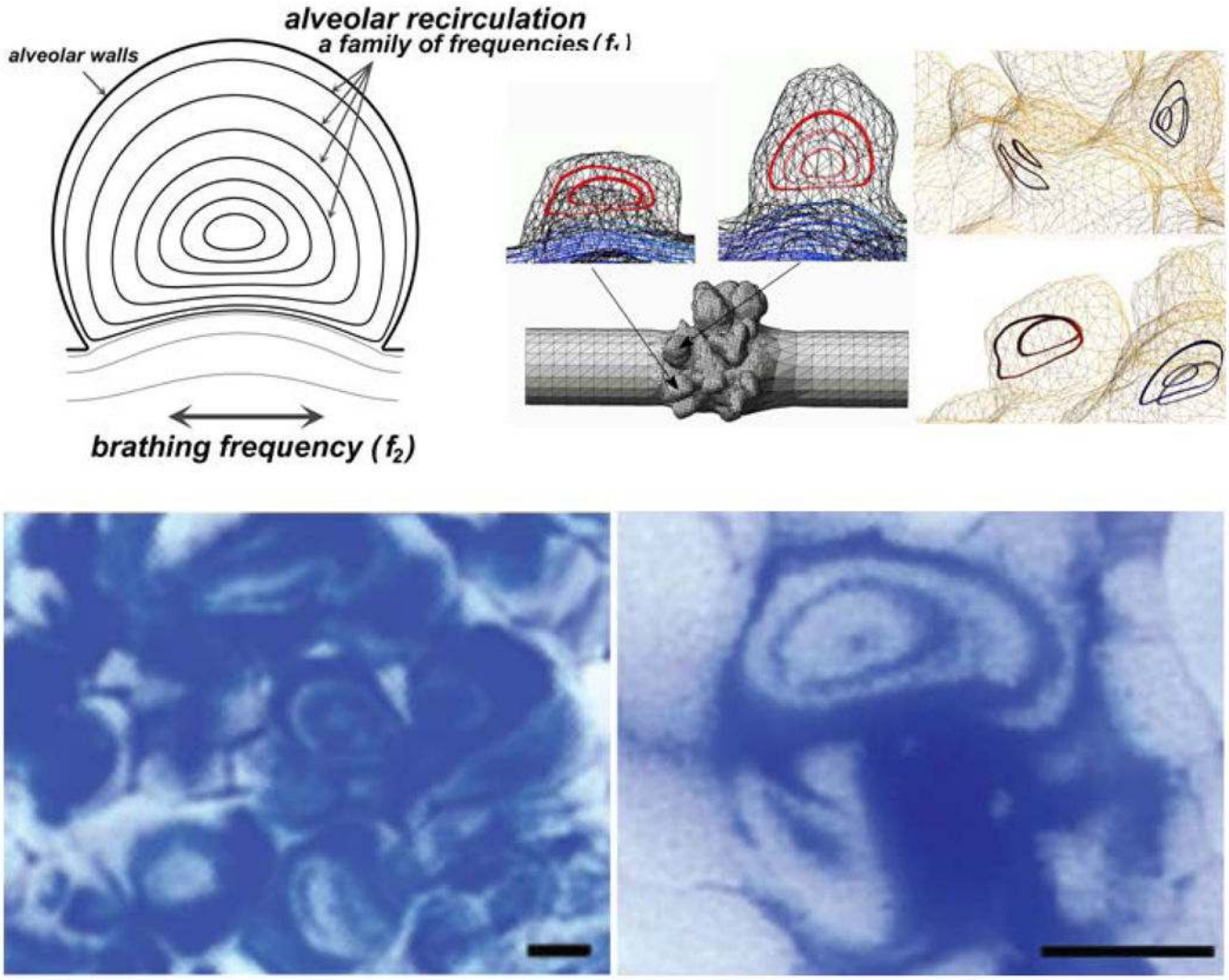

Figure 11.

Alveolar recirculation. *Top*: computational predictions. *Top Left*: idealized model [modified from Tsuda et al. (1995)[310]]. *Top Middle & Right*: synchrotron-based realistic alveolar model. From Filipovic et al. (2010)[95]; Bottom: Experimental observation of rotational flow patterns in the alveoli of excised rat lung. Bar = 100um. From Tsuda et al. (2002)[312].

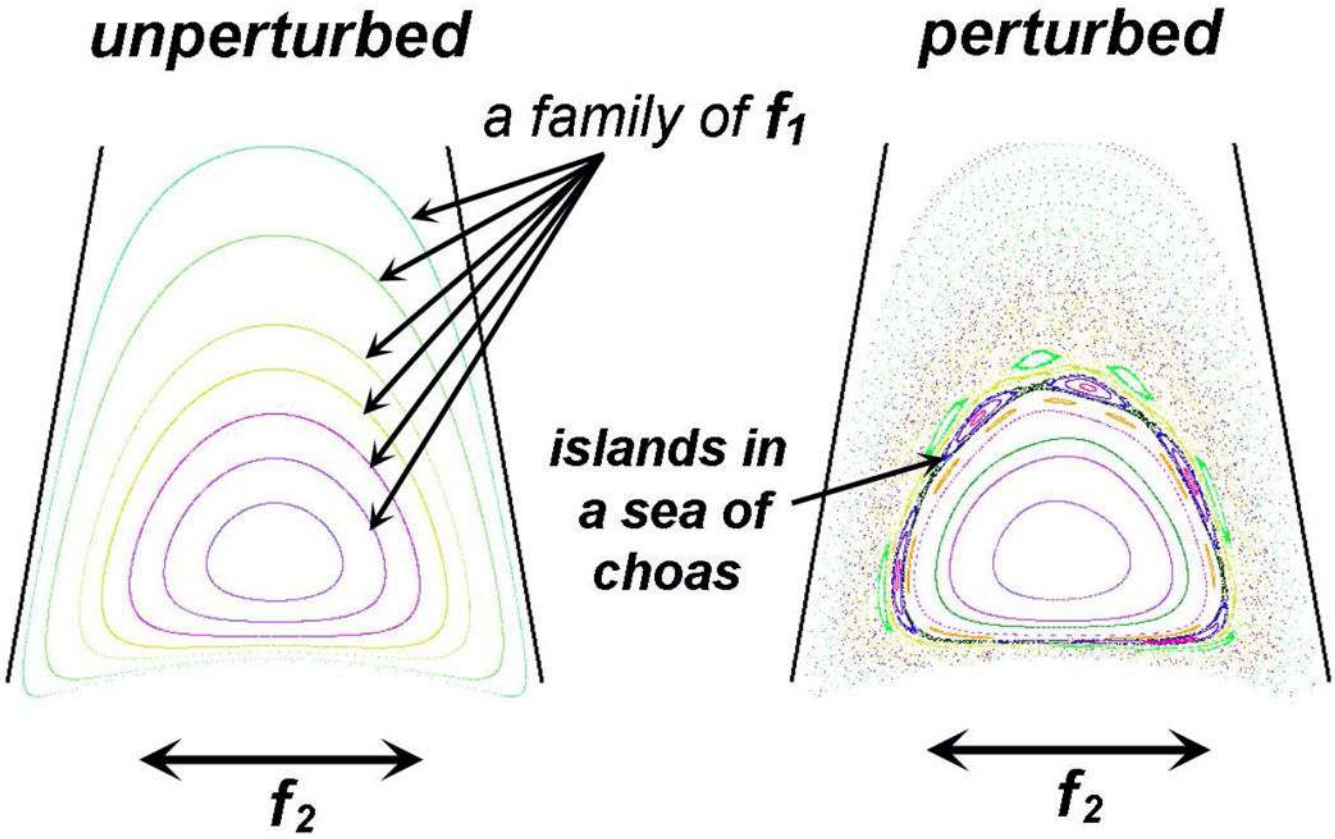

Figure 12.

Poincaré sections of particle transport; each color represents a different trajectory. *Left*: Stokes flow in a cavity – no perturbation present and seven particle paths shown. *Right*: The addition of a perturbation by wall motion creates islands in a sea of chaos; eight more particle paths have been added to the original seven for further detail. Modified from Tsuda, Laine-Pearson & Hydon (2011)[315].

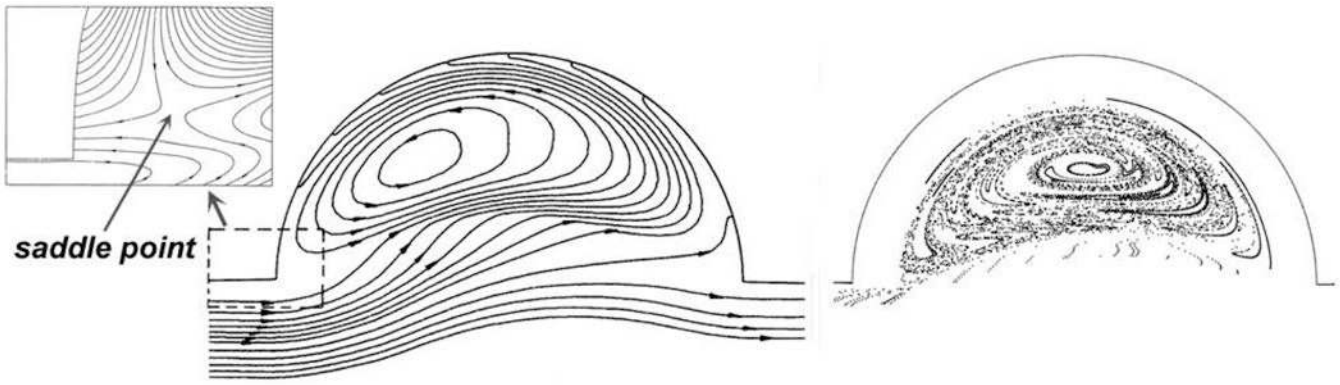

Figure 13.

Streamlines at peak inspiration (*Left*) and the Poincaré map (*Right*) on the symmetry mid-plane of a hemispherical alveolar model with rhythmically expanding walls. The streamlines exhibit recirculations and a stagnation saddle point near the alveolar entrance. The Poincaré map shows that regions of stochasticity seem to appear bounded by quasi-periodic surfaces. From Haber et al. (2000)[125].

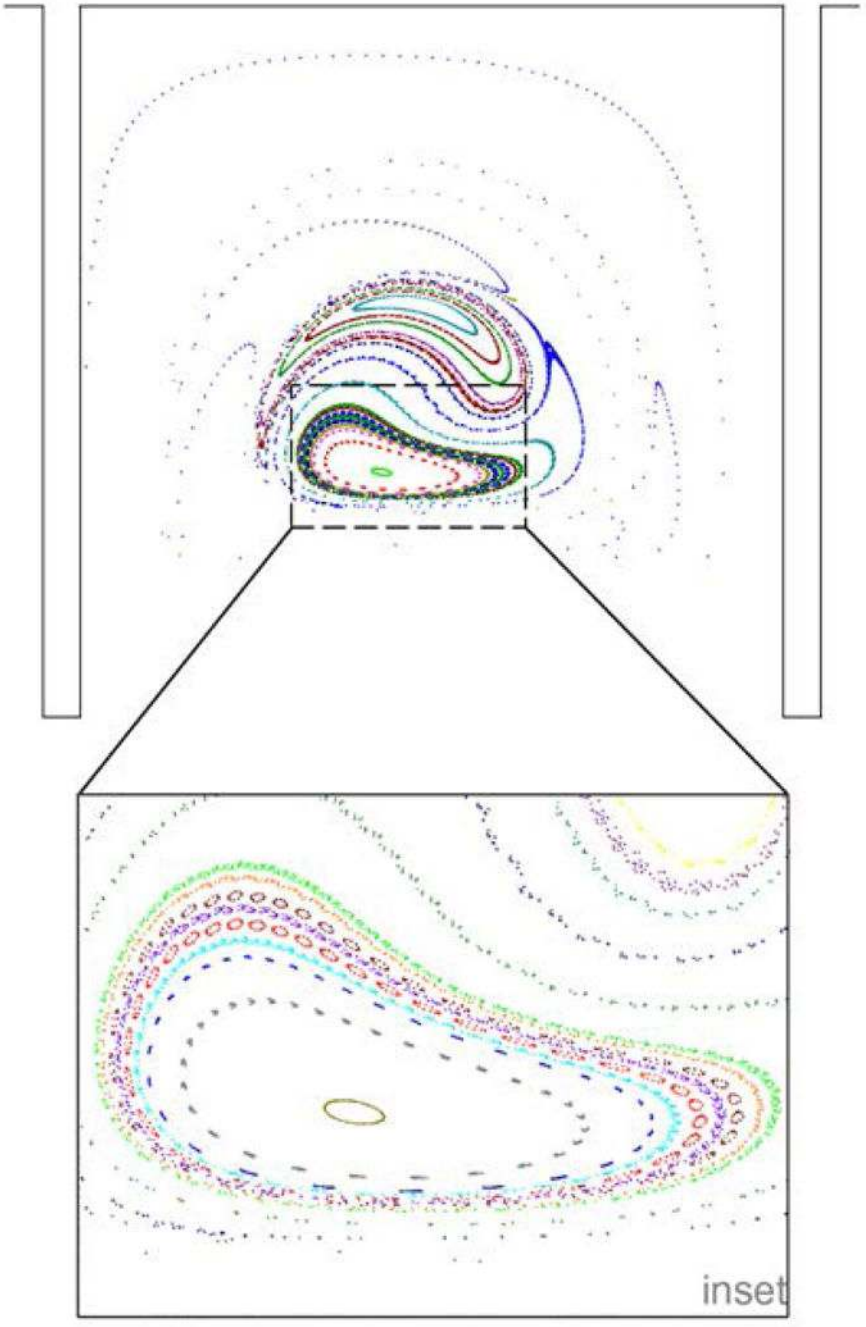

Figure 14.
Poincaré sections for a flow with Re=1.0, showing the presence of chaos even in an alveolus with stationary walls. From Henry et al. (2009)[144].

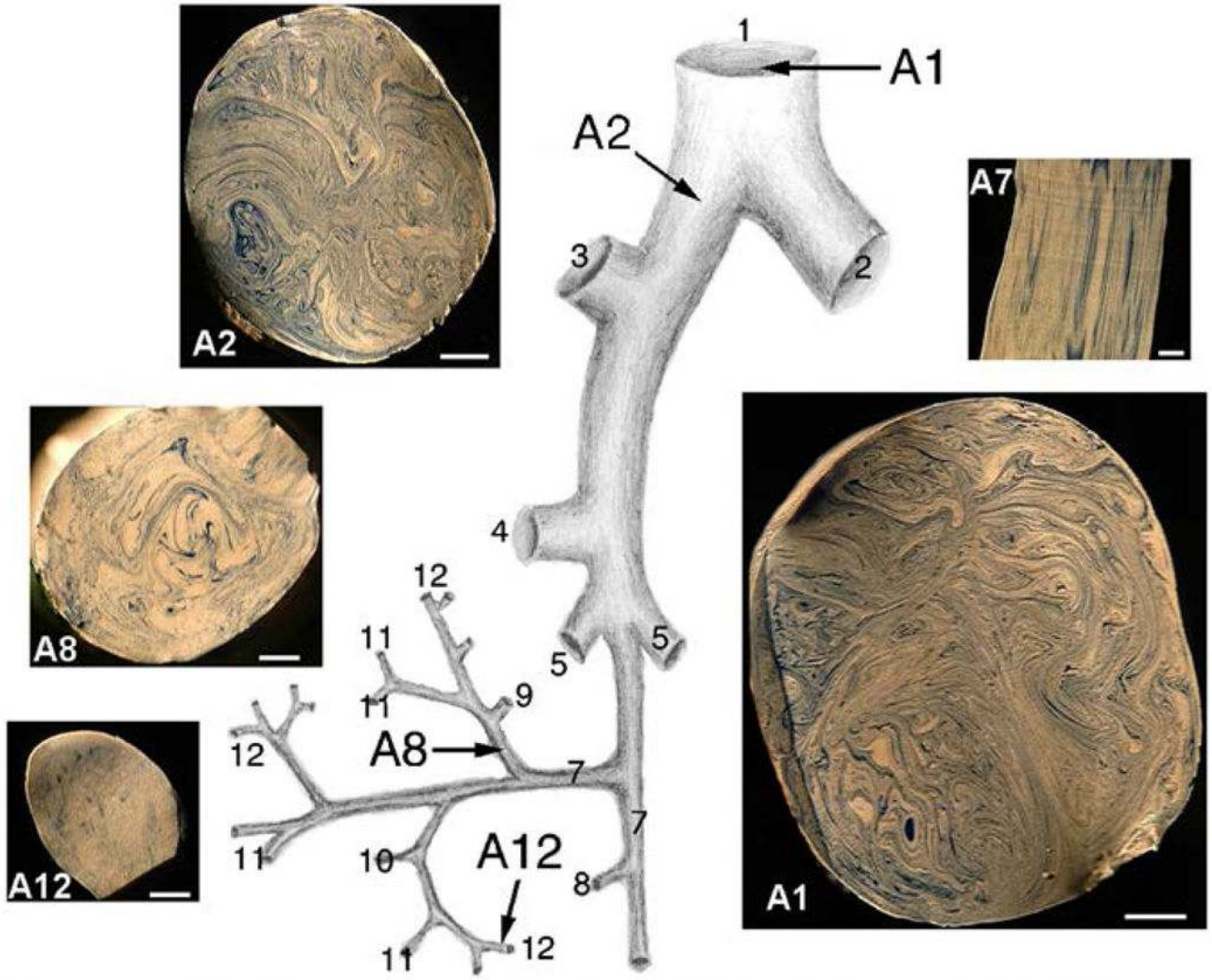

Figure 15.

Complex convoluted "stretch-and-fold" flow patterns on the cross-sections of large airways of rat lung. From Tsuda, et al. (2002)[312].

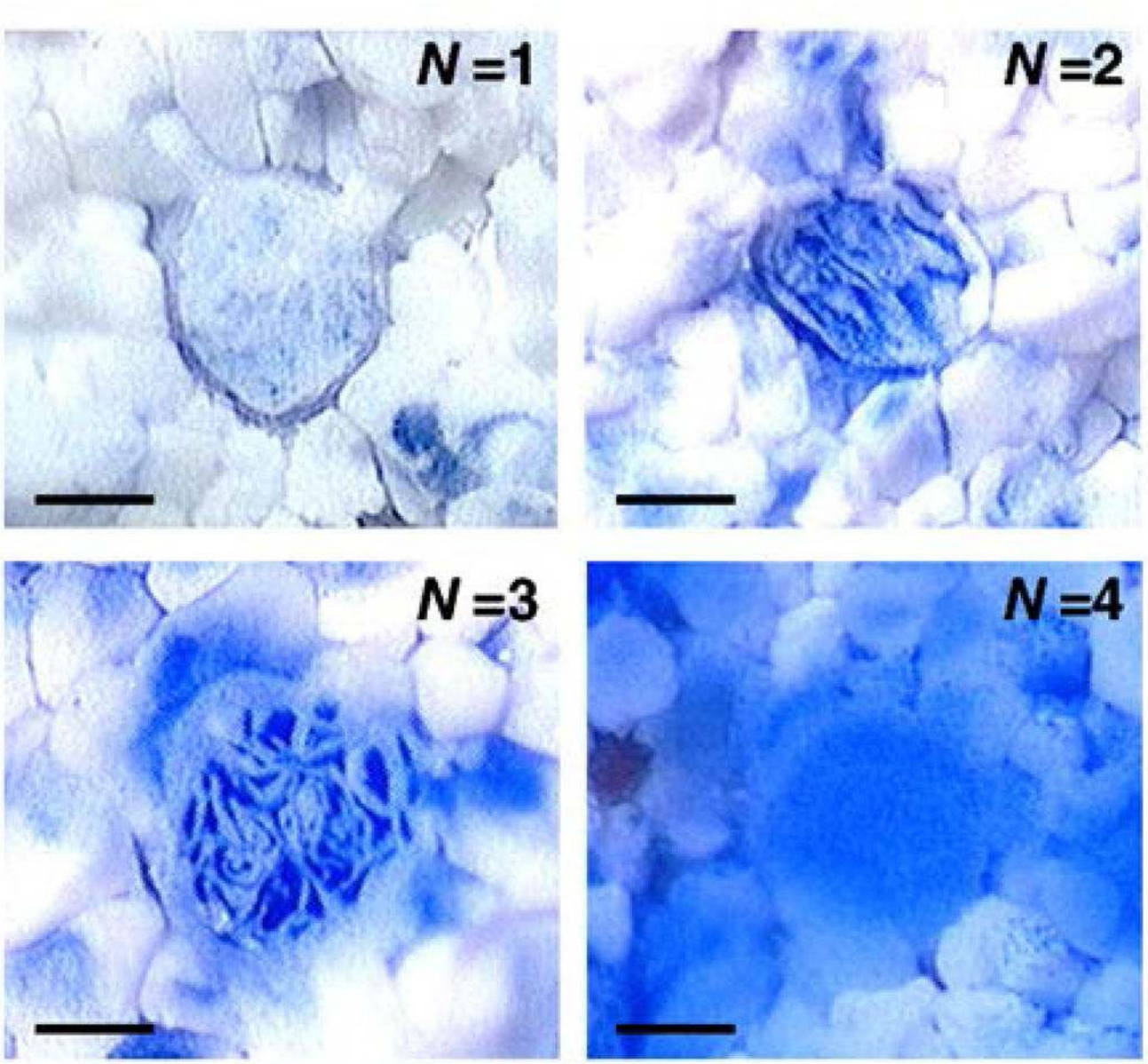

Figure 16.
Typical mixing pattern of two colors observed in ~200μm acinar airway of adult rats after *N*=1,2,3,& 4 cycles. Bar=100μm. From Tsuda, et al. (2002)[312].

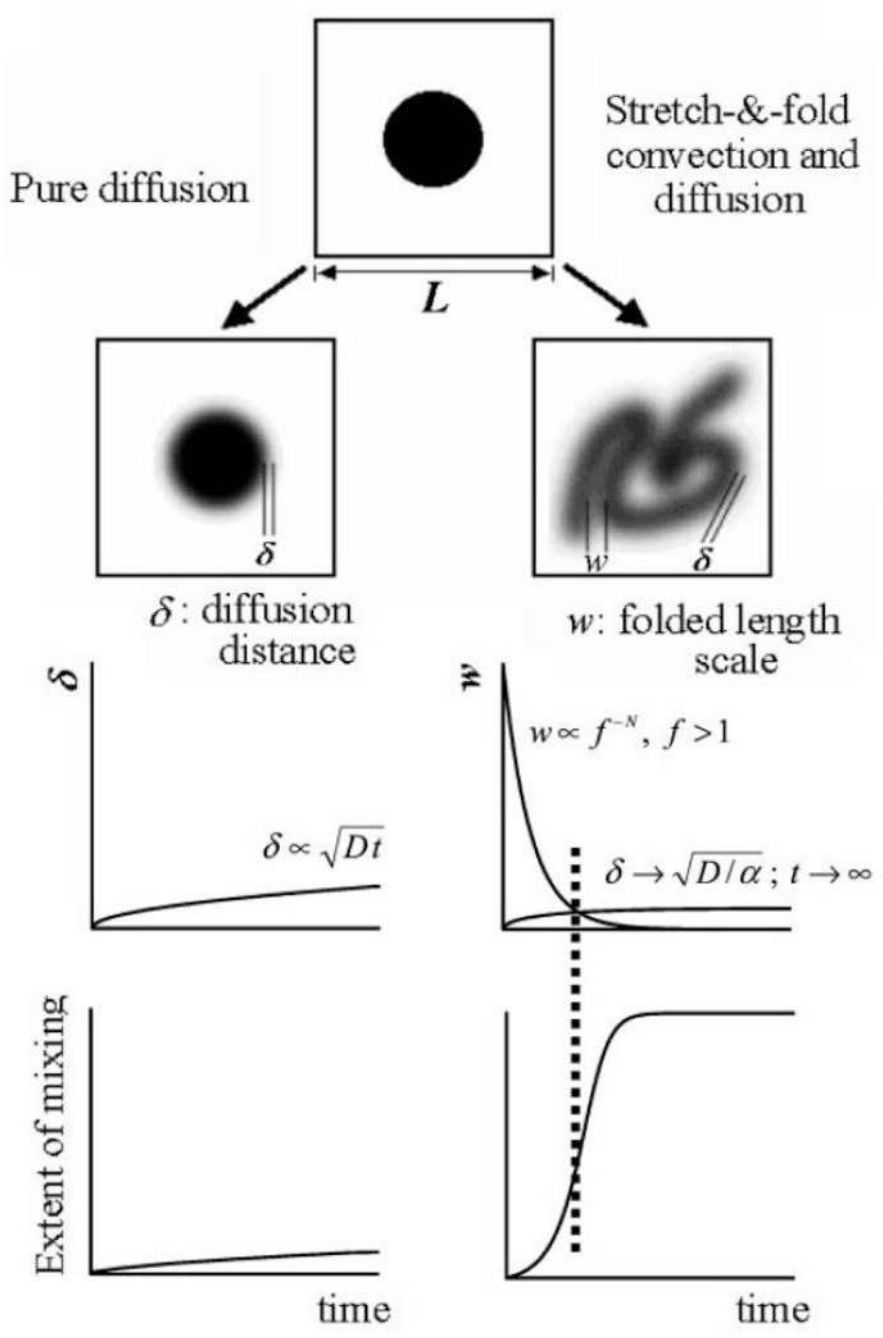

Figure 17.

Comparison of Brownian tracer mixing between a system with pure diffusion and a system with stretch and fold convection and diffusion. (*Top*) Schematic view of these two systems. (*Middle Left*) The slowly increasing length scale for mixing (δ) in pure diffusion. (*Middle Right*) With stretch and fold convection, δ also increases slowly (but approaches an asymptotic value); by contrast, the folding length scale, w, decreases exponentially rapidly. (*Bottom*) Representation of the evolving extent of mixing corresponding to diffusion alone and to diffusion coupled with stretch and fold convection. At the time when the two length

scales are comparable (vertical dotted line), there is sharp jump in mixing (entropy burst). (from Tsuda et al., 2002[312])

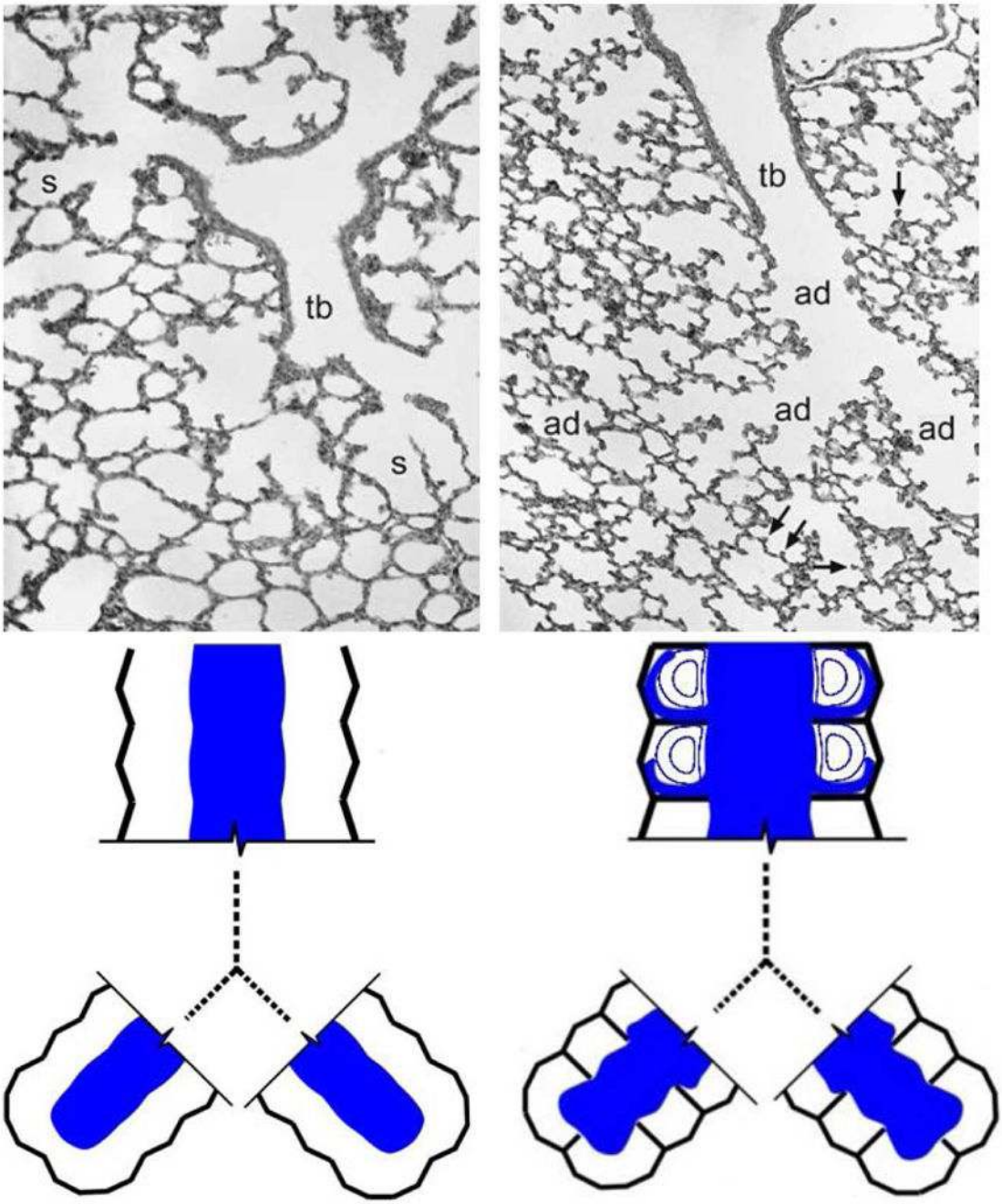

Figure 18.

Top: Acinar structure of the immature lung of a 1-day old rat (left) and the lung of a 21 day old rat whose alveolar shape is nearly fully developed, but small in size (right) (from Schittny & Burri, 2008[273]). tb: terminal bronchioles, S: saccules, ad: alveolar ducts, arrows: secondary septa. *Bottom*: schematics of predicted patterns of particle-laden inhaled airflow (shown in blue).

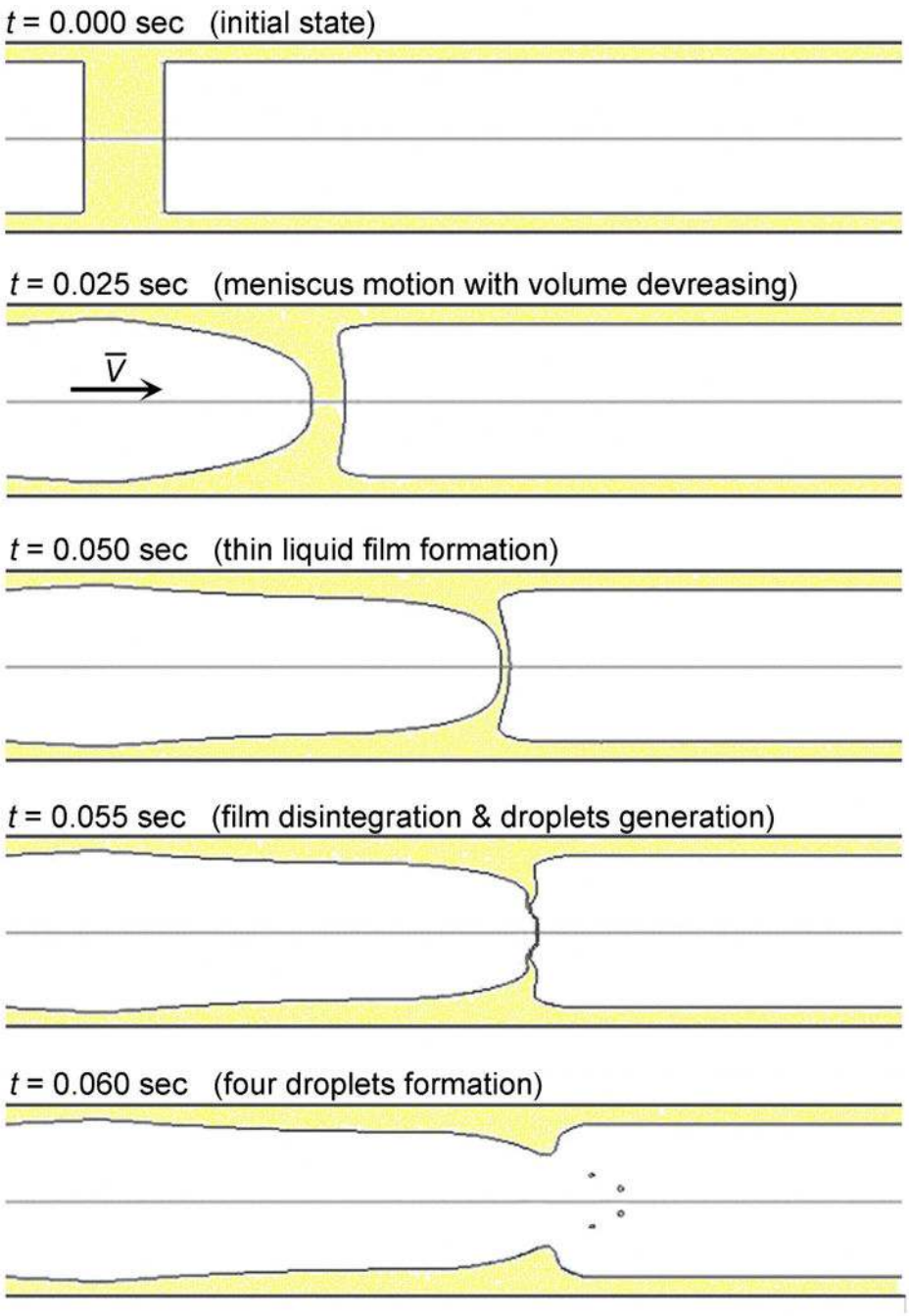

Figure 19.

Formation of droplets at the level of small airways. At Ca above the critical values, a meniscus traveling along the airway thins and then disintegrates into small droplets. Re=0.67, *Ca*=1. See Malasheko et al. (2009)[214] for details.

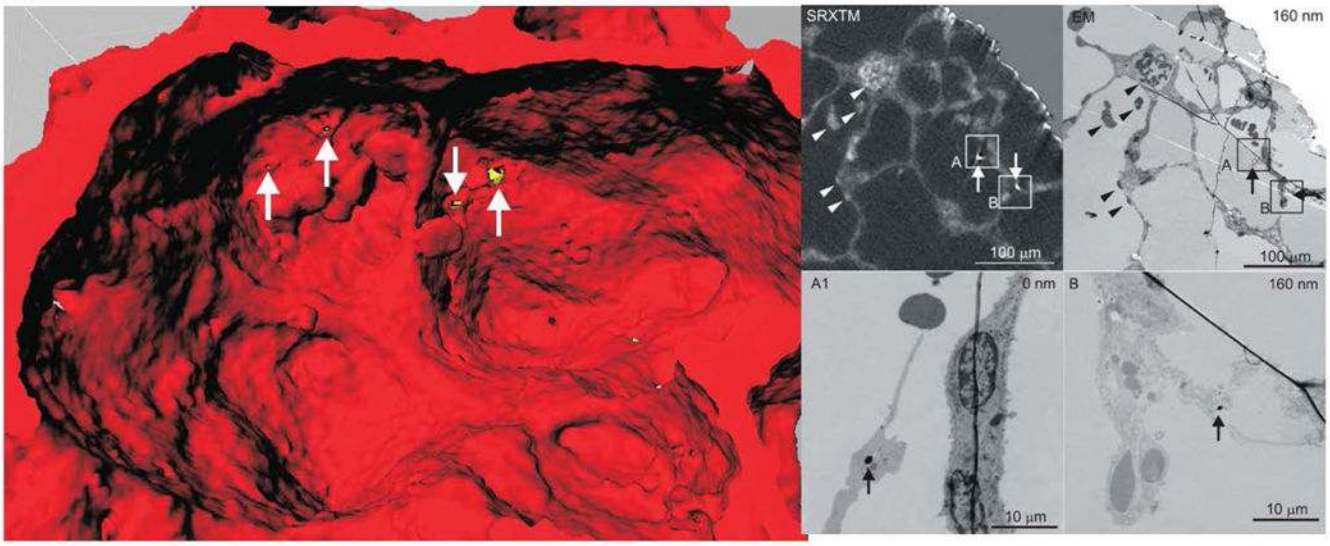

Figure 20.

A demonstration of multimodal imaging techniques: combined synchrotron radiation-based X-ray tomographic microscopy (SRXTM)-based skeletonization technique, which locates an alveolus of interest within the acinar tree[128] and high-resolution transmission electron microscopy (TEM), which is necessary to visualize nanosize particles in the alveolar structure. The concept is illustrated in this figure by the visualization of 700nm gold particles (as surrogates for nanosize particles) instilled into an adult rat lung. First, a tissue sample was imaged by SRXTM and 3D reconstruction of the acinus was performed[312]. Then, by using skeletonization techniques[128], an alveolus containing gold particles on its septal wall was identified in the distal region of the acinus (Panel A). The same particles were also identified in one section of a 3D stack of SRXTM images (Panel B). Using the registered coordinates of this region of interest, serial sectioning was performed in that area. The resulting TEM images of that alveolus and the gold particles located in it are shown in Panel C. A higher magnification of the region A & B in Panel C are shown in Panel D and E, respectively. From Haberthür et al. (2009b)[129], Schittny et al. (2010)[274].

Table 1

Particle size and transport properties. d_p: particle diameter; C_s: Cunningham slip correction factor; D: Diffusion coefficient; V_g: terminal settling velocity; τ_{mon}: momentum relaxation time; $(D*t)^{1/2}$: diffusion distance for t=1 sec; V_g*t: sedimentation distance for t=1sec. See Particle Transport for the definition of the symbols.

d_P [μm]	C_s	D [cm^2/s]	V_g [cm/s]	τ_{mom} [sec]	$(D*t)^{1/2}$ [μm]	V_g*t [μm]
0.01	22.1	5.07E-04		6.20E-09	2.25E+02	
0.02	11.4	1.30E-04		1.27E-08	1.14E+02	
0.05	4.9	2.27E-05		3.47E-08	4.76E+01	
0.1	2.9	6.54E-06	2.75E-05	8.00E-08	2.56E+01	2.75E-01
0.2	1.9	2.14E-06	1.10E-04	2.09E-07	1.46E+01	1.10E+00
0.5	1.3	6.08E-07	6.86E-04	9.30E-07	7.80E+00	6.86E+00
1	1.2	2.66E-08	2.75E-03	3.26E-06	1.63E+00	2.75E+01
2	1.1		1.10E-02	1.21E-05		1.10E+02
5	1		6.86E-02	7.23E-05		6.86E+02

Table 2

Adult data at Total Lung Capacity (TLC) derived from Weibel (1963)[324] and Weibel et al. (2005)[325]. Weibel's airway generation number (gen); airway duct diameter (*d*); airflow velocity (*V*); airflow Reynolds number (*Re*), Péclet number (*Pe*), gravity number and Stokes number for 0.01 and 0.1 μm for rest and exercise conditions are calculated.

		Rest									Exercise								
gen	**d [cm]**	**V [cm/s]**	**Re**	**Pe (0.01μ)**	**Pe (0.1μ)**	**V_g/V (1μ)**	**V_g/V (5μ)**	***Stk* (1μ)**	***Stk* (5μ)**	**Stk/(Vg/V)**	**V [cm/s]**	**Re**	**Pe (0.01μ)**	**Pe (0.1μ)**	**V_g/V (1μ)**	**V_g/V (5μ)**	***Stk* (1μ)**	***Stk* (5μ)**	**Stk/(Vg/V)**
0	1.8	96	859.7	3.39E+05	2.63E+07	2.87E-05	7.19E-04	1.49E-03	3.72E-02	5.2	769	6921	2.73E+06	2.12E+08	3.57E-06	8.93E-05	1.20E-02	2.99E-01	335
1	1.22	104	631.4	2.49E+05	1.93E+07	2.65E-05	6.63E-04	2.38E-03	5.94E-02	9.0	833	5083	2.01E+06	1.55E+08	3.30E-06	8.24E-05	1.91E-02	4.78E-01	580
2	0.666	174	577.8	2.28E+05	1.77E+07	1.58E-05	3.96E-04	7.30E-03	1.82E-01	46.1	1397	4652	1.84E+06	1.42E+08	1.97E-06	4.91E-05	5.58E-02	1.47E+00	2990
3	0.449	191	428.3	1.69E+05	1.31E+07	1.44E-05	3.60E-04	1.19E-02	2.98E-01	82.6	1536	3448	1.36E+06	1.05E+08	1.79E-06	4.47E-05	9.58E-02	2.40E+00	5360
4	0.361	148	266.2	1.05E+05	8.14E+06	1.86E-05	4.65E-04	1.14E-02	2.86E-01	61.4	1187	2143	8.46E+05	6.55E+07	2.31E-06	5.78E-05	9.21E-02	2.30E+00	3980
5	0.281	122	170.8	6.75E+04	5.22E+06	2.26E-05	5.64E-04	1.21E-02	3.03E-01	53.7	979	1376	5.43E+05	4.20E+07	2.80E-06	7.01E-05	9.76E-02	2.44E+00	3480
6	0.225	95	106.6	4.21E+04	3.26E+06	2.90E-05	7.24E-04	1.18E-02	2.95E-01	40.7	763	858	3.39E+05	2.62E+07	3.60E-06	9.00E-05	9.50E-02	2.37E+00	2640
7	0.185	70	64.8	2.56E+04	1.98E+06	3.92E-05	9.80E-04	1.06E-02	2.65E-01	27.0	564	522	2.06E+05	1.59E+07	4.87E-06	1.22E-04	8.54E-02	2.13E+00	1750
8	0.149	54	40.2	1.59E+04	1.23E+06	5.09E-05	1.27E-03	1.01E-02	2.54E-01	19.9	434	323	1.28E+05	9.89E+06	6.32E-06	1.58E-04	8.16E-02	2.04E+00	1290
9	0.124	39	24.1	9.52E+03	7.37E+05	7.06E-05	1.76E-03	8.79E-03	2.20E-01	12.4	313	194	7.66E+04	5.93E+06	8.77E-06	2.19E-04	7.07E-02	1.77E+00	806
10	0.104	28	14.4	5.67E+03	4.39E+05	9.94E-05	2.49E-03	7.44E-03	1.86E-01	7.5	222	116	4.56E+04	3.53E+06	1.24E-05	3.09E-04	5.99E-02	1.50E+00	484
11	0.085	21	8.8	3.46E+03	2.68E+05	1.33E-04	3.33E-03	6.80E-03	1.70E-01	5.1	166	71	2.79E+04	2.16E+06	1.65E-05	4.13E-04	5.47E-02	1.37E+00	331
12	0.069	16	5.4	2.13E+03	1.65E+05	1.76E-04	4.39E-03	6.35E-03	1.59E-01	3.6	126	43	1.71E+04	1.33E+06	2.18E-05	5.45E-04	5.11 E-02	1.28E+00	234
13	0.056	12	3.3	1.31E+03	1.01E+05	2.32E-04	5.79E-03	5.93E-03	1.48E-01	2.6	95	27	1.05E+04	8.17E+05	2.88E-05	7.19E-04	4.77E-02	1.19E+00	166
14	0.045	9.16	2.1	8.14E+02	6.30E+04	3.00E-04	7.49E-03	5.71E-03	1.43E-01	1.9	74	17	6.55E+03	5.07E+05	3.72E-05	9.30E-04	4.59E-02	1.15E+00	123
15	0.036	7.14	1.29	5.08E+02	3.93E+04	3.84E-04	9.61E-03	5.56E-03	1.39E-01	1.44	58	10.4	4.09E+03	3.16E+05	4.77E-05	1.19E-03	4.47E-02	1.12E+00	94
16	0.036	3.55	0.64	2.52E+02	1.95E+04	7.74E-04	1.93E-02	2.76E-03	6.90E-02	0.36	29	5.1	2.03E+03	1.57E+05	9.61E+05	2.40E-03	2.22E-02	5.56E-01	23
17	0.036	1.75	0.31	1.24E+02	9.61E+03	1.57E-03	3.93E-02	1.36E-03	3.40E-02	0.09	14	2.5	1.00E+03	7.74E+04	1.95E-04	4.88E-03	1.09E-02	2.74E-01	6
18	0.029	1.31	0.19	7.51E+01	5.82E+03	2.09E-03	5.23E-02	1.27E-03	3.17E-02	0.06	11	1.5	6.05E+02	4.68E+04	2.60E-04	6.50E-03	1.02E-02	2.55E-01	4
19	0.028	0.67	0.094	3.72E+01	2.88E+03	4.08E-03	1.02E-01	6.73E-04	1.68E-02	0.02	5.41	0.76	2.99E+02	2.32E+04	5.07E-04	1.27E-02	5.42E-03	1.35E-01	1.07
20	0.026	0.36	0.047	1.86E+01	1.44E+03	7.59E-03	1.90E-01	3.90E-04	9.75E-03	0.01	2.91	0.38	1.49E+02	1.16E+04	9.43E-04	2.36E-02	3.14E-03	7.84E-02	0.33
21	0.025	0.17	0.021	8.22E+00	6.36E+02	1.65E-02	4.12E-01	1.87E-04	4.66E-03	0.00	1.34	0.17	6.62E+01	5.12E+03	2.05E-03	5.12E-02	1.50E-03	3.76E-02	0.07
22	0.023	0.07	0.008	3.05E+00	2.36E+02	4.09E-02	1.02E+00	8.18E-05	2.05E-03	0.00	0.54	0.06	2.46E+01	1.90E+03	5.08E-03	1.27E-01	6.59E-04	1.65E-02	0.01
23	0.021	0.04	0.004	1.48E+00	1.15E+02	7.67E-02	1.92E+00	4.78E-05	1.19E-03	0.00	0.29	0.03	1.19E+01	9.25E+02	9.53E-03	2.38E-01	3.84E-04	9.61E-03	0.00

Table 3

Eigenfunction expansion. Graetz analytic solution (Eq. 9) can be discretized for every unit cell ($x=KL_{cell}$) as, $n(K, r^*) = C_1\exp[K\ln(\bar{\lambda_1})][S_1(r^*)] + C_2\exp[K\ln(\bar{\lambda_2})][S_2(r^*)] + C_3\exp[K\ln(\bar{\lambda_3})][S_3(r^*)] + \ldots..$, and therefore, rewritten as Eq. 10. See Glossary for definition of abbreviations.

	cylindrical pipe	alveolated duct
C_1	1.477	1.468
C_2	-0.81	-0.835
C_3	0.385	0.541
λ_1	-14.63	-14.38
λ_2	-89.22	-92.13
λ_3	-228	-260
$\bar{\lambda_1}$	0.864	0.866
$\bar{\lambda_2}$	0.409	0.398
$\bar{\lambda_3}$	0.102	0.074

r^*	$S_1(r^*)$	$S_2(r^*)$	$S_3(r^*)$
0.00	1	1	1
0.05	0.9818	0.8923	0.753
0.10	0.9290	0.6067	0.206
0.15	0.8456	0.2367	-0.290
0.20	0.7382	-0.1062	-0.407
0.25	0.6147	-0.3399	-0.204
0.30	0.4833	-0.4317	0.104
0.35	0.3506	-0.3985	0.278
0.40	0.2244	-0.3051	0.278
0.45	0.1069	-0.1637	0.144
0.50	0	0	0